

**PHOTOPHYSICAL PROPERTIES OF  
ZINC CARBOXY  
PHTHALOCYANINE-QUANTUM  
DOT CONJUGATES**

**A thesis submitted in fulfilment of the requirements**

**for the degree of**

**MASTER OF SCIENCE**

**Of**

**RHODES UNIVERSITY**

**By**

**KUTLOANO EDWARD SEKHOSANA**

**February 2013**

---

**Dedication**

**To**

**My Mother**

**MASEBOKA ANNA SEKHOSANA**

*May God give you strength to continue loving guiding and supporting us.*

**My Sisters**

**MALEHLONONO, RORISANG, REFILOE, FUSI  
AND RELEBOHILE**

**My Brothers**

**TANKISO AND THAROLLO**

**My Cousin**

**ELELLOANG MOHLAKOANA**

**My Father**

**PHEELLO HENRY SEKHOSANA**

*Who passed away before this program could be finished, may your soul rest in peace.*

## Acknowledgements

**“my sincere gratitude to God for His protection over me and strengthening me throughout this particular program”**

My truthful thankfulness is extended to my supervisor **Prof. Tebello Nyokong**. Her patience, guidance and frequent interaction with me, while grooming me up in the process, made this program a success. I like express my cordial gratitude to **Dr. Christian Litwinski** (my former supervisor), who took me through the first but pivotal steps of this program, as well as **Dr. Edith Antunes**, who has always been there for me, helping in every possible way she could. My thanks also go to **Dr. Wadzanai Chidawanyika, Dr. John Mack, Dr. Samson Khene, Mr. Nkosiphile Masilela and Ms Sarah D’Souza** for their kind assistance.

I would also like to thank **Dr. Eugeny Ermilov and Dr. Michael Höpfner** for their supervision as host supervisors at Charité University - Berlin, Germany – many thanks to their group as a whole.

Let me thank the following sponsors for their the Research Foundation (NRF) of South Africa through DST/NRF South African Research Chairs Initiative for Professor of Medicinal Chemistry and Nanotechnology and Rhodes University for financial support, Dr Desmond E. Goddard bursary.

Thanks also to S22 research group colleagues for making the working environment feel like home – I have enjoyed your company. Thanks also to all my friends.

## Abstract

This thesis presents work based on the interactions of water soluble carboxylated zinc phthalocyanines (Pcs) and core-shell quantum dots (QDs). The Pcs are  $\text{ZnPc}(\text{COOH})_8$  and  $\text{ZnPc}(\text{COOH})_4$  and core-shell QDs are  $\text{CdTe@ZnS-GSH}$ . GSH = L-glutathione. Characterization and photophysical studies of conjugates were carried out. The approach of coordinating Pcs to QDs was achieved using an organic cross linker, N-N'-dicyclohexylcarbodiimide (DCC) at pH 10 at room temperature. Employing atomic force microscopy (AFM), transmission electron microscopy (TEM), X-ray diffraction (XRD), Raman, infrared and X-ray photoelectron spectroscopies, the formation of the conjugates was confirmed. Upon conjugation with Pc derivatives, the fluorescence quantum yield of  $\text{CdTe@ZnS-GSH}$  decreased due to energy transfer from the QDs to the Pc. The average fluorescence lifetime of the  $\text{CdTe@ZnS-GSH}$  QD also decreased upon conjugation. The Förster resonance energy transfer (FRET) behaviour of  $\text{CdTe@ZnS-GSH-ZnPc}(\text{COOH})_4$  conjugates was compared to that of  $\text{CdTe@ZnS-GSH-ZnPc}(\text{COOH})_8$ . Higher FRET efficiencies were observed for  $\text{CdTe@ZnS-GSH-ZnPc}(\text{COOH})_4$ -mixed or  $\text{CdTe@ZnS-GSH-ZnPc}(\text{COOH})_4$ -linked compared to the corresponding  $\text{CdTe@ZnS-GSH-ZnPc}(\text{COOH})_8$ -mixed or  $\text{CdTe@ZnS-GSH-ZnPc}(\text{COOH})_8$ -linked. Triplet quantum yield ( $\Phi_T$ ) and lifetime ( $\tau_T$ ) of  $\text{ZnPc}(\text{COOH})_8$  were found to increase in the presence of core-shell QDs. Though the singlet quantum yield ( $\Phi_A$ ) value of  $\text{ZnPc}(\text{COOH})_8$  was lower than  $\Phi_T$ , there was a slight upsurge in the  $\Phi_T$  in the presence of QDs.

---

# Table of Contents

|  |      |
|--|------|
| Dedication .....   | ii   |
| Acknowledgements .....   | iii  |
| Abstract .....   | iv   |
| Table of Contents .....  | v    |
| List of Symbols .....  | viii |
| List of Abbreviations .....  | x    |
| List of Figures .....  | xii  |
| List of Tables .....   | xvi  |
| CHAPTER ONE .....  | 1    |
| INTRODUCTION .....   | 1    |
| 1.1 Phthalocyanines .....  | 2    |
| 1.1.1 Structure and general applications of phthalocyanines .....        | 2    |
| 1.1.2 Synthesis of octa- and tetracarboxy phthalocyanines .....          | 4    |
| 1.1.3 Phthalocyanine spectra and effects of aggregation on spectra ..... | 7    |
| 1.2 Quantum dots .....   | 11   |
| 1.2.1 General applications of quantum dots .....                         | 11   |
| 1.2.2 Synthesis of water soluble core and coreshell QDs .....            | 12   |
| 1.2.3 Fluorescence behaviour .....                                       | 16   |
| 1.3 Förster resonance energy transfer .....                              | 18   |

|  |    |
|--|----|
| 1.4 Photophysical parameters .....   | 26 |
| 1.4.1 Fluorescence quantum yields and lifetimes .....  | 27 |
| 1.4.2 Triplet quantum yields and lifetimes .....   | 29 |
| 1.4.3 Singlet oxygen quantum yield .....   | 31 |
| 1.4.4 FRET parameters .....  | 34 |
| 1.5 Summary of aims .....  | 35 |
| CHAPTER TWO .....  | 39 |
| EXPERIMENTAL .....   | 39 |
| 2.1 Materials .....  | 40 |
| 2.2 Instrumentation .....  | 40 |
| 2.3 Synthesis .....  | 47 |
| 2.4 Photophysical studies .....  | 48 |
| 2.4.1 Fluorescence quantum yields and lifetimes .....  | 48 |
| 2.4.2 FRET Parameters .....  | 48 |
| 2.4.3 Triplet quantum yields ( $\Phi_T$ ) and lifetimes ( $\tau_T$ ) .....   | 49 |
| 2.4.4 Singlet oxygen ( $\Phi_\Delta$ ) .....   | 49 |
| CHAPTER THREE .....  | 50 |
| RESULTS AND DISCUSSION .....   | 50 |
| 3.1 Characterization of conjugates of quantum dots with ZnPc(COOH) <sub>8</sub> and<br>ZnPc(COOH) <sub>4</sub> ..... | 52 |
| 3.1.1 FTIR spectra .....   | 54 |

|   |    |
|---|----|
| 3.1.2 Raman spectra .....   | 57 |
| 3.1.3 XRD .....   | 58 |
| 3.1.4 Microscopic data .....  | 62 |
| 3.1.5 XPS spectra of coreshell QD alone and in the presence of ZnPc(COOH) <sub>8</sub><br>..... | 64 |
| 3.1.6 UV-Vis spectra.....   | 65 |
| 3.2 Photophysical parameters .....  | 70 |
| 3.2.1 Fluorescence quantum yields and lifetimes.....  | 70 |
| 3.2.2 Triplet quantum yields, lifetimes and singlet oxygen quantum yields ...                   | 75 |
| 3.2.3 Förster Resonance Energy Transfer (FRET) Parameters .....                                 | 78 |
| CHAPTER FOUR .....  | 86 |
| CONCLUSIONS .....   | 86 |
| General conclusions .....   | 87 |
| References.....   | 88 |

# List of Symbols

|                          |   |   |
|--------------------------|---|---|
| $\Delta A$               | = | Change in absorbance following laser pulse                      |
| $I$                      | = | Intensity of light  |
| $I_{\text{abs}}$         | = | Intensity of light absorbed                                     |
| $F$                      | = | Fluorescence intensity  |
| $\alpha$                 | = | Non-peripheral position   |
| $\beta$                  | = | Peripheral position   |
| $\varepsilon$            | = | Molar extinction coefficient                                    |
| $\varepsilon_S$          | = | Singlet state extinction coefficient                            |
| $\varepsilon_T$          | = | Triplet state extinction coefficient                            |
| $\lambda_{\text{emi}}$   | = | Wavelength of emission spectrum maximum                         |
| $\lambda_{\text{exci}}$  | = | Wavelength of excitation spectrum maximum                       |
| $h\nu$                   | = | Light   |
| $n$                      | = | Refractive index  |
| $\Phi_{\Delta}$          | = | Singlet oxygen quantum yield                                    |
| $\Phi_F$                 | = | Fluorescence quantum yield                                      |
| $\Phi_T$                 | = | Triplet state quantum yield                                     |
| $\tau$                   | = | Fluorescence lifetime   |
| $\tau_{\text{av}}$       | = | Average lifetime  |
| $\tau_T$                 | = | Triplet state lifetime  |
| $\chi^2$                 | = | Reduced Chi-squared statistic                                   |
| $J$                      | = | Overlap integral  |
| $R_0$                    | = | Förster distance (critical distance at which efficiency is 50%) |
| $r$                      | = | Centre-to-centre separation distance                            |
| $k^2$                    | = | Dipole orientation factor                                       |
| $^1\text{O}_2$           | = | Singlet oxygen  |
| $\text{O}_2(^1\Delta_g)$ | = | Singlet oxygen  |
| $^3\text{O}_2$           | = | Triplet molecular oxygen  |



|                      |   |                                      |
|----------------------|---|--------------------------------------|
| <b>O<sub>2</sub></b> | = | <b>Ground state molecular oxygen</b> |
| <b>S<sub>0</sub></b> | = | <b>Ground singlet state</b>          |
| <b>S<sub>1</sub></b> | = | <b>Excited singlet state</b>         |
| <b>T<sub>1</sub></b> | = | <b>First excited triplet state</b>   |
| <b>T<sub>2</sub></b> | = | <b>Second excited triplet state</b>  |

---

# List of Abbreviations

|                   |   |   |
|-------------------|---|---|
| A                 | = | Absorbance  |
| ADMA              | = | Tetrasodium a,a-(anthracene-9,10-diyl) dimethylmalonate |
| AFM               | = | Atomic force microscope                                 |
| AlPcSmix          | = | Mixed-sulfonated aluminium phthalocyanine               |
| CT                | = | Charge-transfer transitions                             |
| DBU               | = | 1,8-diazabicyclo[5.4.0]undec-7-ene                      |
| DMSO              | = | Dimethylsulphoxide                                      |
| ET                | = | Energy transfer   |
| F                 | = | Fluorescence  |
| GSH               | = | L-glutathione   |
| H <sub>2</sub> Pc | = | Metal-free phthalocyanine                               |
| HOMO              | = | Highest occupied molecular orbital                      |
| IC                | = | Internal conversion                                     |
| IR                | = | Infrared  |
| ISC               | = | Intersystem crossing                                    |
| L-cys             | = | L-cysteine  |
| LMCT              | = | Ligand-to-metal charge transfer                         |
| LUMO              | = | Lowest unoccupied molecular orbital                     |
| MLCT              | = | Metal-to-ligand charge transfer                         |
| MOCPC             | = | Metallo-ctacarboxy phthalocyanine                       |
| MPA               | = | 3-Mercaptopropionic acid                                |
| MPc               | = | Metallophthalocyanine                                   |
| NaOH              | = | Sodium hydroxide  |
| Pc                | = | Phthalocyanine  |
| ZnSPc             | = | Zinc sulphonated phthalocyanine                         |
| MTCPC             | = | Metallo-tetracarboxamido phthalocyanine                 |
| MTCAPc            | = | Metallo-tetracarboxy phthalocyanine                     |

|        |   |  |
|--------|---|--|
| OD     | = | Optical density                        |
| PDT    | = | Photodynamic therapy                   |
| Ph     | = | Phosphorescence                        |
| SOC    | = | Spin-orbit coupling                    |
| ROS    | = | Reactive Oxygen Species                |
| TCSPC  | = | Time-correlated single photon counting |
| TEM    | = | Transmission electron microscope       |
| TET    | = | Triplet energy transfer                |
| TGA    | = | Thioglycolic acid                      |
| UV/Vis | = | Ultraviolet/visible                    |
| VR     | = | Vibrational relaxation                 |
| XPS    | = | X-ray photo-electron spectroscopy      |
| XRD    | = | X-ray diffractometer                   |
| ZnS    | = | Zinc sulphide                          |

---

# List of Figures

|  |    |
|--|----|
| <b>Figure 1.1:</b> Structure of a metallophthalocyanine showing positions for functionalization and of a porphyrin molecule.....           | 2  |
| <b>Figure 1.2:</b> Industrial applications of phthalocyanines (Pcs) .....  | 4  |
| <b>Figure 1.3:</b> Ground state absorption spectra of metallated and unmetallated Pcs .....  | 7  |
| <b>Figure 1.4:</b> Electronic transitions in phthalocyanines.....  | 8  |
| <b>Figure 1.5:</b> Absorption spectra of a typical water soluble aggregated Pcs.....   | 10 |
| <b>Figure 1.6:</b> Industrial and biological applications of quantum dots (QDs).....   | 12 |
| <b>Figure 1.7:</b> Water soluble ligands commonly used in the preparation of quantum dots.....   | 13 |
| <b>Figure 1.8:</b> Structures of core CdTe QDs and coreshell CdTe@ZnS QDs capped with MPA. ....  | 15 |
| <b>Figure 1.9:</b> The fluorescence spectra of quantum dots red-shifting as the size increases. ....                                       | 17 |
| <b>Figure 1.10:</b> Representation of Förster resonance transfer energy (FRET).....  | 19 |
| <b>Figure 1.11:</b> Stimulated emission spectra of AlTSPc in the presence of L-Cys-capped CdTe.....  | 20 |
| <b>Figure 1.12:</b> The Jablonski diagram.....   | 26 |
| <b>Figure 1.13:</b> Triplet lifetime decay curve of ZnSPc dissolved in water.....  | 30 |
| <b>Figure 1.14:</b> Schematic representation of singlet oxygen generation by phthalocyanines at triplet state in the presence of QDs. .... | 32 |

**Figure 2.1:** Schematic diagram of time-correlated single photon counting (TCSPC) setup.....42

**Figure 2.2:** Schematic diagram for a laser flash photolysis setup.....45

**Figure 2.3:** Schematic diagram for the singlet oxygen detection setup using its phosphorescence. ....46

**Figure 3.1:** IR spectra of GSH, CdTe@ZnS-GSH, CdTe@ZnS-GSH-ZnPc(COOH)<sub>8</sub>-linked and ZnPc(COOH)<sub>8</sub> alone. ....56

**Figure 3.2:** FTIR spectra of ZnPc(COOH)<sub>4</sub>, CdTe@ZnS-GSH and CdTe@ZnS-GSH-ZnPc(COOH)<sub>4</sub>-linked.....56

**Figure 3.3:** Raman spectra of CdTe@ZnS-GSH-ZnPc(COOH)<sub>8</sub>, CdTe@ZnS-GSH and ZnPc(COOH)<sub>8</sub>.....58

**Figure 3.4:** XRD spectra of CdTe-TGA, CdTe@ZnS-GSH and CdTe@ZnS-GSH-ZnPc(COOH)<sub>8</sub>-linked. ....60

**Figure 3.5:** XRD spectra of CdTe@ZnS-GSH and CdTe@ZnS-GSH-ZnPc(COOH)<sub>4</sub>-linked. ....61

**Figure 3.6:** TEM images of CdTe@ZnS-GSH QDs and CdTe@ZnS-GSH-ZnPc(COOH)<sub>8</sub>-linked. ....62

**Figure 3.7:** AFM size distribution histograms for CdTe@ZnS-GSH QDs and CdTe@ZnS-GSH-ZnPc(COOH)<sub>8</sub>-linked. ....64

**Figure 3.8:** XPS spectra of CdTe@ZnS-GSH QDs and CdTe@ZnS-GSH-ZnPc(COOH)<sub>8</sub>-linked. ....65

|   |    |
|---|----|
| <b>Figure 3.9:</b> (A) Absorption and fluorescence spectra of CdTe-TGA and CdTe@ZnS-GSH and (B) absorbance spectra of CdTe@ZnS-Zn(COOH) <sub>8</sub> -mixed, CdTe@ZnS-Zn(COOH) <sub>8</sub> -linked and Zn(COOH) <sub>8</sub> .....                                     | 67 |
| <b>Figure 3.10:</b> Absorbance spectra of ZnPc(COOH) <sub>4</sub> , CdTe@ZnS-GSH-ZnPc(COOH) <sub>4</sub> -linked, CdTe@ZnS-GSH-ZnPc(COOH) <sub>4</sub> -mixed and ZnPc(COOH) <sub>4</sub> . ....  | 69 |
| <b>Figure 3.11:</b> Fluorescence decay curves of CdTe@ZnS-GSH and CdTe@ZnS-GSH-ZnPc(COOH) <sub>4</sub> -linked. ....  | 71 |
| <b>Figure 3.12:</b> Triplet lifetime decay curve of CdTe@ZnS-GSH-ZnPc(COOH) <sub>8</sub> -linked in NaOH (pH 11). ....  | 76 |
| <b>Figure 3.13:</b> Singlet oxygen kinetics decay curve of ZnPc(COOH) <sub>8</sub> .....  | 78 |
| <b>Figure 3.14:</b> Absorption spectrum of ZnPc(COOH) <sub>8</sub> and emission spectrum of CdTe@ZnS-GSH. ....  | 79 |
| <b>Figure 3.15:</b> Emission spectra of (A) CdTe@ZnS-GSH, CdTe@ZnS-GSH-ZnPc(COOH) <sub>8</sub> -mixed ZnPc(COOH) <sub>8</sub> and CdTe@ZnS-GSH-ZnPc(COOH) <sub>8</sub> -linked. (B) CdTe-TGA, CdTe-TGA-ZnPc(COOH) <sub>8</sub> -mixed and ZnPc(COOH) <sub>8</sub> ..... | 80 |
| <b>Figure 3.16:</b> Absorption and emission spectra of ZnPc(COOH) <sub>4</sub> and CdTe@ZnS-GSH respectively. ....  | 83 |
| <b>Figure 3.17:</b> Emission spectra for the CdTe@ZnS-GSH QDs, CdTe@ZnS-GSH-ZnPc(COOH) <sub>4</sub> -mixed conjugate, CdTe@ZnS-Zn(COOH) <sub>4</sub> -linked conjugate and ZnPc(COOH) <sub>4</sub> alone. ....  | 84 |

---

# List of Schemes

|  |    |
|--|----|
| <b>Scheme 1.1:</b> Synthesis of metallo-octacarboxy phthalocyanine (MOCPc) ..... | 5  |
| <b>Scheme 1.2:</b> Synthesis of metallotetracarboxy phthalocyanine (MTCPC) ..... | 6  |
| <b>Scheme 3.1:</b> Coordination of ZnPc(COOH) <sub>8</sub> to CdTe@ZnS-GSH. .... | 53 |
| <b>Scheme 3.2:</b> Coordination of ZnPc(COOH) <sub>4</sub> to CdTe@ZnS-GSH. .... | 53 |
| <b>Scheme 3.3:</b> Encapsulation of CdTe into a zinc sulphide shell (ZnS) .....  | 54 |

---

# List of Tables

|  |    |
|--|----|
| <b>Table 1.1:</b> FRET parameters for quantum dot-phthalocyanine conjugates (mixed and linked).....                      | 21 |
| <b>Table 1.2:</b> Phthalocyanine complexes that have been coordinated to QDs. ....                                       | 23 |
| <b>Table 1.3:</b> Carboxylated phthalocyanines and coreshells used in this thesis. ....                                  | 37 |
| <b>Table 3.1:</b> Fluorescence quantum yields and lifetime data of QDs, ZnPc(COOH) <sub>8</sub> and the conjugates. .... | 73 |
| <b>Table 3.2:</b> Fluorescence quantum yield and lifetime data of QDs, ZnPc(COOH) <sub>4</sub> and the conjugates. ....  | 74 |
| <b>Table 3.3:</b> Triplet quantum yields and lifetime values of ZnPc(COOH) <sub>8</sub> and its. ....                    | 77 |



# CHAPTER ONE

## INTRODUCTION

## Introduction

### 1.1 Phthalocyanines

The aim of this thesis is to conjugate CdTe@ZnS coreshell quantum dots capped with glutathione to zinc octacarboxy phthalocyanines ( $\text{ZnPc}(\text{COOH})_8$ ) and zinc tetracarboxy phthalocyanines ( $\text{ZnPc}(\text{COOH})_4$ ).

#### 1.1.1 Structure and general applications of phthalocyanines

Metallophthalocyanines (MPcs) (**Figure 1.1**) are large compounds consisting of four groups of isoindole that are linked by nitrogen atoms [1, 2]. They differ from biologically essential porphyrins (**Figure 1.1**) by an extended  $\pi$ -system characterized by four benzene rings, and the presence of nitrogens at the meso positions [3, 4].

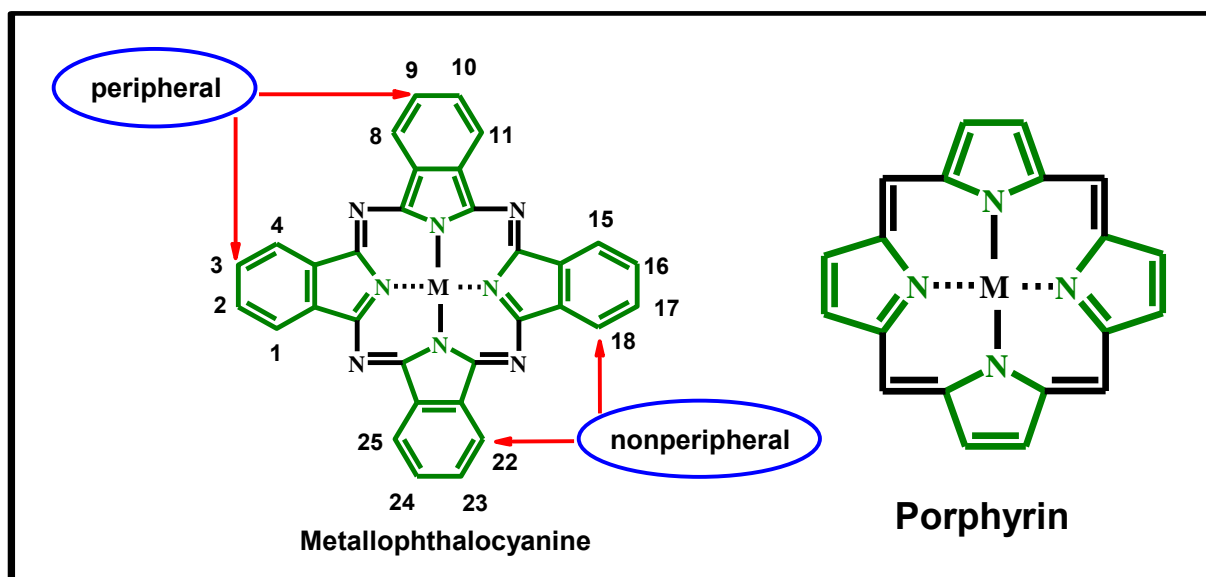


Figure1.1: Structure of a metallophthalocyanine (left) showing positions for functionalization and of a porphyrin molecule (right).

More than 70 metallic or metalloic atoms can be inserted into the phthalocyanine (Pc) ring to form metallophthalocyanines (MPcs) [5]. Zinc phthalocyanines (ZnPcs) are some of the most common phthalocyanines studied. This is due to the closed shell  $Zn^{2+}$  ion which results in high triplet quantum yields and relatively longer triplet lifetimes [6]. The incorporation of different substituents on the peripheral {(2, 3), (9, 10), (16, 17) or (23, 24)} or non-peripheral {(1, 4), (8, 11), (15, 18) or (22, 25)} positions of the ring (**Figure 1.1**) results in Pcs with different properties. Phthalocyanines (Pcs) have found applications in many fields such as jet printing inks [7], nonlinear optics [8-10], photodynamic therapy [11-14], data storage [15], solar cells [16-18], catalysts [19], sensors [20], organic light emitting devices [21], dyes [22], electronics and optoelectronics [23]. **Figure 1.2** shows a summary of the applications of phthalocyanines.

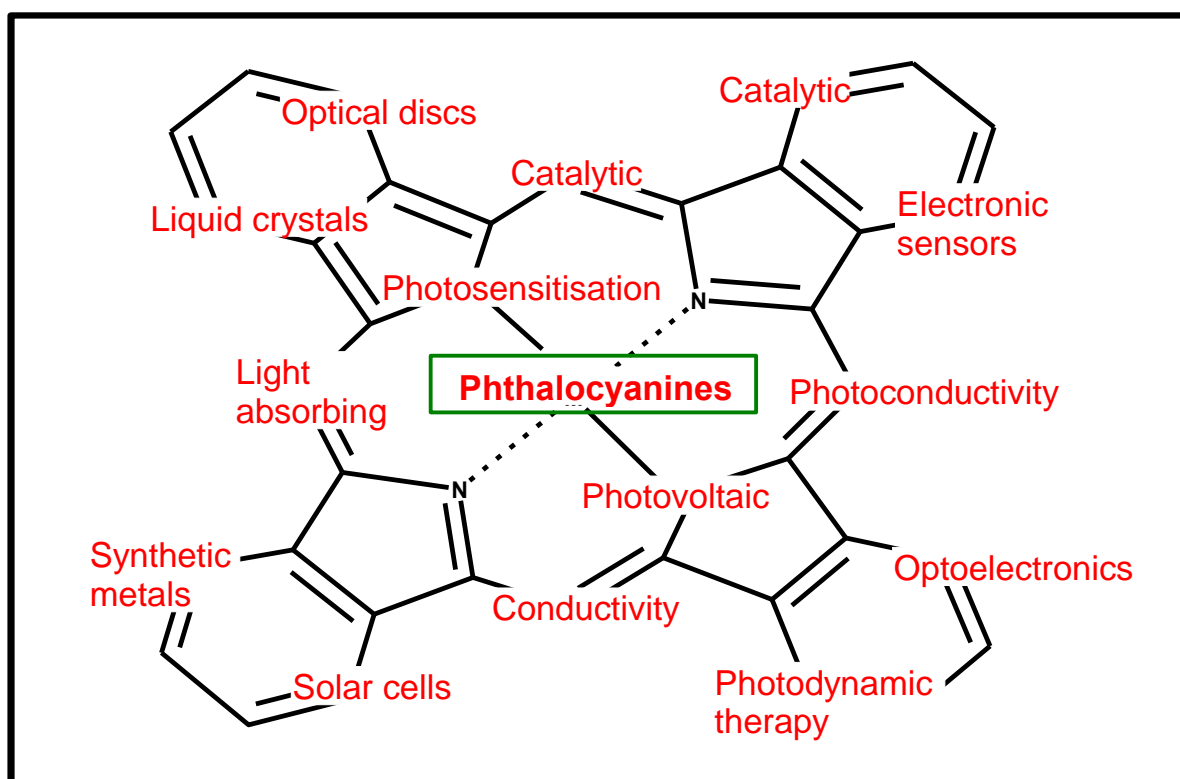
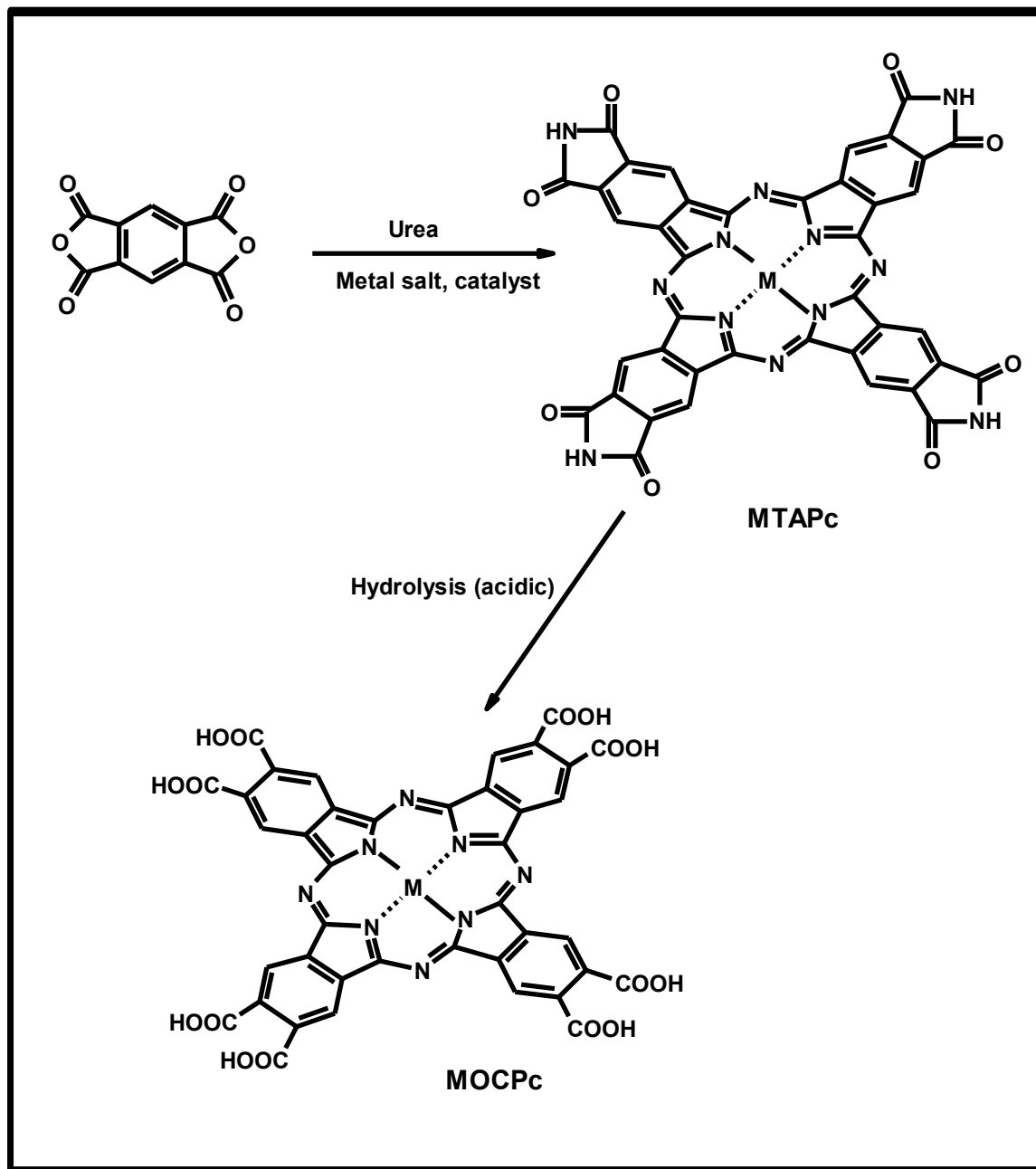


Figure 1.2: Industrial applications of phthalocyanines

### 1.1.2 Synthesis of octa- and tetracarboxy phthalocyanines

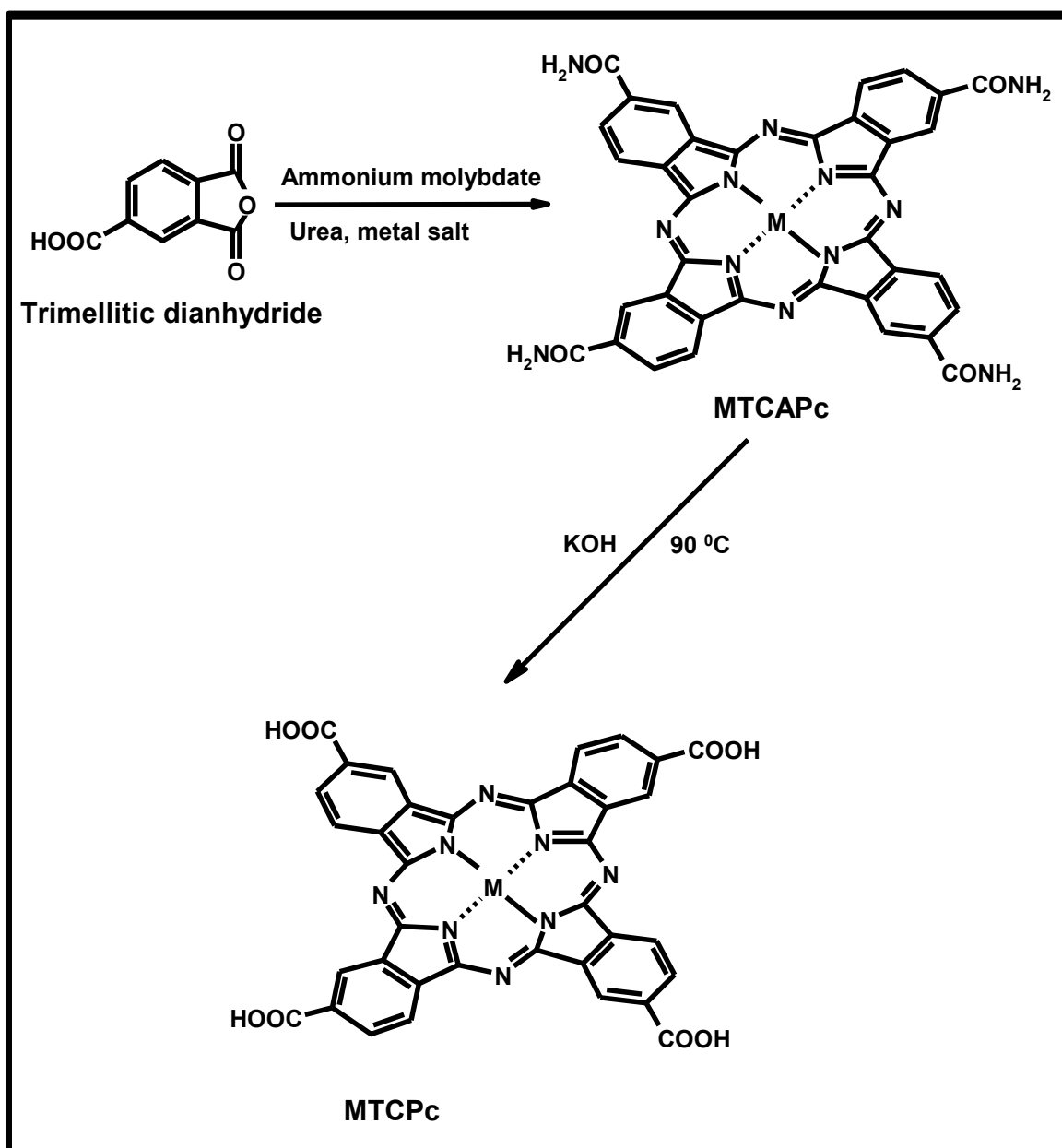
Since only metallo-octacarboxy phthalocyanines (MOCPcs) and metallo-tetracarboxy phthalocyanines (MTCPcs) will be employed in this thesis, their general syntheses are discussed. Both compounds are well known. The synthesis of octacarboxylic acid-substituted metallo-phthalocyanines is generally achieved by reacting pyromellitic dianhydride, urea (as a solvent and a source of nitrogen), 1,8-diazabicyclo[5.4.0]undec-7-ene (DBU) (as a catalyst) and a suitable amount of a metal salt, **Scheme 1.1** [24, 25]. MTCPcs, **Scheme 1.2**, are obtained from tetracarboxamido phthalocyanato metal (II) (MTCAPc) which is an intermediate formed from reacting trimellitic anhydride, urea ammonium molybdate and a metal

salt, followed by treatment with potassium hydroxide at elevated temperature [24, 26-30].



Scheme 1.1: Synthesis of metallo-octacarboxy phthalocyanine (MOCPc) [24, 25].

MTAPc = metallotetra-amido phthalocyanine.



Scheme 1.2: Synthesis of metallo-tetracarboxy phthalocyanine (MTCPc) [24].

MTCAPc = metallo-tetracarboxamido phthalocyanine.

### 1.1.3 Phthalocyanine spectra and effects of aggregation on spectra

Two main distinct absorption bands, arising as a result of  $\pi$ - $\pi^*$  transitions within the delocalized 18- $\pi$  electron system of the ring, characterise Pc spectra, **Figure 1.3**.

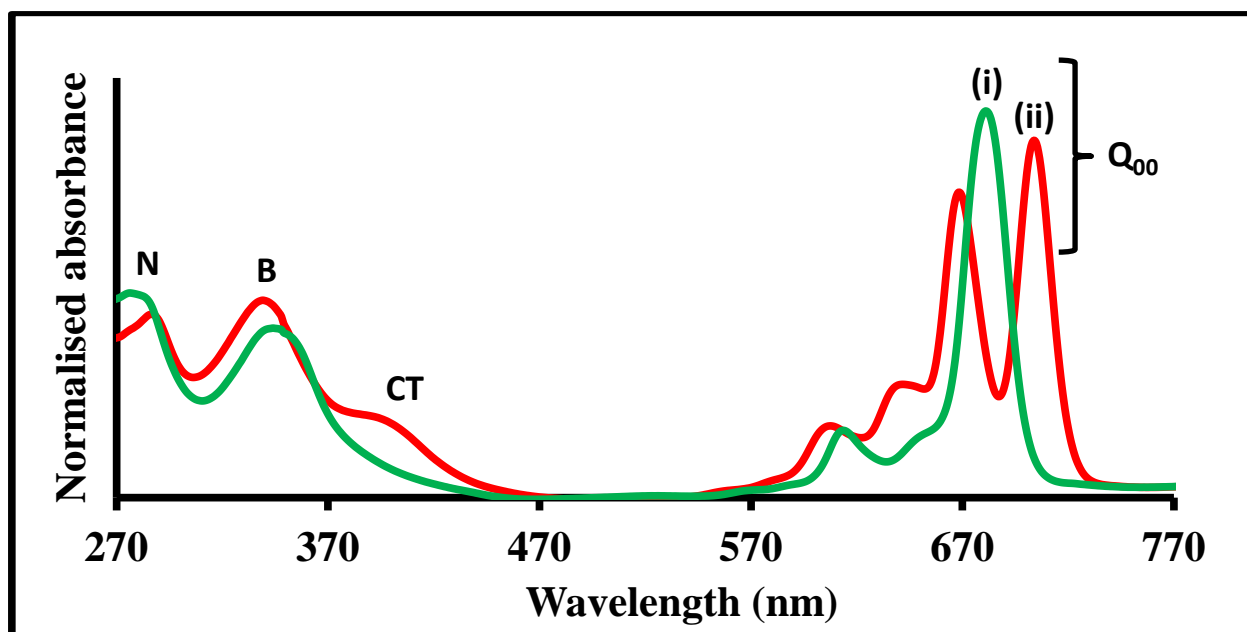


**Figure 1.3:** Ground state absorption spectra of metallated ((i) black) and unmetallated ((ii) red) Pc

The split in the Q-band of the absorption spectrum of the unmetallated phthalocyanine ( $H_2Pc$ ) is caused by  $D_{2h}$  symmetry, and results from presence of the two protons at the core of the ring. For  $H_2Pc$ , the lowest unoccupied molecular orbital (LUMO) is non-degenerate (**Figure 1.4**), giving rise to two allowed electronic transitions. The metallated Pc show an unsplit Q-band due to a  $D_{4h}$  symmetry and a degenerate LUMO. The Q-band ( $Q_{00}$ ) is the highly intense absorption band that is observed towards the near infrared region of the visible spectrum and is due to transitions from the  $a_{1u}$  of the highest occupied molecular orbital (HOMO) to the  $e_g$

of the LUMO, **Figure 1.4**. The B-band (also called Soret band) is the second band of lower intensity observed in the region between 300 to 400 nm and is a superimposition of  $B_1$  and  $B_2$  bands [31, 32]. Three other bands normally observed towards the UV region, the N, L and C bands, are mainly observed when using transparent solvents. The charge transfer (CT) absorption bands, **Figure 1.3**, are observed only when the metal d-orbitals lie within the HOMO-LUMO gap, **Figure 1.4**, and are not common in all phthalocyanine complexes [33, 34]. They can be assigned to either metal to ligand (MLCT) or a ligand to metal charge (LMCT) transfer.

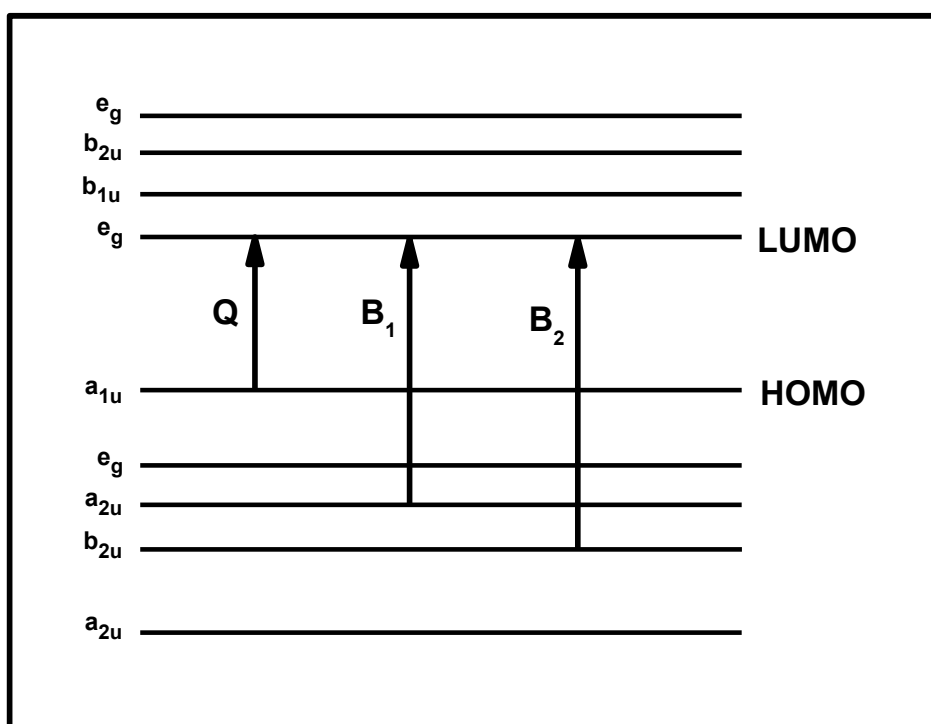


**Figure 1.4:** Electronic transitions in phthalocyanines



There are a number of factors which may affect Pc spectrum. Amongst them is aggregation which is commonly found in water soluble Pcs. Aggregation, referred to as an intrinsic property of this class of compounds, diminishes the efficiency of phthalocyanines as photosensitisers [35]. Aggregation generally occurs as a result of co-planar association of phthalocyanine rings progressing from a monomer to a dimer and higher order aggregates [36-38]. Aggregation can be due to high concentrations of MPc complexes which brings the neighbouring MPc rings in a close proximity. The presence of a surfactant helps collapse the band due to aggregates (dimer) and the band due to the monomer becomes more pronounced [39-43], **Figure 1.5**.

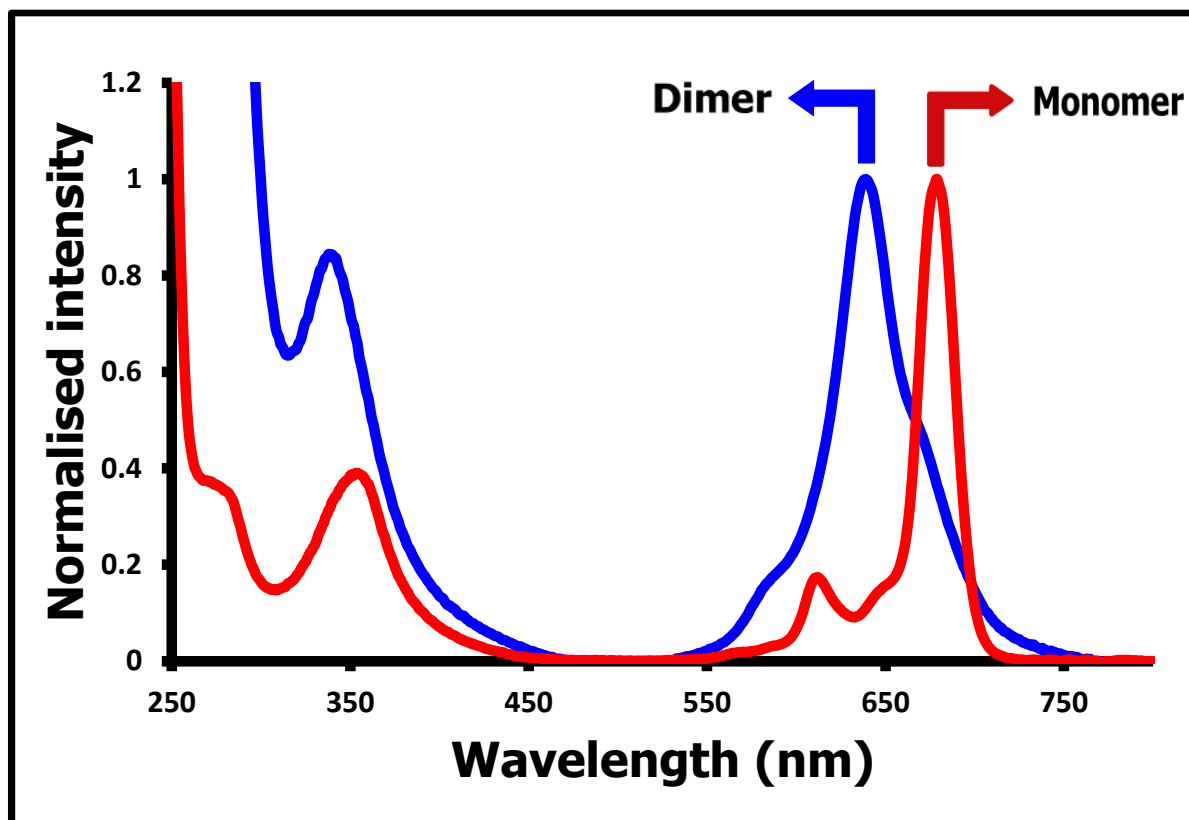


Figure 1.5: Absorption spectra of a typical water soluble aggregated phthalocyanine; (blue line) and in the presence of a surfactant (red line) [unpublished].

Playing a huge role in aggregation of Pc complexes is the nature of a solvent and aggregation is more pronounced in polar solvents such as water than in non-polar solvents [39–43]. The distance between the planar macrocycle rings that carry the  $\pi$  electrons can be increased by peripheral or non-peripheral substitution and axial ligation, thereby making solvation easier and reducing aggregation [44]. Aggregation is less in non-peripheral compared to peripheral substitution.

## 1.2 Quantum dots

### 1.2.1 General applications of quantum dots

Quantum dots (QDs), have become a fundamental tool for fluorescence imaging. The unique and fascinating optical properties are the basic rationale for using QDs. These properties are generally not available for individual molecules or bulk semiconductor solids. QDs have distinctive characteristics such as size-tunable light emission, improved signal brightness, resistance against photobleaching and simultaneous excitation of multiple fluorescence colours, which are not present in conventional organic dyes and fluorescent proteins [45-49].

QDs are applied in many various fields as drug carriers [45, 50], in diagnostics [45], photovoltaic devices [51, 52], microelectronics [53], biomedicine [53, 54], spintronic applications, [52, 55] and on-chip light-emitting sources [56]. **Figure 1.6** summarizes the various applications of quantum dots.

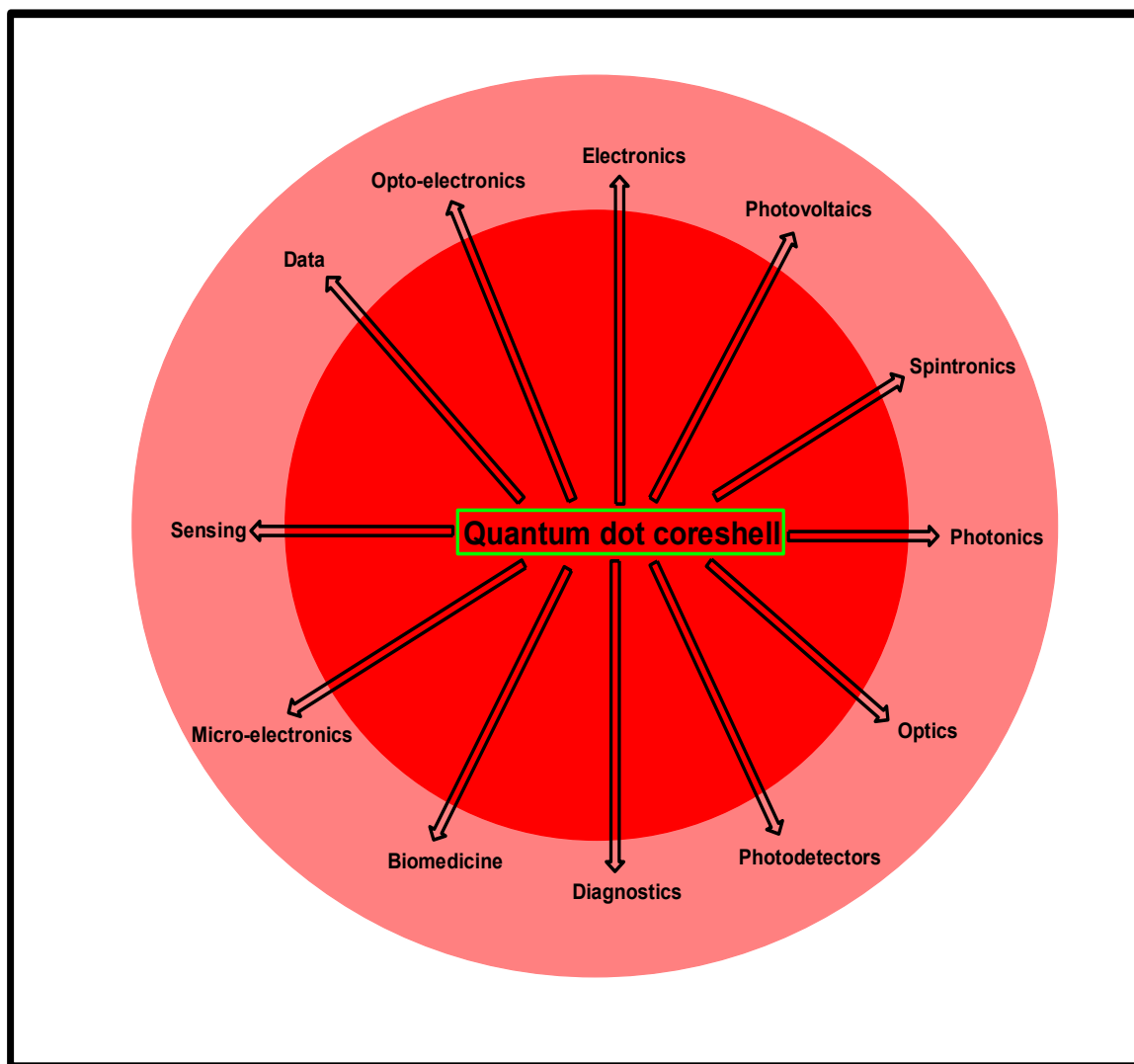


**Figure 1.6: Industrial and biological applications of quantum dots (QDs)**

### 1.2.2 Synthesis of water soluble core and coreshell QDs

The solubility and size are some of the important features of quantum dots that determine their applicability, with the former dependent on the nature of a capping agent while the latter can be controlled in the synthesis. Capping ligands commonly used are shown in **Figure 1.7**.

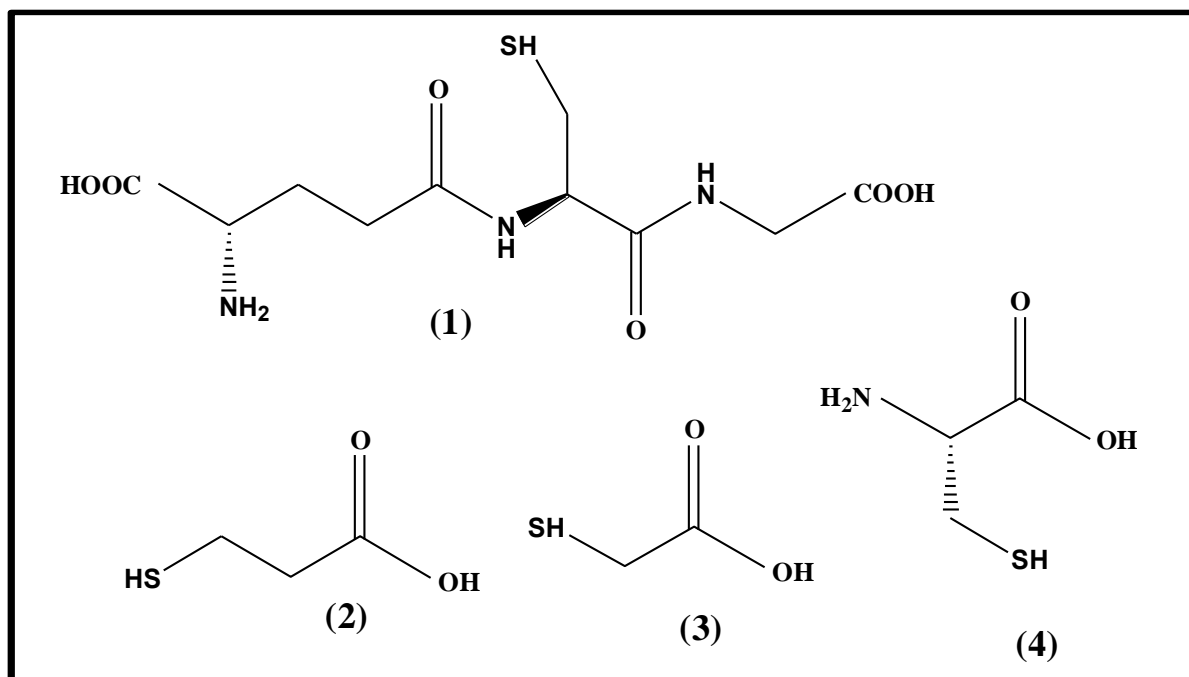


**Figure 1.7: Water soluble ligands commonly used in the preparation of quantum dots. (1) = glutathione (GSH), (2) = 3-mercaptopropionic acid (MPA), (3) = Thioglycolic acid (TGA), (4) = L-cysteine.**

QDs need to be bio-compatible in order to meet the paraphernalia of applications in the field of medicine. They have to be hydrophilic and non-toxic and this can be achieved using ligands such as the ones shown in **Figure 1.7** in the synthesis and modifying the surface by encapsulating core QDs into shells. A lot of procedures have been reported for the synthesis of both the core and the coreshell QDs. For core QDs such as CdTe [57-61], sodium hydrogen telluride and cadmium chloride precursor, whose pH is adjusted by sodium hydroxide, are mixed together under inert atmosphere, followed by heating at elevated temperatures to get core QDs of different sizes. Zinc sulphide (ZnS) is one of the most important shell materials for

coreshell preparation. The passivation of the core QDs may be inefficient if the shell is too thin, resulting in reduced photostability [62]. Coreshell QDs such as CdTe@ZnS capped with GSH may be prepared at higher temperatures from as-prepared CdTe core QDs in the presence of GSH-zinc containing precursor [63], with GSH acting as both a capping agent and a source for sulphur for the formation of a ZnS shell. **Figure 1.8** shows structures of core and coreshell QDs capped with water soluble ligands.

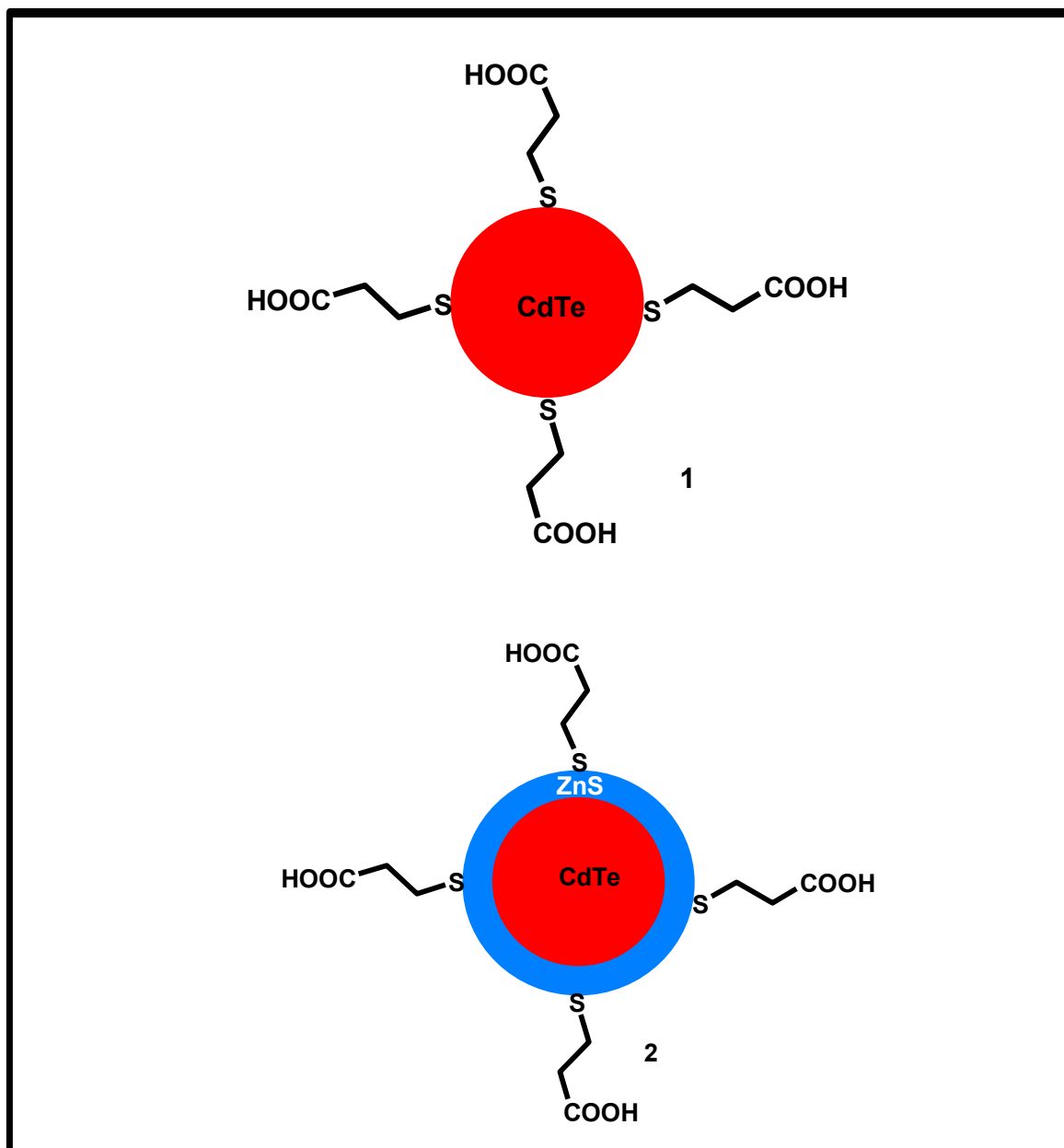


Figure 1.8: Structures of (1) core CdTe QDs and (2) coreshell CdTe@ZnS QDs capped with MPA.

### 1.2.3 Fluorescence behaviour

Colloidal semiconductor QDs exhibit size dependent optical properties and therefore have generated considerable interest over the past three decades. Quantum dots show a broad absorption spectrum, a narrow and symmetric emission spectrum, and a high fluorescence quantum yield [64]. The narrow fluorescence peaks are a result of direct recombination of an electron with a hole and the broad fluorescence band is due to trapped carrier recombination (shallow/ deep trap states) [65]. Comparing core, for example, CdTe with core-shell, e.g., CdTe@ZnS used in this work shows that the shell plays a crucial role on the luminescence properties and the photochemical stability of the QDs. Defect states and dangling bonds at the core surface, which otherwise favour the undesired nonradiative recombination of the photogenerated electron-hole pairs, become saturated by a shell with the fluorescence quantum yield (QY) significantly increasing [64]. After extensive investigations of various parameters such as precursor reagents, temperature, chelating ligands and precursor ratios, synthesis of QDs with high fluorescence QYs (>50%) has become straightforward [66]. The fluorescence spectra of the QDs are red-shifted as the core size increases (**Figure 1.9**).



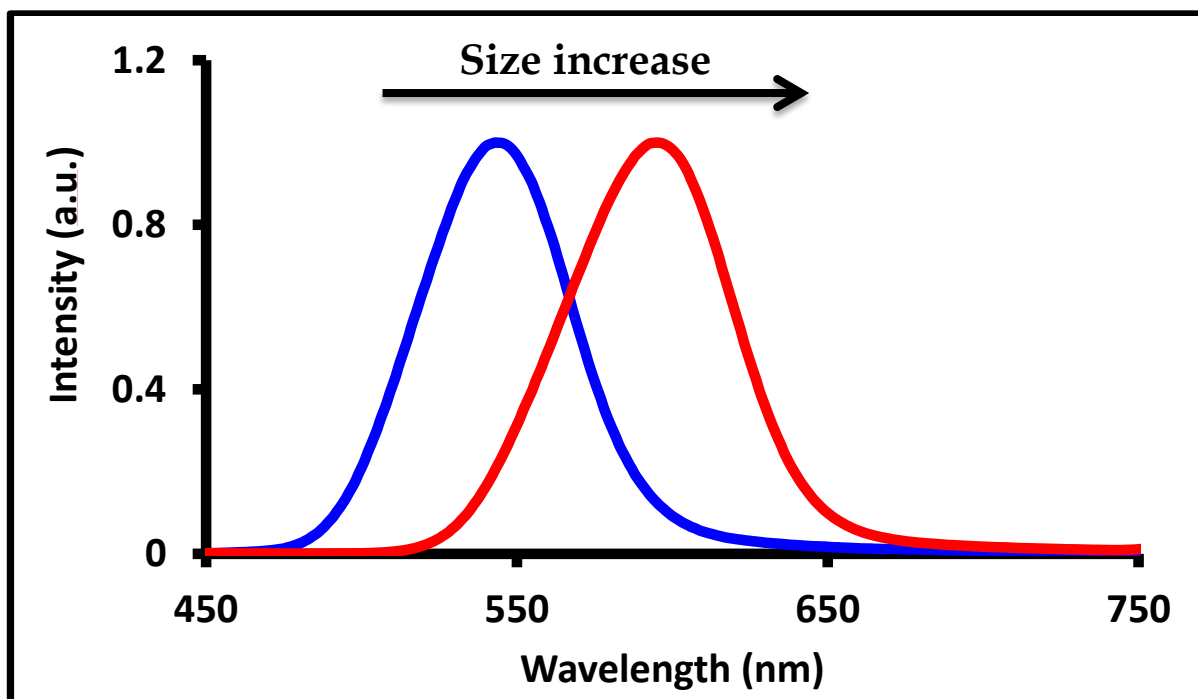


Figure 1.9: The fluorescence spectra of quantum dots red-shifting as the size increases [unpublished].

Emission intensities are dependent on QD concentrations, solvents, and aging effect [67]. The storage of samples of quantum dot results in several events: (i) “blue” spectral shift of the photoluminescence (PL) band position, (ii) decrease of the PL intensity and (iii) increase in the full width at half maximum (FWHM) of the fluorescence band. All three features can be apportioned to “aging” mechanism [68]. Colour of stored solutions of quantum dots can explain the mechanism of aging. Literature results indicate that greenish-yellow coloured solution did not show any change in colour up to a certain number of hours of aging at room temperature. Only on keeping the QDs for about one week at room temperature, did their colour slowly change to light orange, and then to orange. This is probably due to slow aggregation of the initially produced nanoparticles, as monitored by UV-Vis spectroscopy [69].

The effects of pH and temperature on QDs spectroscopic characteristics need to be paid attention to. Highly fluorescent core may be achieved in a pH range of 9–12 [70] while the brightest coreshells are obtained at lower ~pH 8 (slightly alkaline) [63].

### 1.3 Förster resonance energy transfer

Quantum dots in their “dark states” are capable of transferring energy through a mechanism termed as triplet energy transfer (TET) to molecular oxygen, leading to the generation of reactive oxygen species (ROS). At triplet state, they can generate singlet oxygen ( $^1\text{O}_2$ ), with yields which have been reported to be as low as 5% for CdSe [71] and 28% for coreshells [72]. Alternatively, quantum dots can act as cofactors to promote the effect of conventional photosensitizing agents used in photodynamic therapy (PDT) via Förster resonance energy transfer (FRET), **Figure 1.10**. The advantage of combining quantum dots with PDT photosensitizers is that the use of an excitation wavelength where the photosensitizer alone does not absorb is enabled. FRET from CdSe QD to Pc photosensitiser was first demonstrated by Samia et al. [73].

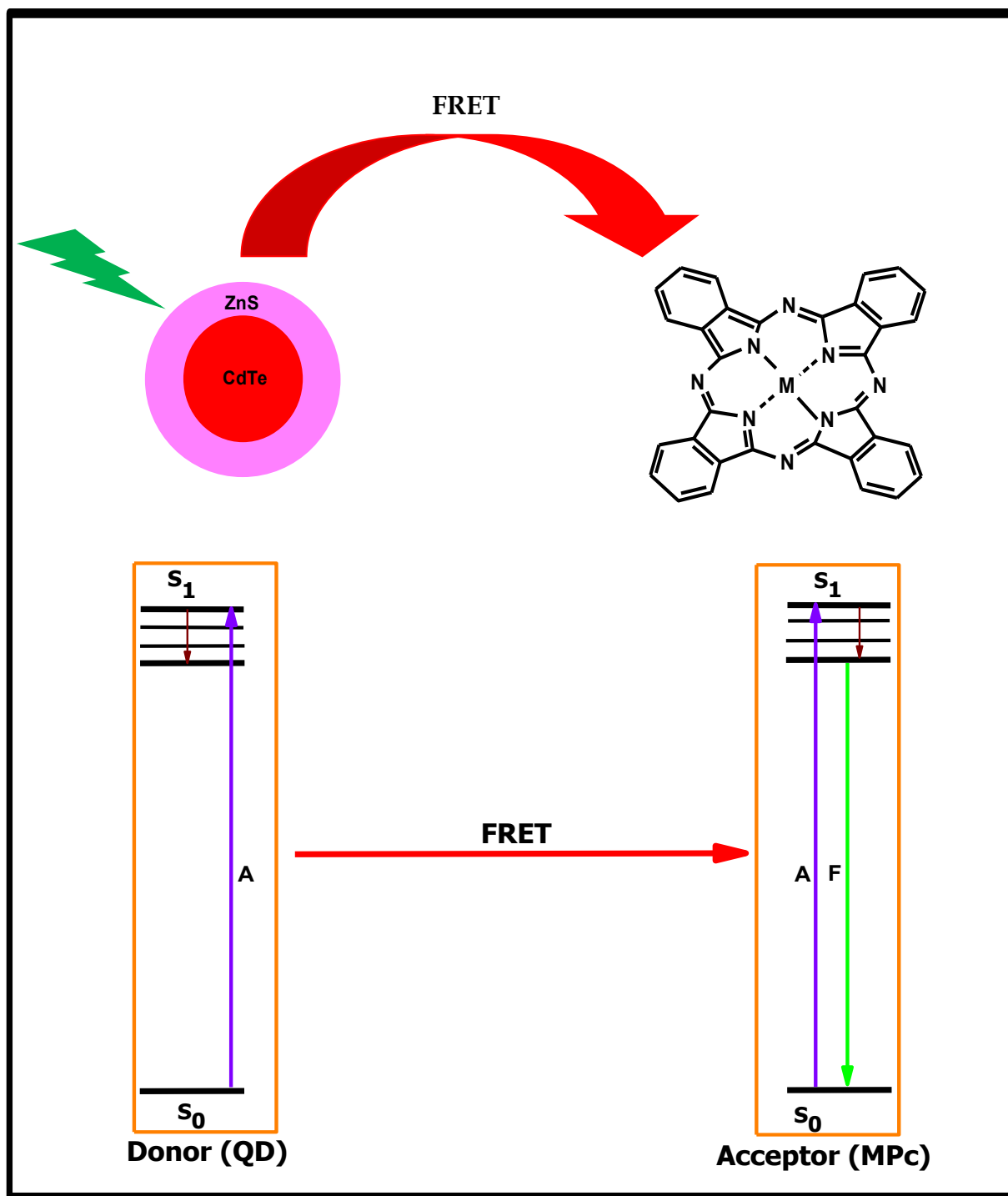
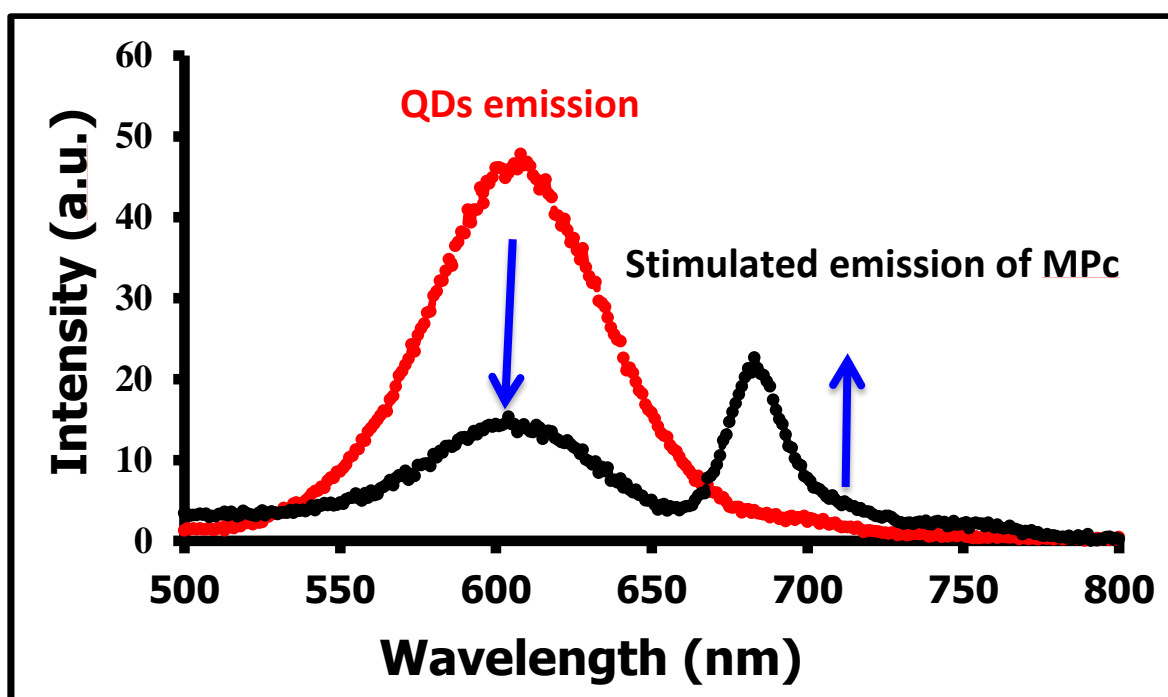


Figure 1.10: Representation of förster resonance transfer energy (FRET).

Energy transfer from QDs to different phthalocyanine photosensitizers (where the two components are mixed or linked together) has been demonstrated in a number of studies [73-87] through FRET. **Figure 1.11** shows the emission spectrum of aluminium tetrasulphonated phthalocyanine (AITSPc) indirectly stimulated by L-cysteine-capped CdTe QDs.



**Figure 1.11:** Stimulated emission spectra of AITSPc in the presence of L-Cys-capped CdTe [75].

FRET parameters have been reported mainly in mixtures [74-78]. Linking Pc to QDs is preferred since controlled conjugates are formed. Only a few studies have been reported for Pc linked to QDs, **Table 1.1**.

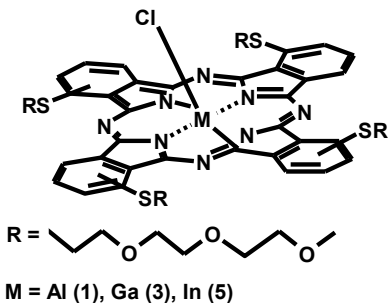
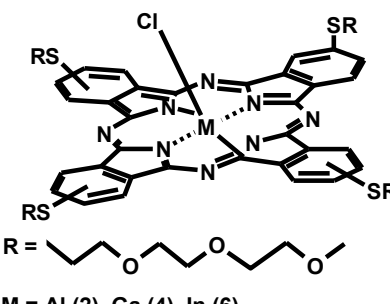
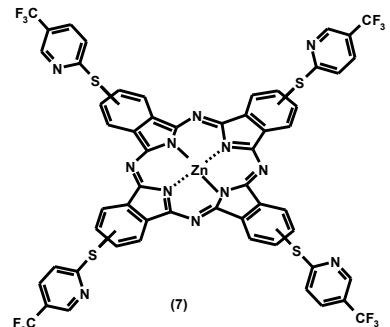
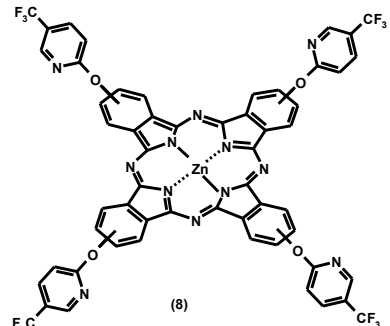
**Table 1.1: FRET parameters for quantum dot-phthalocyanine conjugates (mixed and linked). Structures for 1 - 9 are shown in Table 1.2.**

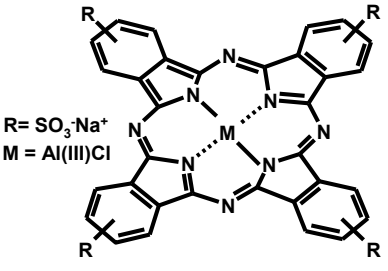
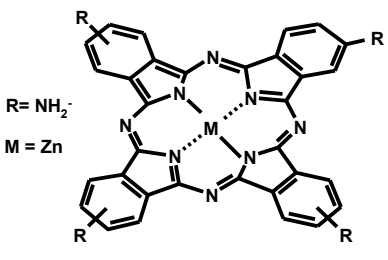
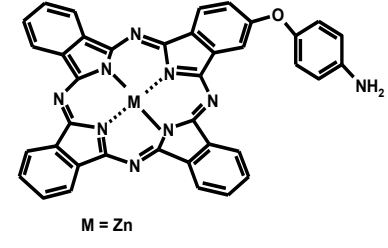
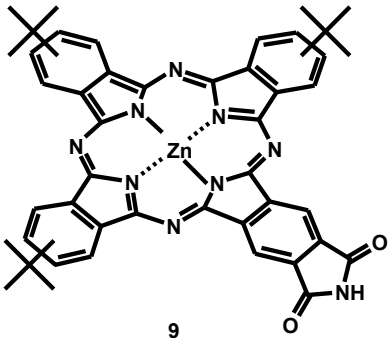
| Pc derivatives                   | QD capping | J<br>( $10^{-14}\text{cm}^6$ ) | $R_0$<br>(Å) | r<br>(Å) | Eff<br>(%) | Ref. |
|----------------------------------|------------|--------------------------------|--------------|----------|------------|------|
| Al (1) (mixed)                   | TGA        | 6.60                           | 54.22        | 54.38    | 0.49       | [74] |
| Al (2) (mixed)                   | TGA        | 0.106                          | 42.77        | 35.29    | 0.76       | [74] |
| Ga (3) (mixed)                   | TGA        | 4.96                           | 37.43        | 32.75    | 0.69       | [74] |
| Ga (4) (mixed)                   | TGA        | 1.13                           | 42.98        | 43.85    | 0.47       | [74] |
| In (5) (mixed)                   | TGA        | 4.68                           | 37.06        | 20.76    | 0.97       | [74] |
| In (6) (mixed)                   | TGA        | 0.107                          | 42.59        | 26.07    | 0.95       | [74] |
| ZnOCPc (mixed)                   | Cys        | 79.7                           | 62.56        | 60.91    | 0.54       | [75] |
| (OH)AlOCPc (mixed)               | Cys        | 79.5                           | 62.54        | 52.99    | 0.73       | [75] |
| (OH) <sub>2</sub> SiOCPc (mixed) | Cys        | 57.9                           | 59.31        | 60.91    | 0.80       | [75] |
| (OH) <sub>2</sub> GeOCPc (mixed) | Cys        | 51.3                           | 58.14        | 47.98    | 0.76       | [75] |
| ZnTSPc-mixed                     | TGA        | 1.80                           | 57.0         | 67.0     | 0.30       | [76] |
| ZnTCPc (mixed)                   | TGA        | 0.72                           | 49.0         | 63.0     | 0.20       | [76] |
| TtfmMPyZnPc (mixed) (7)          | MPA        | 107                            | 51.59        | 58.95    | 0.31       | [77] |
| TtfmPyZnPc (mixed) (8)           | MPA        | 117                            | 52.15        | 53.56    | 0.45       | [77] |
| ZnTAPc (mixed)                   | MPA        | 3.43                           | 30.8         | 25.9     | 0.74       | [84] |
| ZnTAPc (linked)                  | MPA        | 3.43                           | 30.8         | 20.0     | 0.93       | [84] |
| ZnTAPc (mixed)                   | TGA        | 2.18                           | 24.8         | 22.0     | 0.68       | [84] |
| ZnTAPc (linked)                  | TGA        | 2.18                           | 24.8         | 21.6     | 0.70       | [84] |
| MAPPc (mixed)                    | MPA        | 1.36                           | 46.52        | 42.57    | 0.63       | [86] |
| MAPPc (linked)                   | MPA        | 1.09                           | 44.38        | 29.54    | 0.92       | [86] |
| MAPPc (mixed)                    | TGA        | 1.24                           | 45.71        | 60.26    | 0.16       | [86] |
| MAPPc (linked)                   | TGA        | 0.84                           | 42.53        | 26.04    | 0.95       | [86] |
| MAPPc (mixed)                    | L-Cys      | 0.78                           | 26.46        | 34.46    | 0.17       | [86] |
| MAPPc (linked)                   | L-Cys      | 1.30                           | 29.37        | 20.36    | 0.90       | [86] |
| ZnttbIPc (mixed) (9)             | MPA        | 64                             | 44.68        | 44.08    | 0.52       | [87] |
| ZnttbIPc (linked)                | MPA        | 64                             | 44.68        | 34.70    | 0.82       | [87] |

MAPPc = 4-Monoaminophenoxy zinc phthalocyanine, TAPc = tetraamino Phthalocyanine, OCPc = octacarboxy phthalocyanine, TSPc = tetrasulfo phthalocyanine, TCPc = tetracarboxy phthalocyanine, ZnttbIPc = Tris[9(10),16(17),23(24)-tertbutyl] imidophthalocyaninato] zinc (II), TtfmMPyZnPc = 4-(Tetrakis-5-(trifluoromethyl)-2-mercaptopyridinephthalocyaninato]-phthalonitrile.  $J$  = Förster overlap integral,  $R_0$  = Förster distance,  $r$  = Centre-to-centre separation distance between the donor and the acceptor,  $Eff$  = efficiency.

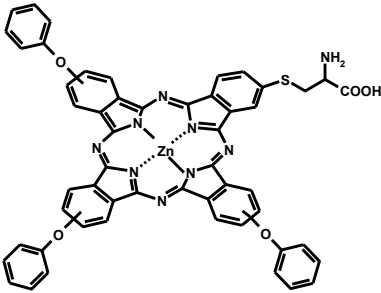
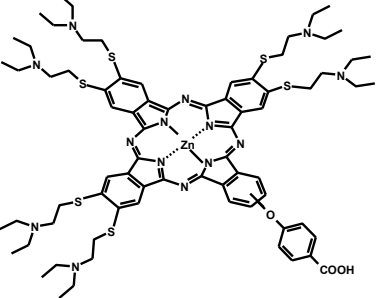
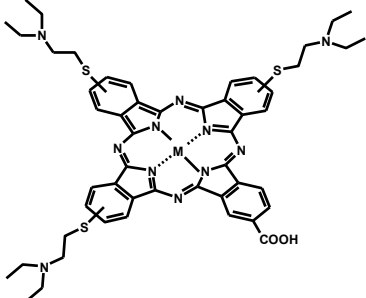
Various Pc complexes that have been coordinated to QDs via covalent linking or mixing are shown in **Table 1.2** [74, 77, 78, 80, 84, 86-88]. Data presented in **Table 1.1** show FRET parameters reported between water soluble QD core and phthalocyanines (hydrophilic and hydrophobic). For phthalocyanines that are hydrophobic, solvent mixtures were employed to accommodate both the quantum dots and the phthalocyanines. This thesis reports for the first time the formation of conjugates in water only. In this way, solvent mixtures were completely avoided, while at the same time, studying the mixed and linked coreshell-phthalocyanine conjugates.

Table 1.2: Phthalocyanine complexes that have been coordinated to QDs.

| Complex   | Abbreviation               | Ref. |
|---|----------------------------|------|
|  <p>R = <chem>CCCCOCCOCCO</chem><br/>M = Al (1), Ga (3), In (5)</p>  | Al (1)<br>Ga (3)<br>In (5) | [74] |
|  <p>R = <chem>CCCCOCCOCCO</chem><br/>M = Al (2), Ga (4), In (6)</p> | Al (2)<br>Ga (4)<br>In (6) | [74] |
|  <p>(7)</p>  | TtfmMPyZnPc                | [77] |
|  <p>(8)</p>  | TtfmPyZnPc                 | [77] |

|   |          |          |
|---|----------|----------|
|  <p>R = SO<sub>3</sub>Na<sup>+</sup><br/>M = Al(III)Cl</p> | AlTSPc   | [78, 80] |
|  <p>R = NH<sub>2</sub><br/>M = Zn</p>                      | ZnTAPc   | [84]     |
|  <p>M = Zn</p>  | MAPPc    | [86]     |
|  <p>9</p>  | ZnttbIPc | [87]     |



|  |   |      |
|--|---|------|
|   | ZnMCsPc                                     | [88] |
|   | ZnMPCPc                                     | [88] |
|  <p>M = (OH)<sub>2</sub>Ge<br/>OTi<br/>(ac)<sub>2</sub>Sn</p> | GeMCPc,<br>TiMCPc,<br>SnMCPc {ac = acetate} | [88] |

## 1.4 Photophysical parameters

Figure 1.12 shows Jablonski diagram illustrating the processes that occur during the absorption of light, leading to the generation of singlet oxygen [89].

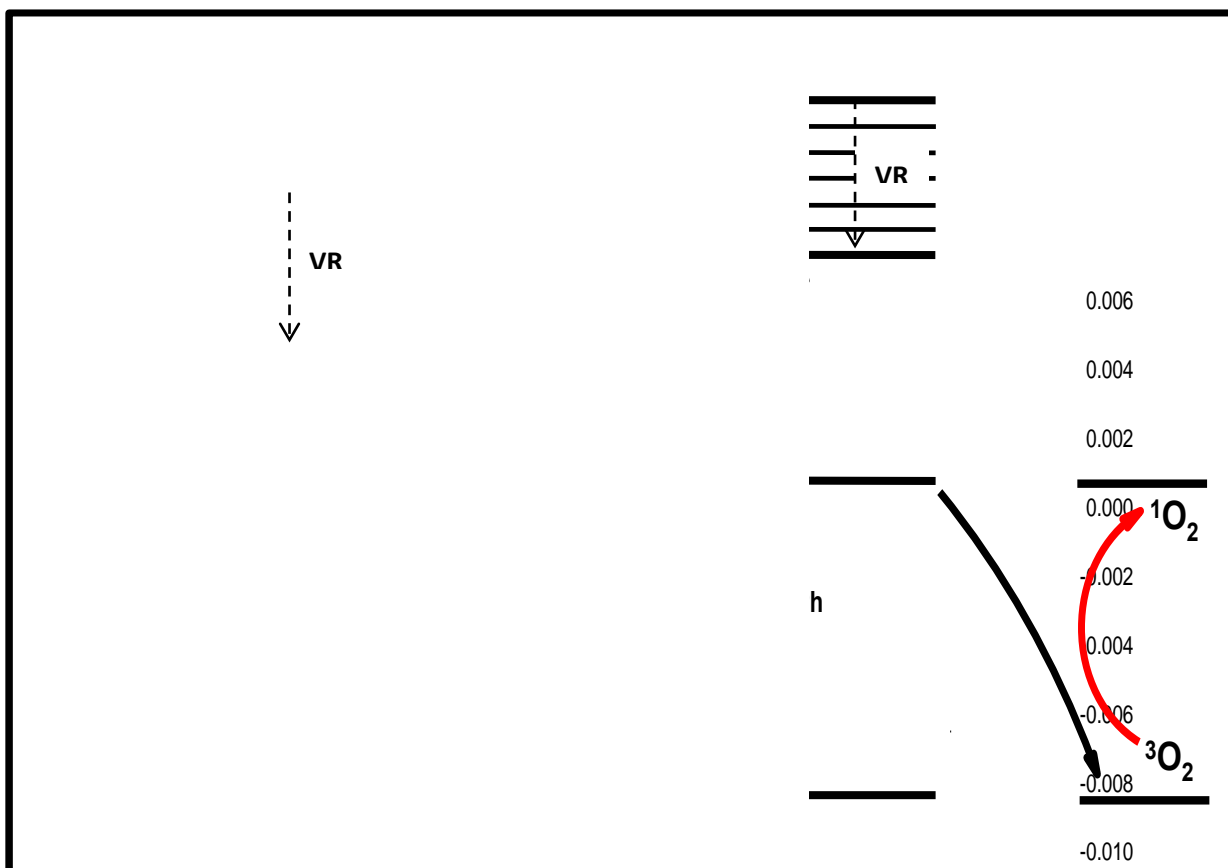


Figure 1.12: The Jablonski diagram displaying transitions of a molecule from its lower energy ground state to its higher energy excited state following absorption with light; A = absorption, VR = vibrational relaxation, ISC = intersystem crossing, F = fluorescence, IC = internal conversion, Ph = phosphorescence,  $S_0$  = singlet ground state,  $S_1$  = singlet excited state and  $T_1$  = 1st excited triplet excited state,  $T_2$  = second excited triplet state.

The processes taking place during excitation of a photosensitiser can be explained as follows: When a molecule gains energy through absorption (**A**), it is excited from its lower energy singlet ground state ( $S_0$ ) to the higher vibronic energy level of the first singlet excited state ( $S_1$ ). The molecule will then lose some energy, relaxing from the higher vibronic level through some vibrational relaxation processes (**VR**) to a lower vibronic energy level. From the lowest vibronic level of ( $S_1$ ), the molecule can relax to the ground state ( $S_0$ ) through (i) fluorescence (**F**), or (ii) internal conversion (**IC**). Another possibility is that the molecule can undergo intersystem crossing (**ISC**) to the first excited triplet state energy level ( $T_1$ ). According to the selection rules, the change of multiplicity in ISC is spin-forbidden yet it still occurs to some extent as a result of the spin-orbit coupling (**SOC**). At the triplet state the molecules can still lose energy through emitted light in the form of phosphorescence (**Ph**). The molecule can also give its energy to the ground state molecular oxygen to generate singlet oxygen through photosensitization, **Figure 1.12**. The ideal photosensitiser should meet at least the following requirements: minimum photobleaching [90], a high extinction coefficient in the far-red or near infrared (NIR) spectral region and a high yield of the long lived triplet excited state [91]. Paramagnetic compounds or large atoms (heavy atoms) such as indium [92, 93] and lead enhance the intersystem crossing (**ISC**).

### 1.4.1 Fluorescence quantum yields and lifetimes

Fluorescence quantum yield ( $\Phi_F$ ) is the number of emitted photons relative to the number of absorbed photons. The emission rates of fluorescence are typically  $10^8 \text{ s}^{-1}$ , so that a typical fluorescence lifetime is near 10 ns ( $10 \times 10^{-9} \text{ s}$ ) [89]. Fluorescence lifetime ( $\tau_F$ ) is the average time an excited fluorophore spends in the excited state

before it releases energy and decays to its basic ground state [89, 94]. Fluorescence lifetime may be determined by a time correlated single photon counting [95] and this is employed in this work.

Fluorescence quantum yield ( $\Phi_F$ ) may be determined by comparison with a standard using Eq. 1.1 [96]:

$$\Phi_F = \Phi_{F_{std}} \frac{F \cdot A_{std} n^2}{F_{std} \cdot A \cdot n_{std}^2} \quad 1.1$$

where  $F$  and  $F_{Std}$  are the areas under the fluorescence curves for sample and standard, respectively.  $A$  and  $A_{Std}$  are the absorbances of the sample and reference at the excitation wavelength respectively, while  $n$  and  $n_{Std}$  are the refractive indices of solvents in which the sample and reference were dissolved, respectively. The fluorescence quantum yields of QDs in the conjugates may be obtained using Eqs. 1.2 when mixed  $\Phi_{F(QD)}^{Mix}$  with Pcs or when linked  $\Phi_{F(QD)}^{linked}$  to Pcs:

$$\Phi_{F(QD)}^{Mix} = \Phi_{F(QD)} \frac{F_{QD}^{Mix}}{F_{QD}} \quad 1.2a$$

$$\Phi_{F(QD)}^{linked} = \Phi_{F(QD)} \frac{F_{QD}^{linked}}{F_{QD}} \quad 1.2b$$

where  $\Phi_{F(QD)}$  is the fluorescence quantum yield of the QDs alone and is used as standard,  $F_{QD}^{Mix}$  (or  $F_{QD}^{linked}$ ) is the fluorescence intensity of QDs, in the mixture (or

linked) with Pc when excited at the excitation wavelength of the QDs and  $F_{\text{QD}}$  is the fluorescence intensity of the QD alone.

### 1.4.2 Triplet quantum yields and lifetimes

A technique called laser flash photolysis is used to determine the triplet lifetime and the change in absorbance in the triplet state, which is directly related to the triplet quantum yield [97]. The efficiency of the triplet state is determined and quantified by the use of the triplet quantum yield ( $\Phi_{\text{T}}$ ). The triplet absorption is  $\sim 500$  nm for phthalocyanines, which is far from the ground singlet state absorption making it possible to conduct these measurements. The triplet state parameters include the triplet quantum yield ( $\Phi_{\text{T}}$ ), and the triplet lifetime ( $\tau_{\text{T}}$ ). Either the triplet absorption or singlet depletion method determines the triplet quantum yields. In this work the triplet absorption method was employed hence it is discussed. **Figure 1.13** shows triplet lifetime decay curve of a water soluble zinc sulphonated phthalocyanine (ZnSPc).

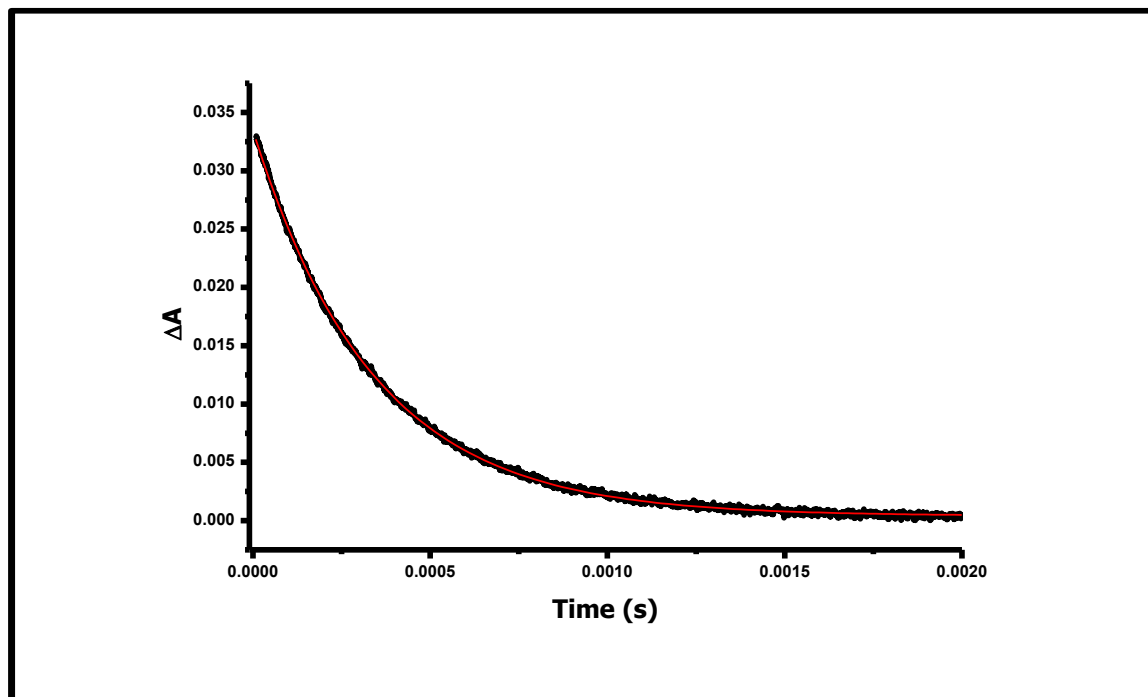


Figure 1.13: Triplet lifetime decay curve of ZnSPc dissolved in water [unpublished].

A comparative method [98] using standard may be employed for the calculations of  $\Phi_T$ , Eq. 1.3

$$\Phi_T = \Phi_T^{Std} \frac{\Delta A_T \cdot \varepsilon_T^{Std}}{\Delta A_T^{Std} \cdot \varepsilon_T} \quad 1.3$$

where  $\Delta A_T$  and  $\Delta A_T^{Std}$  are the changes in the triplet state absorbances of the Pc derivative and the standard respectively;  $\varepsilon_T$  and  $\varepsilon_T^{Std}$ , the triplet state molar extinction coefficients for the Pc derivative and the standard respectively;  $\Phi_T^{Std}$ , the triplet quantum yield for the standard.  $\varepsilon_T$  and  $\varepsilon_T^{Std}$  are determined from the molar extinction coefficients of their respective ground singlet state ( $\varepsilon_S$  and  $\varepsilon_S^{Std}$ ), the

changes in absorbances of the ground singlet states ( $\Delta A_S$  and  $\Delta A_S^{Std}$ ) and changes in the triplet state absorptions, ( $\Delta A_T$  and  $\Delta A_T^{Std}$ ) according to Eqs. 1.4a and 1.4b:

$$\varepsilon_T = \varepsilon_S \frac{\Delta A_T}{\Delta A_S} \quad 1.4a$$

$$\varepsilon_T^{Std} = \varepsilon_S^{Std} \frac{\Delta A_T^{Std}}{\Delta A_S^{Std}} \quad 1.4b$$

### 1.4.3 Singlet oxygen quantum yield

Photodynamic therapy (PDT) is a cancer treatment based on light-induced, local production of a reactive oxygen species, such as singlet oxygen, which destroys the surrounding tissue [91, 99-105]. Conjugating Pcs to QDs results in the production of  $^1O_2$  via the FRET route, **Figure 1.14**. In PDT, Pcs and QDs can be applied separately or in combination. It is essential to determine the singlet oxygen quantum yield ( $\Phi_\Delta$ ) for Pcs or their conjugates with QDs. This thesis presents  $\Phi_\Delta$  of carboxyl phthalocyanines alone and in the presence of QDs.

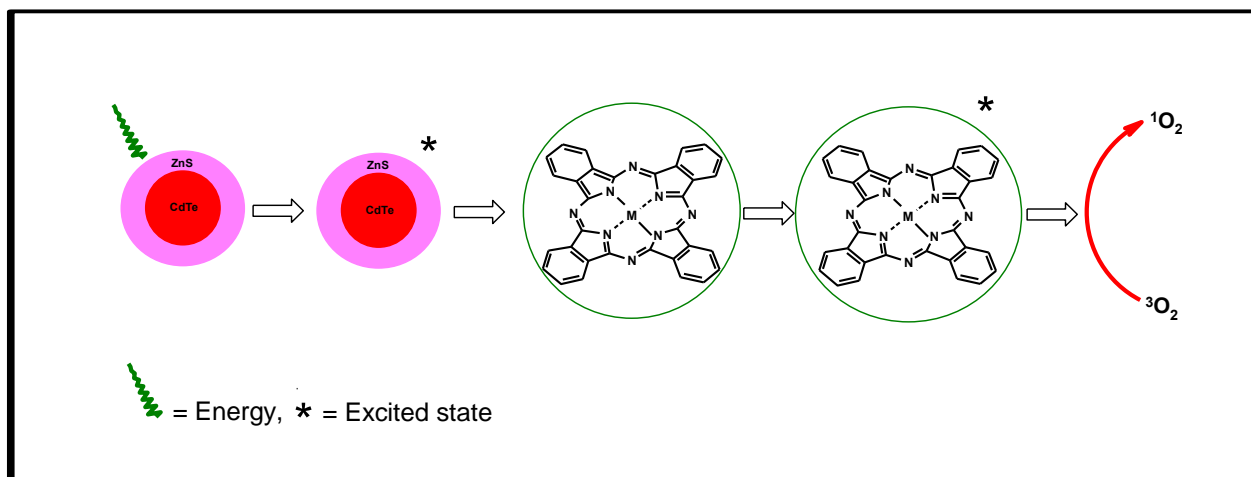


**Figure 1.14:** Schematic representation of singlet oxygen generation by phthalocyanines at triplet state in the presence of QDs.

There are different experimental procedures employed in the determination of  $\Phi_{\Delta}$ . The singlet-oxygen quantum yields for the MPc complexes may be conveniently determined using a singlet-oxygen quencher such as 1,3-diphenylisobenzofuran (DPBF) in organic solvents or by using the singlet-oxygen luminescence method (SOLM) [106].

Employing the comparative method, the singlet oxygen quantum yield of the phthalocyanine can be determined according to Eq. 1.5 [107-109]:

$$\Phi_{\Delta} = \Phi_{\Delta}^{Std} \frac{WI_{Abs}^{Std}}{W^{Std}I_{Abs}} \quad 1.5$$

where  $\Phi_{\Delta}^{std}$  is the singlet oxygen quantum yield for the standard,  $W$  and  $W^{Std}$  are the DPBF photobleaching rates in the presence of MPc derivatives under examination



and the standard, respectively.  $I_{Abs}^{Std}$  and  $I_{Abs}$  are the rates of light absorption by the MPc derivative and standard, respectively.

For the SOLM, the dynamic course of  $^1O_2$  concentration can be clearly recorded, following Eq. 1.6 as described theoretically in the literature [110]:

$$I(t) = B \frac{\tau_D}{\tau_T - \tau_D} [e^{-t/\tau_T} - e^{-t/\tau_D}] \quad 1.6$$

where  $I(t)$  is the phosphorescence intensity of singlet oxygen ( $O_2(^1\Delta_g)$ ) at time  $t$ ,  $\tau_D$  is the lifetime of  $O_2(^1\Delta_g)$  phosphorescence decay,  $\tau_T$  is the triplet state lifetime of standard or sample and  $B$  is a coefficient involved in sensitizer concentration and singlet oxygen quantum yield. The singlet oxygen quantum yield,  $\Phi_\Delta$ , of the phthalocyanine is then determined by a comparative method using Eq. 1.7 [110]:

$$\Phi_\Delta = \Phi_\Delta^{Std} \cdot \frac{B \cdot OD^{Std}}{B^{Std} \cdot OD} \quad 1.7$$

where  $\Phi_\Delta^{Std}$  is the singlet oxygen quantum yield for the standard usually unsubstituted zinc phthalocyanine.  $B$  and  $B^{Std}$  refer to coefficient involved in sensitizer concentration and  $^1O_2$  quantum yield for the sample and standard respectively and;  $OD$  and  $OD^{Std}$  are the optical density of the sample and standard correspondingly at the excitation wavelength.

### 1.4.4 FRET parameters

Föster resonance energy transfer (FRET) efficiency ( $Eff$ ) may be determined experimentally from the fluorescence quantum yields of the donor in the absence ( $\Phi_{F(QD)}$ ) and presence ( $\Phi_{F(QD)}^{Mix}$  or  $\Phi_{F(QD)}^{linked}$ ) of the acceptor using Eq. 1.8 [111, 112]:

$$Eff = 1 - \frac{(\Phi_{F(QD)}^{Mix})}{(\Phi_{F(QD)})} \quad 1.8$$

or using weighted fluorescence lifetimes, employing Eq. 1.9 [89, 113]:

$$Eff = 1 - \frac{\tau_{DA}}{\tau_D} \quad 1.9$$

where  $\tau_{DA}$  and  $\tau_D$  express the average fluorescence lifetimes of the donor QDs in the presence and absence of the acceptor respectively. FRET efficiency ( $Eff$ ) is related to  $r$  ( $\text{\AA}$ ) by Eq. 1.10 [89]

$$Eff = \frac{R_0^6}{R_0^6 + r^6} \quad 1.10$$

where  $r$  expresses the centre-to-centre separation distance (in  $\text{\AA}$ ) between donor and acceptor,  $R_0$  (the Förster distance,  $\text{\AA}$ ) is the critical distance between the donor and the acceptor molecules at which the efficiency of energy transfer is 50% and depends on the quantum yield of the donor Eq. 1.11 [89, 113]:

$$R_0^6 = 8.8 \times 10^{23} \kappa^2 n^{-4} \Phi_{F(QD)} J \quad 1.11$$

where  $\kappa$  is the dipole orientation factor,  $n$  the refractive index of the medium,  $\Phi_F$  the fluorescence quantum yield of the donor (QD), and  $J$  is the Förster overlap integral, given by Eq. 1.12:

$$J = \int f_{QD}(\lambda) \varepsilon_{ZnPc}(\lambda) \lambda^4 d\lambda \quad 1.12$$

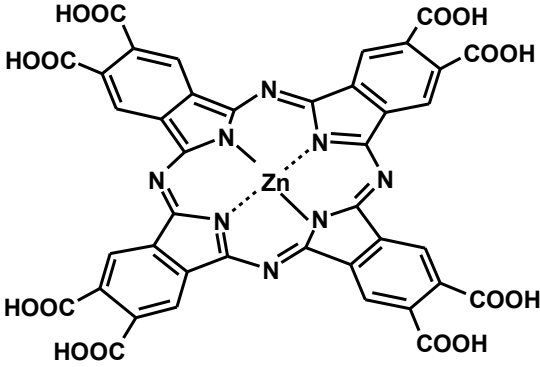
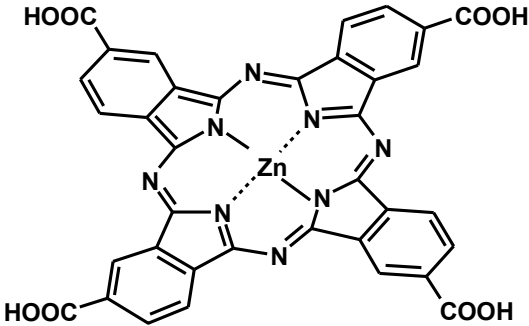
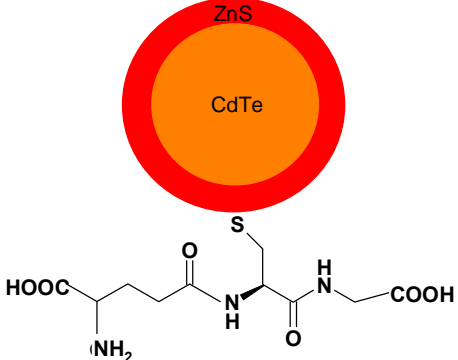
where  $f_{QD}$  is the normalized QD emission spectrum and  $\varepsilon_{ZnPc}$  is the molar extinction coefficient of ZnPc derivatives,  $\lambda$  is the wavelength of the acceptor, at the Q-band. It is assumed that  $\kappa^2$  is 2/3 (0.667) for mixed QDs with ZnPc. Such assumptions are usually made for donor-acceptor pairs in a liquid medium, which are considered to be isotropically oriented during their lifetime. This value of  $\kappa^2$  is also employed for the linked conjugate. FRET parameters may be computed using the program PhotochemCAD [114].

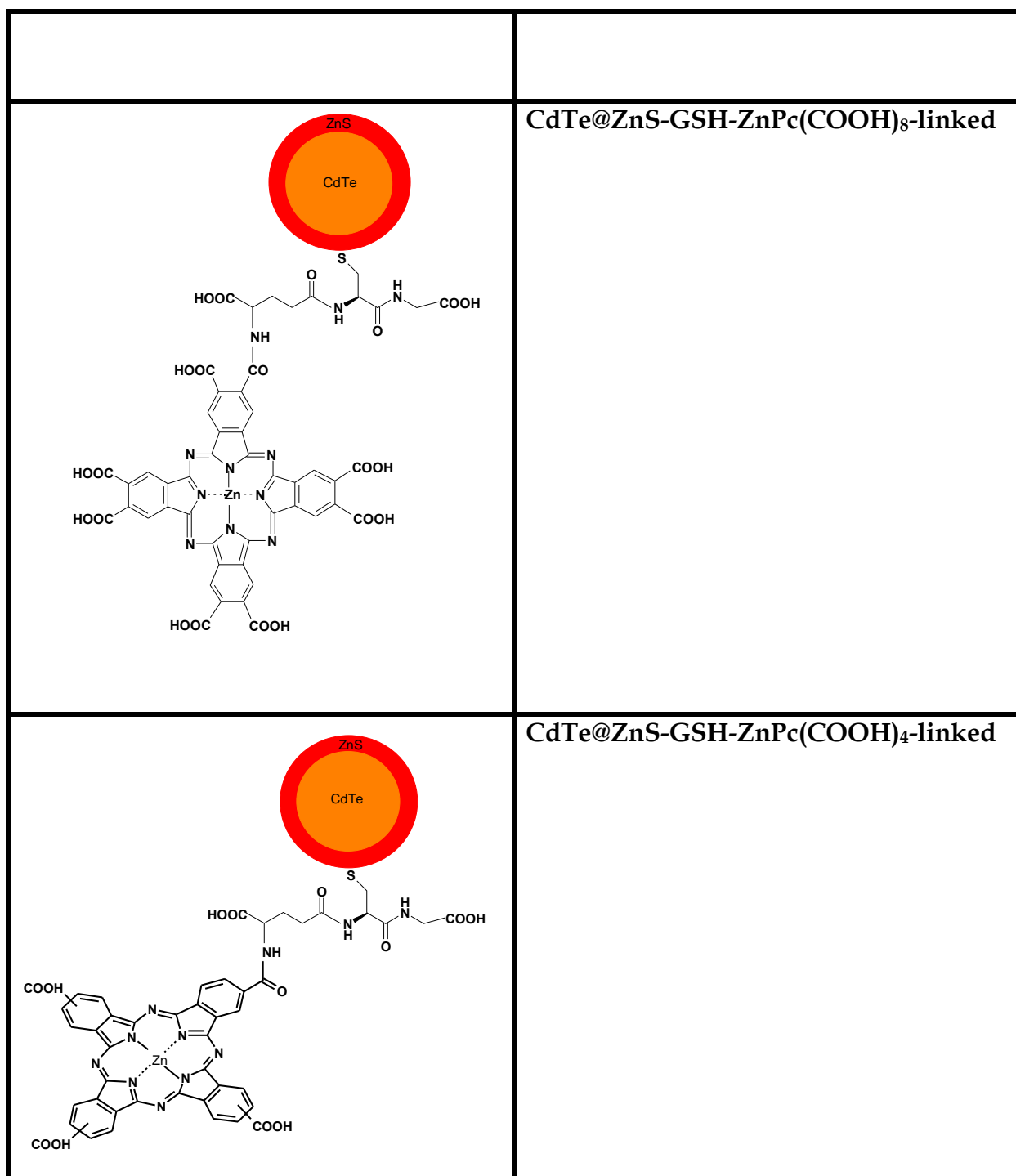
## 1.5 Summary of aims

1. To link carboxylated phthalocyanines (zinc tetra- and octacarboxy phthalocyanines) to CdTe@ZnS-QDs capped with glutathione. **Table 1.3** shows the Pc and the conjugates to be studied.
2. Characterize the samples using UV-Visible spectroscopy, fluorescence spectroscopy, infrared spectroscopy, Raman spectroscopy, time-correlated single photon counting, flash photolysis, X-ray diffraction, atomic force microscopy, transmission electron microscopy, as well as X-ray photoelectron spectroscopy.

3. To study their photophysical and photochemical behaviour (including fluorescence quantum yields, triplet quantum yields and lifetimes, singlet oxygen) and,
4. To study the FRET behaviour of the conjugates.

Table 1.3: Carboxylated phthalocyanines and coreshells used in this thesis.

| Molecule   | Abbreviation            |
|--|-------------------------|
|  <p>The structure shows a central zinc atom (Zn) coordinated to four nitrogen atoms in a phthalocyanine ring. Each of the four phenyl rings attached to the nitrogen atoms has two carboxylic acid groups (COOH) at the 2 and 6 positions, resulting in a total of eight COOH groups.</p>   | ZnPc(COOH) <sub>8</sub> |
|  <p>The structure shows a central zinc atom (Zn) coordinated to four nitrogen atoms in a phthalocyanine ring. Each of the four phenyl rings attached to the nitrogen atoms has a single carboxylic acid group (COOH) at the 4 position, resulting in a total of four COOH groups.</p>   | ZnPc(COOH) <sub>4</sub> |
|  <p>The diagram illustrates a core-shell structure. At the center is a CdTe core (orange circle), surrounded by a ZnS shell (red ring). Below the shell is the chemical structure of L-glutathione (GSH), showing its characteristic gamma-L-glutamyl-L-cysteinylglycine backbone with a free amino group (NH<sub>2</sub>) and a free carboxylic acid group (COOH).</p> | CdTe@ZnS-GSH            |



# **CHAPTER TWO**

## **EXPERIMENTAL**

## Experimental

### 2.1 Materials

Cadmium acetate dehydrate, L-glutathione (GSH) was purchased from Fluka. Tellurium powder (Te), thioglycolic acid (TGA) and N-N'-dicyclohexylcarbodiimide (DCC) were purchased from Sigma-Aldrich. 1,8-Diazabicyclo[5.4.0]-undec-7-ene (DBU), sulphuric acid and sodium hydroxide pellets were purchased from Merck. Aqueous solutions were prepared using Millipore water Milli-Q Water Systems (Millipore Corp., Bedford, MA, USA). Zinc chloride and N,N-dimethylformamide (DMF) were purchased from SAARCHEM. Isopropanol was purchased from B & M Scientific cc. Ammonium molybdate was purchased from uniLAB. Mixed-sulfonated aluminium phthalocyanine (AlPcSmix) standard was synthesized following a method published elsewhere [115]. Rhodamine 6G was purchased from Sigma.

### 2.2 Instrumentation

- ❖ Infrared spectra were recorded on a Perkin Elmer 100 ART FT-IR spectrometer.
- ❖ Ultraviolet-visible spectra (UV-Vis) were recorded on a Shimadzu UV-Vis 2550 spectrophotometer. All spectral measurements were performed in a quartz cell of 1 cm path length.
- ❖ The emission spectra were recorded on a Varian Cary Eclipse fluorescence spectrophotometer.



- ❖ Luminescence lifetimes were measured using time correlated single photon counting setup (TCSPC) (PicoQuant FluoTime 200), **Figure 2.1**. The excitation source was a diode laser (LDH-P-C-485, 480 nm, 10 MHz repetition rate for excitation of QDs, or LDH-P-670 with PDL 800-B, 670 nm, 20 MHz repetition rate Picoquant GmbH, for excitation of  $\text{ZnPc}(\text{COOH})_8$  and  $\text{ZnPc}(\text{COOH})_4$ . Fluorescence was detected under the magic angle with a peltier cooled photomultiplier tube (PMT) (PMA-C 192-N-M, Picoquant) and integrated electronics (PicoHarp 300E, Picoquant GmbH). A monochromator with a spectral width 4 nm was used to select the required emission wavelength. The response function of the system, which was measured with a scattering Ludox solution (DuPont), had a full width at half-maximum (FWHM) of 300 ps. All luminescence decay curves were measured at the maximum of the emission peak and the lifetimes obtained by deconvolution of the decay curves using the FluoFit Software program (PicoQuant GmbH, Germany). The support plane approach [89] was used to estimate the errors of the decay times.

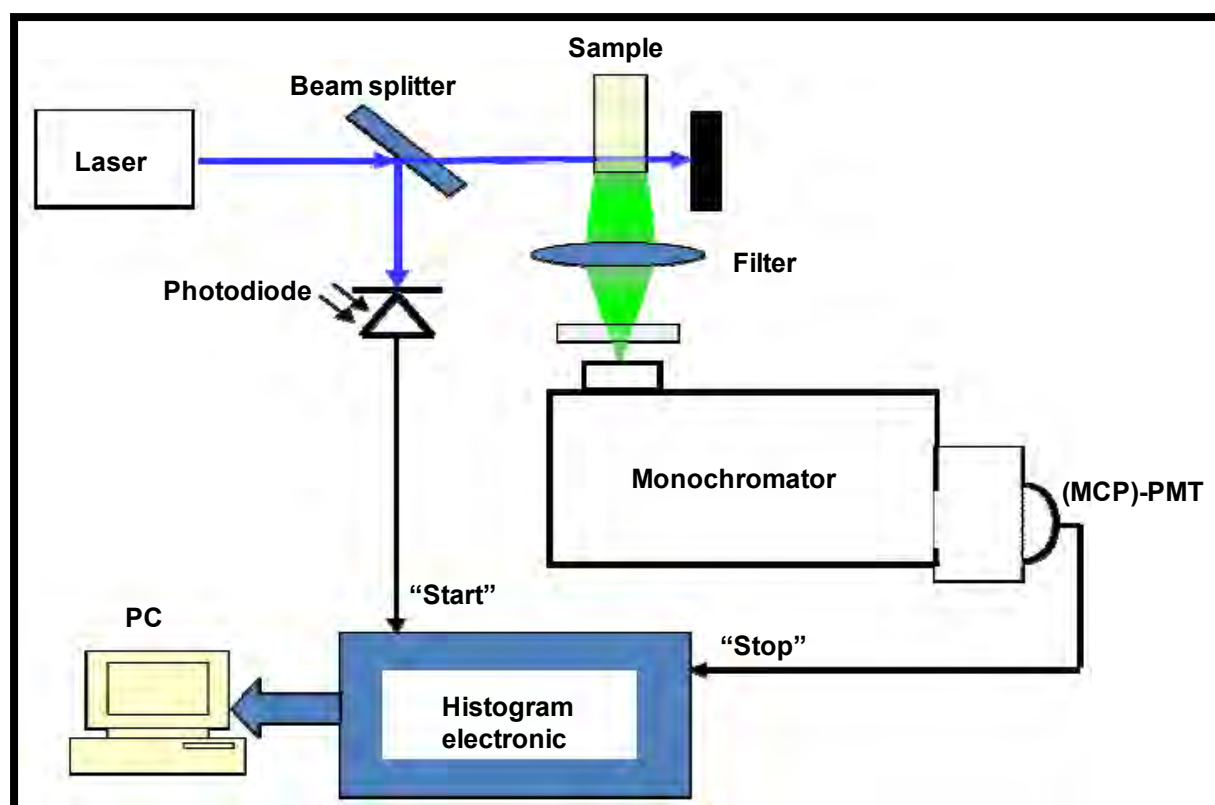


Figure 2.1: Schematic diagram of time-correlated single photon counting (TCSPC) setup. (MCP)-PMT = Monochromator photomultiplier tube, PC = Personal computer.

- ❖ Transmission electron microscopy (TEM) images were obtained using ZESISS LIBRA® 120 transmission electron microscope which operates at 90 kV.
- ❖ Atomic force microscopy (AFM) images, from which distribution histograms were obtained, were recorded in the non-contact mode in air with a CP-11 Scanning Probe Microscope from Veeco Instruments (Carl Zeiss, South Africa) at a scan rate of 1 Hz. Samples for AFM were prepared by spin coating samples of QDs in NaOH (in the absence or presence of  $\text{ZnPc}(\text{COOH})_8$  or  $\text{ZnPc}(\text{COOH})_4$ ).

- ❖ X-ray photoelectron spectra (XPS) were acquired on a Kratos Axis Ultra DLD operating at pressures below  $5 \times 10^{-9}$  torr. A monochromatic Al anode with emission currents and voltages set at 10 mA and 15 kV, together with a charge neutraliser, were used to acquire the spectra. Survey scans were obtained using a hybrid lens, in slot aperture mode with the pass energy set at 160 eV. Scans were acquired from 1200 to -5 eV (binding energy) with steps at 0.1 eV and dwell times at 300 ms.
  
- ❖ X-ray powder diffraction (XRD) patterns were recorded on a Bruker D8, Discover equipped with a proportional counter using Cu-K radiation ( $\lambda = 1.5405$  Å, nickel filter). Data for CdTe-TGA, CdTe@ZnS-GSH and CdTe@ZnS-GSH-ZnPc(COOH)<sub>8</sub>-linked or CdTe@ZnS-GSH-ZnPc(COOH)<sub>4</sub>-linked were collected in the range from  $2\theta = 5^\circ$  to  $60^\circ$ , scanning at  $1^\circ \text{ min}^{-1}$ . The filter time-constant and the slit width were 2.5 s per step and 6.0 mm respectively. Samples were placed on a silicon wafer slide. The X-ray diffraction data were processed using the Eva (evaluation curve fitting) software. Baseline correction was performed on each diffraction pattern by subtracting a spline fitted to the curved background.
  
- ❖ Raman spectra were obtained using a Bruker Vertex 70-Ram II spectrometer equipped with a Nd:YAG laser that emit at 1064 nm and liquid nitrogen cooled germanium detector.

- ❖ Laser flash photolysis experiments were performed with light pulses produced by a Quanta-Ray Nd:YAG laser providing 400 mJ, 9 ns pulses of laser light at 10 Hz, pumping a Lambda-Physik FL3002 dye laser (Pyridin 1 dye in methanol), **Figure 2.2**. Single pulse energy ranged from 2 to 7 mJ. The analyzing beam source was from a Thermo Oriel Xenon arc lamp, and photomultiplier tube (a Kratos Lis Projekte MLIS-X3) was used as a detector. Signals were recorded with a two-channel 300 MHz digital real time oscilloscope (Tektronix TDS 3032C); the kinetic curves were averaged over 256 laser pulses.

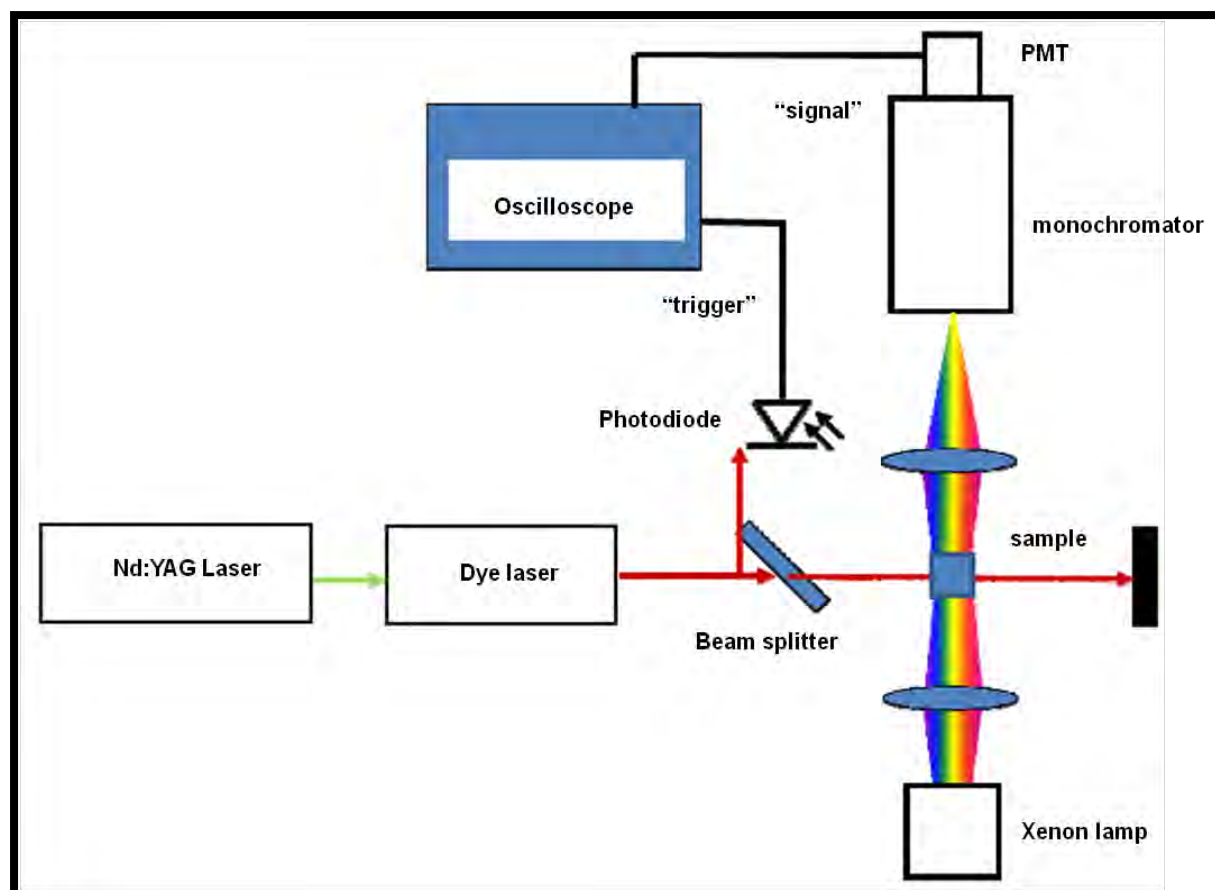


Figure 2.2: Schematic diagram for a laser flash photolysis setup.

- ❖ Time resolved phosphorescence decay of singlet oxygen at 1270 nm was used to determine singlet oxygen quantum yield in NaOH (pH 11). The dynamic phosphorescence decay of singlet oxygen ( $O_2(^1\Delta_g)$ ), was demonstrated using time resolved phosphorescence of  $O_2(^1\Delta_g)$  at 1270 nm. For these studies (Figure 2.3) an ultra sensitive germanium detector (Edinburgh Instruments, EI-P) combined with a 1000 nm long pass filter (Omega, RD 1000 CP) and a 1270 nm band-pass filter (Omega, C1275, BP50) was used to detect  $O_2(^1\Delta_g)$  phosphorescence under the excitation using Quanta-Ray Nd:YAG laser providing 400 mJ, 90 ns pulses of laser light at 10 Hz pumping a Lambda-

Physik FL3002 dye laser (Pyridin 1 dye in methanol), with a pulse period of 7 ns and repetition rate of 10 Hz. The near-infrared phosphorescence of the samples were focused onto the germanium detector by a lens (Edmund, NT 48-157) with detection direction perpendicular to the excitation laser beam. The detected signals were averaged with a digital oscilloscope (Tektronics, TDS 360) to show the dynamic decay of  $O_2(^1\Delta_g)$ .

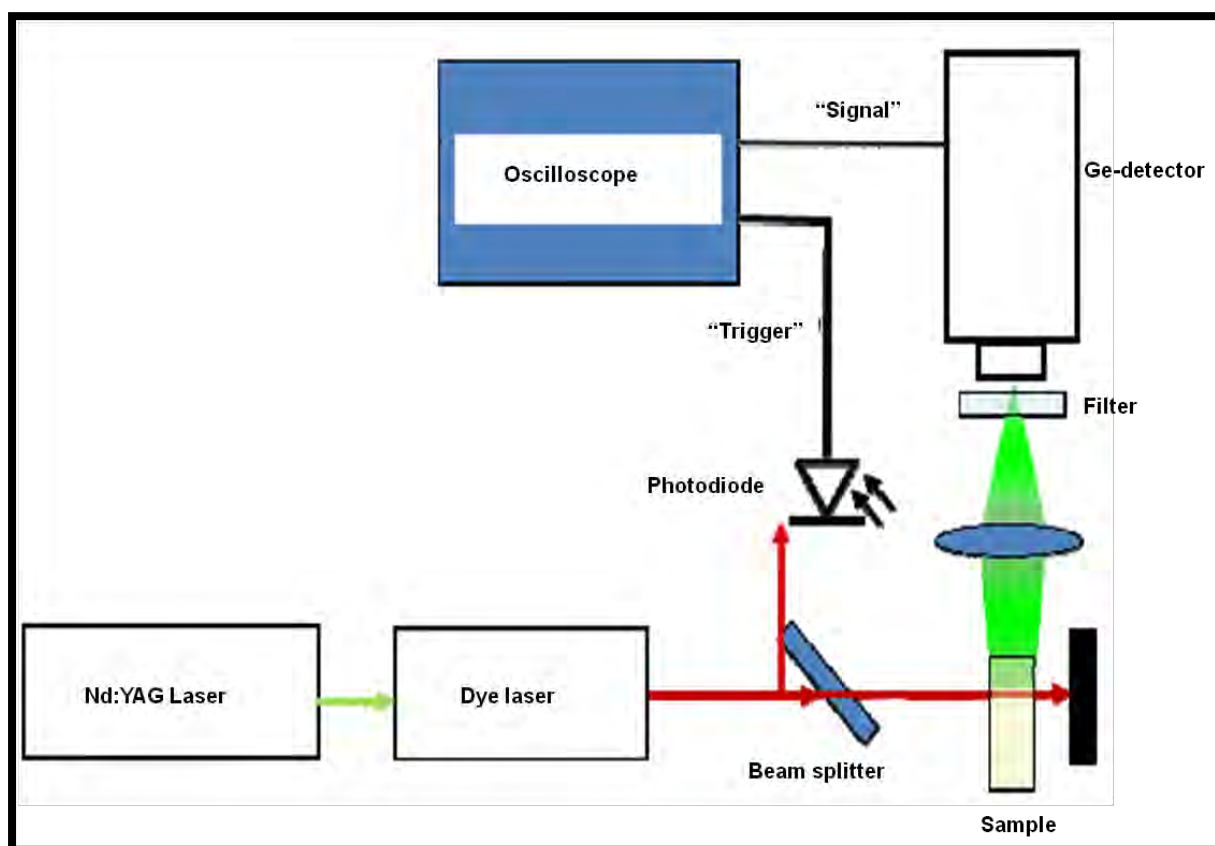


Figure 2.3: Schematic diagram for the singlet oxygen detection setup using its phosphorescence.

### 2.3 Synthesis

The syntheses of  $\text{ZnPc}(\text{COOH})_8$  [25] and  $\text{ZnPc}(\text{COOH})_4$  [24] have been reported before. The syntheses of both CdTe-TGA [60, 116] and CdTe@ZnS-GSH [63] have been reported.

Coordination of phthalocyanines to core-shell quantum dots was achieved by dissolving a  $\text{ZnPc}(\text{COOH})_8$  or  $\text{ZnPc}(\text{COOH})_4$  complex (10.0 mg) in dilute NaOH (pH 10, 10 mL), then DCC (30.00 mg) was added to convert the carboxylic group ( $-\text{COOH}$ ) of the Pc into an activated carbodiimide ester group. The mixture was left to stir at room temperature under argon atmosphere for 68 h. After this time, CdTe@ZnS-GSH (2 mL) was added to the activated Pc and the mixture was stirred for 20 h to allow for conjugation of the Pc to the QDs to take place.

Precipitation and purification of conjugates formed was achieved by centrifugation in isopropanol, addition of DMF to dissolve the unreacted DCC, suspension in isopropanol for the second precipitation and then employing size exclusion chromatography, with an aqueous solution at pH 11 serving as an eluent, to separate MPcs as well as QDs that did not take part in the coordination process.

## 2.4 Photophysical studies

### 2.4.1 Fluorescence quantum yields and lifetimes

Fluorescence quantum yields ( $\Phi_F$ ) of the zinc octacarboxy phthalocyanines [117] and zinc tetracarboxy phthalocyanines [76] have been determined elsewhere. Fluorescence quantum yields ( $\Phi_F$ ) of QDs and conjugates were determined in water by a comparative method, Equation 1.1 and 1.2. Rhodamide 6G was dissolved in ethanol and employed as a standard ( $\Phi_F^{\text{Std}} = 0.94$  [89]). Both the samples and standard were excited at the same wavelength. The absorbances of the solutions at the excitation wavelength were about 0.05 to avoid any inner filter effects.

The fluorescence lifetimes were evaluated from the tri-exponential decay curve of CdTe-TGA and CdTe@ZnS-GSH. A good fitting was judged by weighted residuals and  $\chi^2$  values. The calculation of the average fluorescence lifetime for conjugates and QDs was achieved using the values obtained from the fit by employing Eq. 2.1 [118].

$$\tau_{av} = \sum a_i \tau_i \quad 2.1$$

where  $a_i$  is the relative amplitude contribution to the lifetime  $\tau_i$ .

### 2.4.2 FRET Parameters

Employing QDs (donors) in the presence of Pcs (acceptors), all FRET parameters were obtained spectroscopically using steady state data and lifetime data, with



PhotochemCAD software being employed to determine  $J$ , the Förster overlap integral between the QD and Pc.

### 2.4.3 Triplet quantum yields ( $\Phi_T$ ) and lifetimes ( $\tau_T$ )

The decay kinetics of the triplet absorption of the phthalocyanines were recorded using laser flash photolysis setup, **Figure 2.2**. The absorbance of sample solutions and that of the standard were adjusted to be nearly 1.5 at their Q-band maximum. All samples were introduced into a 1 cm quartz cell and then bubbled with argon for 10 min to remove dissolved oxygen before taking readings. The triplet quantum yields of the sample phthalocyanines alone and in the presence of quantum dots were determined using Equation 1.3. Mixed-sulfonated aluminium phthalocyanine (AlPcSmix) was employed as a standard {AlPcSmix in aqueous medium ( $\Phi_T^{\text{std}} = 0.44$  [117])}. Triplet lifetimes were determined from the kinetic data obtained, using ORIGIN Pro 8 software to fit the kinetics decay curves.

### 2.4.4 Singlet oxygen ( $\Phi_\Delta$ )

The determination of  $\Phi_\Delta$  was achieved by employing an optical method. The optical method involves the observation of the fluorescence kinetic decay of the singlet oxygen generated at 1270 nm in air using equipment shown in **Figure 2.3**. Sodium azide ( $\text{NaN}_3$ ) was used as singlet oxygen quencher. The dynamic course of the singlet oxygen concentrations were clearly recorded following Equation 1.6. The  $\Phi_\Delta$  values were then determined using Equation 1.7, and employing AlPcSmix in  $\text{H}_2\text{O}$  ( $\Phi_\Delta^{\text{Std}} = 0.38$  [119]) as a standard.

# **CHAPTER THREE**

## **RESULTS AND DISCUSSION**

---

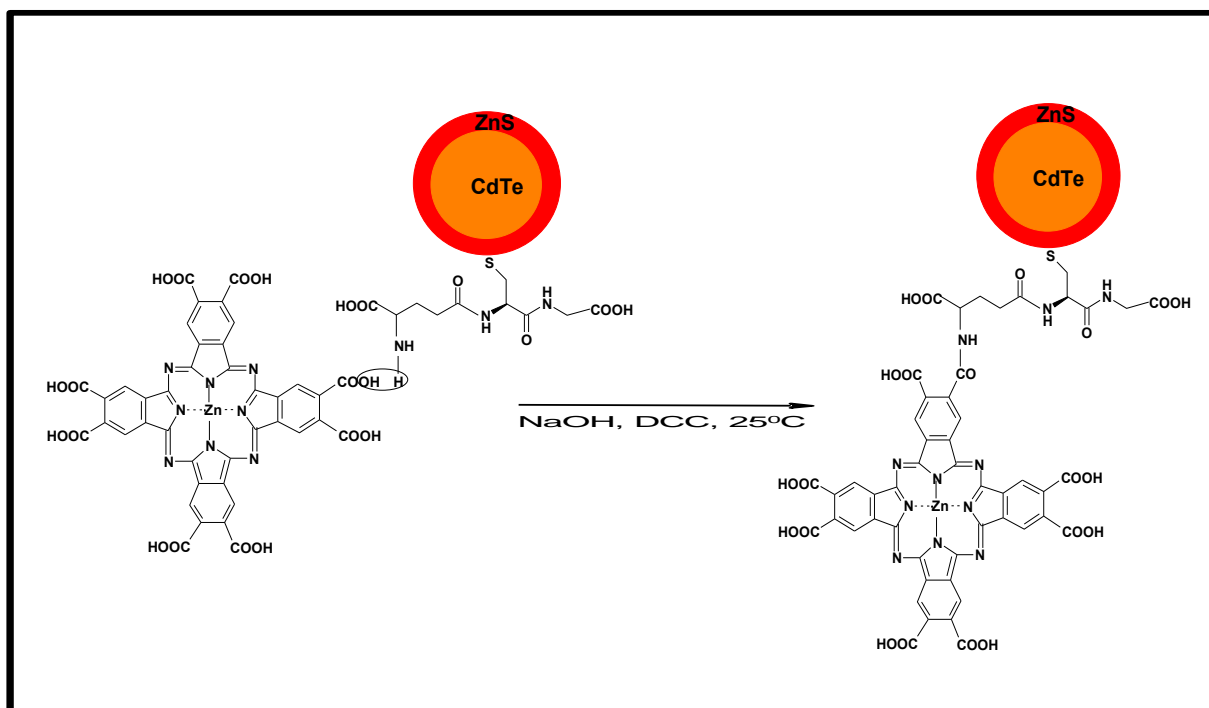
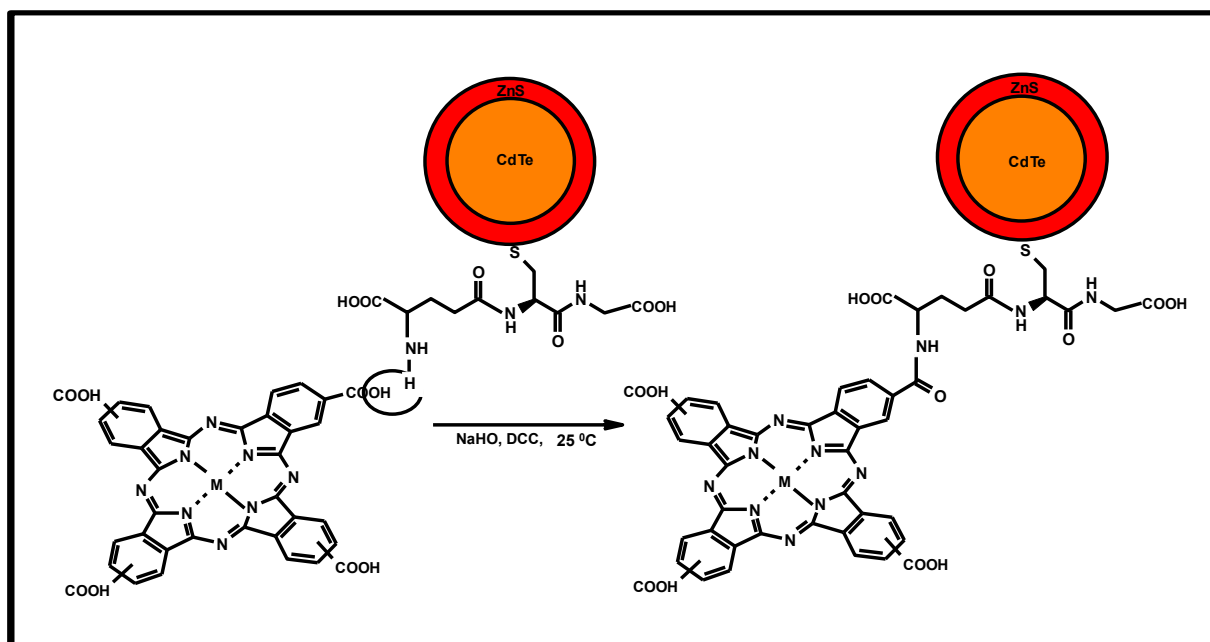
## Results and Discussion

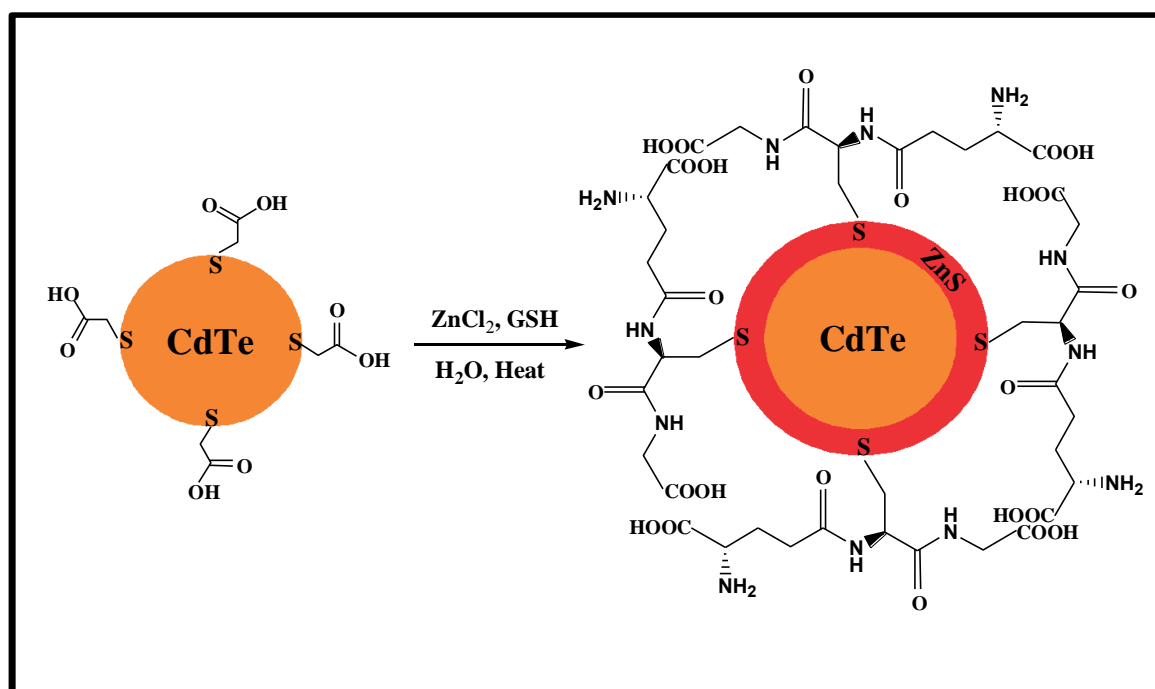
### PUBLICATION(S)

1. Fluorescence behaviour of glutathione capped CdTe@ZnS quantum dots chemically coordinated to zinc octacarboxy phthalocyanines, **Kutloano E. Sekhosana**, Edith Antunes, Samson Khene, Sarah D'Souza and Tebello Nyokong, *J. Lumin.* 136 (2013) 255-264.
2. Glutathione capped CdTe@ZnS quantum dots - zinc tetracarboxy phthalocyanine conjugates: fluorescence behaviour studies in comparison with zinc octacarboxy phthalocyanine, **Kutloano E. Sekhosana**, Edith Antunes and Tebello Nyokong, *Polyhedron* {accepted for publication}.

### 3.1 Characterization of conjugates of quantum dots with ZnPc(COOH)<sub>8</sub> and ZnPc(COOH)<sub>4</sub>

**Schemes 3.1** and **3.2** show the formation of CdTe@ZnS-GSH-ZnPc(COOH)<sub>8</sub>-linked and CdTe@ZnS-GSH-ZnPc(COOH)<sub>4</sub>-linked respectively by linking of the carboxyl group of the phthalocyanine to the amino group of GSH capped QD. It is possible that more than one phthalocyanine molecule will link to the QDs. The number of binding sites for MPcs on QDs has been shown to vary between 1 and 2 depending on the capping agent [84]. **Scheme 3.3** shows the formation of CdTe@ZnS-GSH from core QDs.

Scheme 3.1: Coordination of ZnPc(COOH)<sub>8</sub> to CdTe@ZnS-GSH.Scheme 3.2: Coordination of ZnPc(COOH)<sub>4</sub> to CdTe@ZnS-GSH.



**Scheme 3.3: Encapsulation of CdTe into a zinc sulphide shell (ZnS).**

### 3.1.1 FTIR spectra

The IR spectra, **Figure 3.1**, show a disappearance of the S-H vibration for free GSH following the formation of CdTe@ZnS-GSH, indicating engagement of the S-H functional group on the GSH capped QDs. The N-H broad vibration shifted from  $3259\text{ cm}^{-1}$  of CdTe@ZnPc-GSH to  $3315\text{ cm}^{-1}$  upon formation of the CdTe@ZnS-GSH-ZnPc(COOH)<sub>8</sub>-linked conjugates. The C=O vibrations ( $1623\text{ cm}^{-1}$  on MPc and CdTe@ZnS-GSH-ZnPc(COOH)<sub>8</sub>-linked conjugate) became more resolved on conjugation. In general there is sharpening of peaks between  $2000$  and  $3500\text{ cm}^{-1}$  for the CdTe@ZnS-GSH-ZnPc(COOH)<sub>8</sub>-linked conjugate compared to ZnPc(COOH)<sub>8</sub> or QDs alone, **Figure 3.1**. Amide bonds are also present in the GSH backbone, hence making definite assignments difficult. However it is known that shift in IR bands

confirm structural change [120], as observed in this work. All the changes indicate the formation of a different complex. Similar changes were observed for  $\text{ZnPc}(\text{COOH})_4$ , **Figure 3.2**.

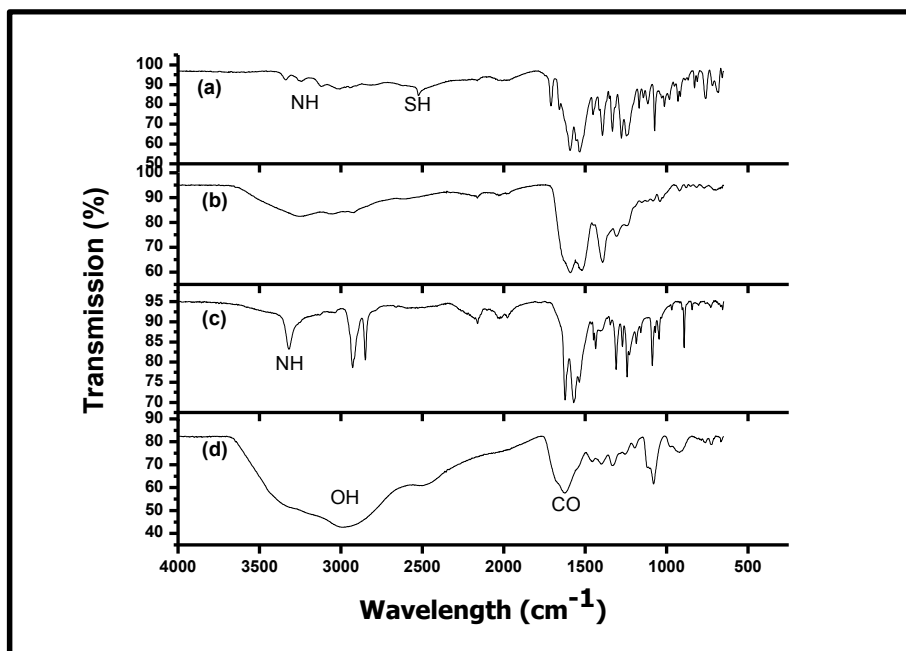


Figure 3.1: IR spectra of (a) GSH, (b) CdTe@ZnS-GSH, (c) CdTe@ZnS-GSH-ZnPc(COOH)<sub>8</sub>-linked and (d) ZnPc(COOH)<sub>8</sub> alone.

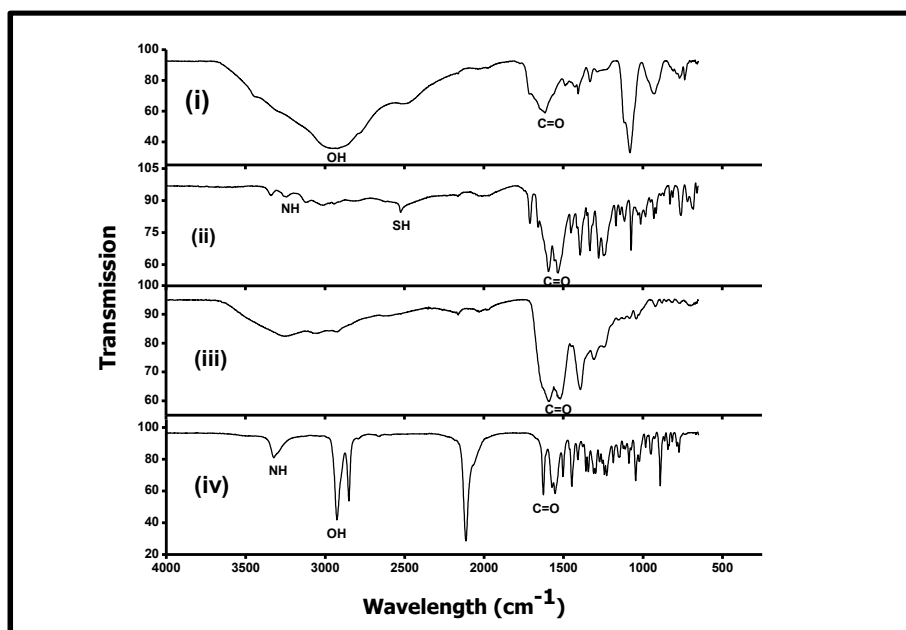


Figure 3.2: FTIR spectra of (i) ZnPc(COOH)<sub>4</sub>, (ii) CdTe@ZnS-GSH and (iii) CdTe@ZnS-GSH-ZnPc(COOH)<sub>4</sub>-linked.



### 3.1.2 Raman spectra

An amide bond formation was further investigated by Raman spectroscopy, **Figure 3.3**. There were shifts and weakening of the OH (near  $3200\text{ cm}^{-1}$ ) and NH vibration (near  $2940\text{ cm}^{-1}$ ) upon conjugation of Pc with CdTe@ZnS-GSH. The amide bond area for the conjugate showed very weak bands compared to CdTe@ZnS-GSH alone or ZnPc(COOH)<sub>8</sub> alone. The insert in **Figure 3.3a**, shows an expansion of the amide bond area of the conjugate. Though weak, the amide bonds (amides I and II) are observed at  $1523\text{ cm}^{-1}$  and  $1444\text{ cm}^{-1}$  in comparison with literature [121]. These values are different from the CO vibration values in this region which are no longer visible in the conjugate. The changes indicate formation of a new complex.

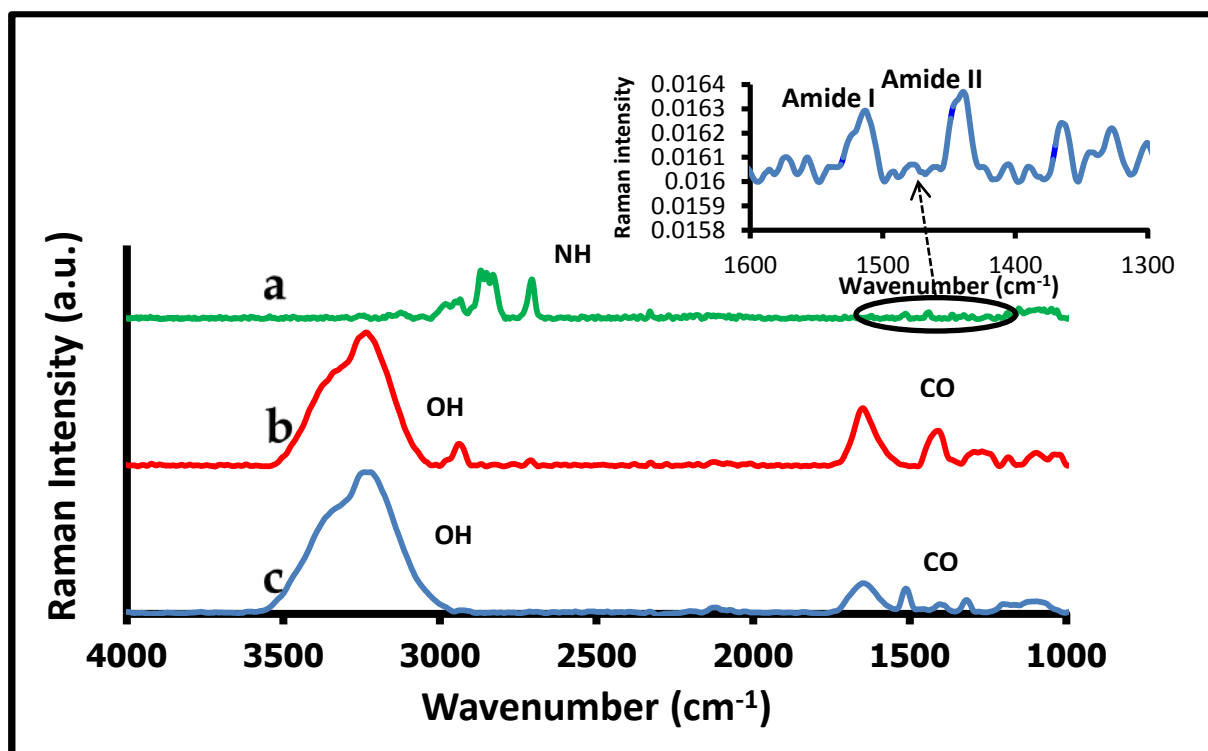


Figure 3.3: Raman spectra of (a) CdTe@ZnS-GSH-ZnPc(COOH)<sub>8</sub>, (b) CdTe@ZnS-GSH and (c) ZnPc(COOH)<sub>8</sub>.

### 3.1.3 XRD

The XRD pattern showed a relatively large shift to higher  $2\theta$  values for the coreshell (CdTe@ZnS-GSH) compared to the core (CdTe-TGA) alone (Figure 3.4A). The diffraction peaks are broad [122] and centred at approximately  $2\theta = 24^\circ, 40^\circ$  and  $47^\circ$  corresponding to the three most intense peaks for bulk CdTe (ZnS-type structure,  $2\theta = 23.8^\circ, 39.3^\circ$ , and  $46.5^\circ$ ) as they appear on the simulated pattern obtained from The International Centre for Diffraction Data (ICDD). The shift and broadening of the diffraction patterns to higher angles due to the growth of ZnS shells has been reported before and is typical of the formation of a shell over the core [123]. The

main XRD peak is shifted further to larger  $2\theta$  values for the XRD pattern of CdTe@ZnS-GSH-ZnPc(COOH)<sub>8</sub>-linked (Figure 3.4B) suggesting phase transformation or additional coating [124]. Only the main peak is observed for the conjugate since the other peaks are too weak to be observed due to the small amount of CdTe@ZnS-GSH QDs within the conjugate. The XRD peak of Pc alone was too broad to be observed. The sizes of CdTe@ZnS-GSH and CdTe@ZnS-GSH-ZnPc(COOH)<sub>8</sub>-linked employed in this work are 2.3 nm and 3.0 nm respectively and were obtained using the Debye-Scherrer Eq. 3.1:

$$d = \frac{0.9\lambda}{\beta \cos \theta} \quad 3.1$$

where  $d$  = the mean diameter in nm,  $\lambda$  is the wavelength of the X-ray source, (1.5405 Å),  $\beta$  is the full width at half maximum of the diffraction peak, and  $\theta$  is the angular position of the peak.

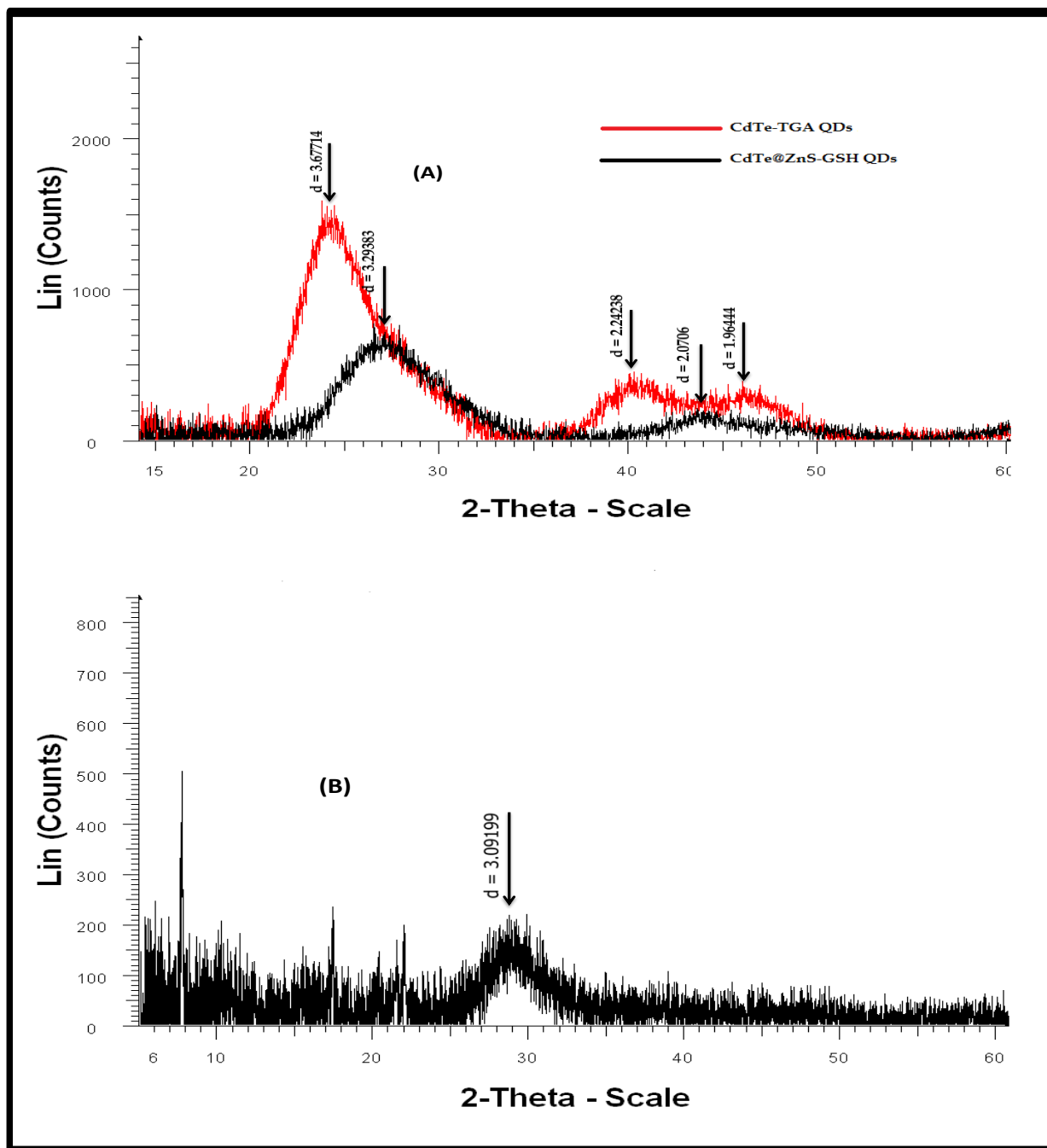


Figure 3.4: XRD spectra of (A) CdTe-TGA and CdTe@ZnS-GSH and (B) CdTe@ZnS-GSH-ZnPc(COOH)<sub>8</sub>-linked.

Figure 3.5 shows the XRD spectra of the CdTe@ZnS-GSH QD alone and that of the CdTe@ZnS-GSH-ZnPc(COOH)<sub>4</sub>-linked complex. The XRD patterns for the CdTe@ZnS-GSH QDs (Figure 3.5) shows one main peak at  $2\theta = 26.5^\circ$  which is shifted to  $28^\circ$  in the conjugates. The size of the CdTe@ZnS-GSH QD and its linked complex, CdTe@ZnS-GSH-ZnPc(COOH)<sub>4</sub>-linked, were found to be 2.3 nm and 3.0 nm respectively. For CdTe@ZnS-GSH-ZnPc(COOH)<sub>4</sub>-linked, the size was found to be the same as that of CdTe@ZnS-GSH-ZnPc(COOH)<sub>8</sub>-linked conjugate.

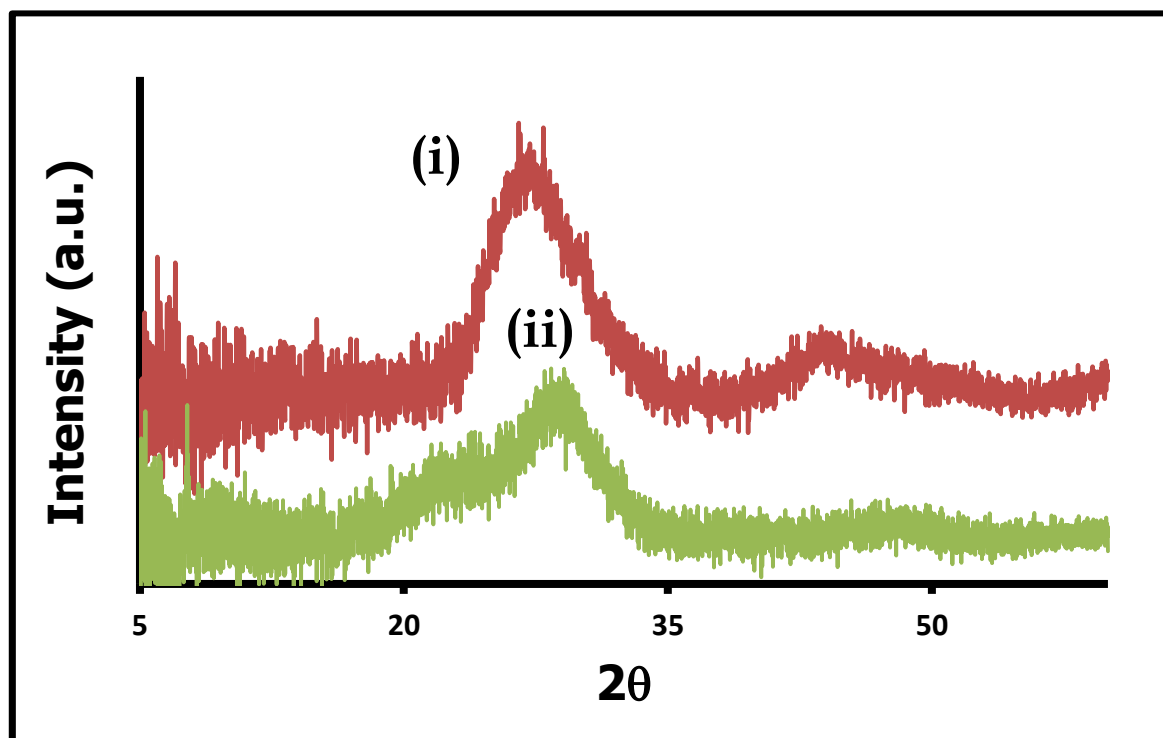


Figure 3.5: XRD spectra of CdTe@ZnS-GSH (i) and CdTe@ZnS-GSH-ZnPc(COOH)<sub>4</sub>-linked (ii).

### 3.1.4 Microscopic data

Figure 3.6 shows the TEM images of (i) CdTe@ZnS-GSH QDs and (ii) CdTe@ZnS-GSH-ZnPc(COOH)<sub>8</sub>-linked. CdTe@ZnS-GSH QDs (Figure 3.6(i)) are slightly aggregated as shown by a chain-like pattern which brings about difficulty in measuring the size of individual particles using TEM technique. The aggregation of CdTe@ZnS-GSH QDs increased upon covalently linking a Pc to form the CdTe@ZnS-GSH-ZnPc(COOH)<sub>8</sub>-linked (Figure 3.6(ii)) complex. TEM characterization for CdTe@ZnS-GSH-ZnPc(COOH)<sub>4</sub>-linked was not performed and therefore is not discussed in this thesis.

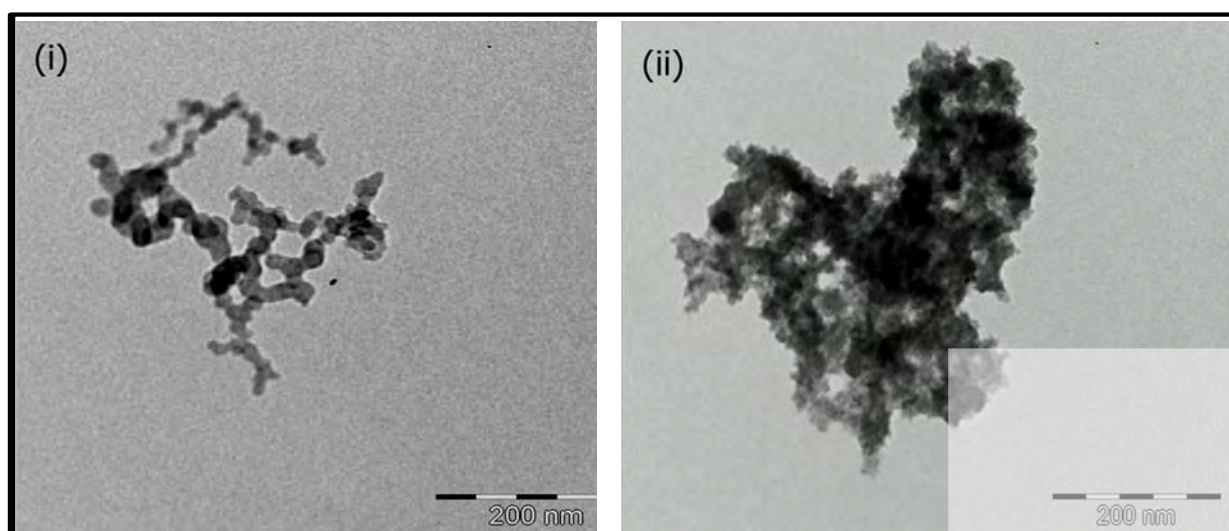
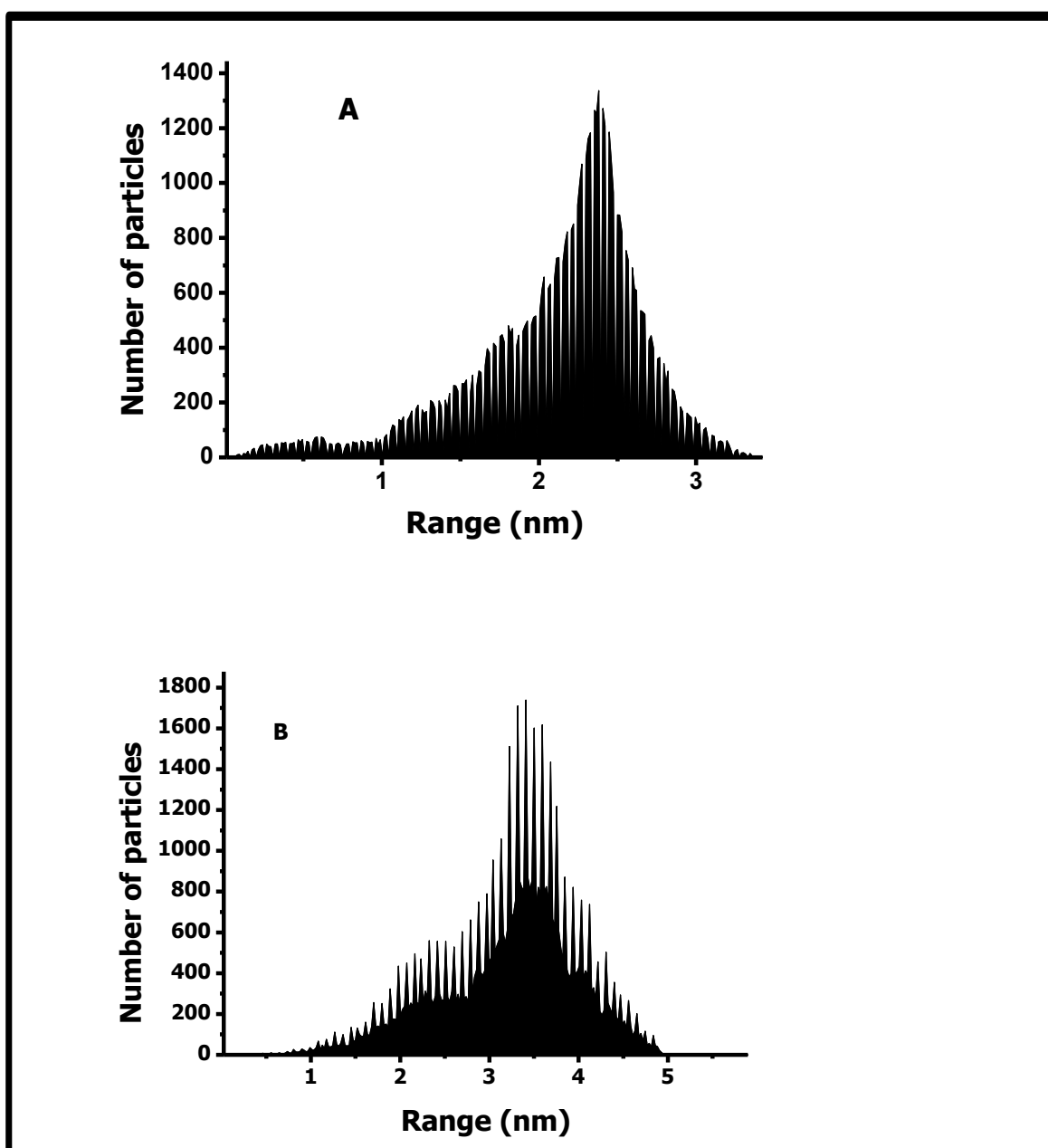


Figure 3.6: TEM images of (i) CdTe@ZnS-GSH QDs and (ii) CdTe@ZnS-GSH-ZnPc(COOH)<sub>8</sub>-linked.

Figure 3.7A shows the size distribution histograms (from AFM) for CdTe@ZnS-GSH QDs and CdTe@ZnS-GSH-ZnPc(COOH)<sub>8</sub>-linked. The average size for CdTe@ZnS-

GSH QDs (Figure 3.7A) was estimated to be 2.4 nm, which is nearly the same as the one determined by XRD (2.3 nm). The average size for CdTe@ZnS-GSH-ZnPc(COOH)<sub>8</sub>-linked (Figure 3.7B) was found to be 3.5 nm which differs slightly from that which was estimated by XRD (3.0 nm). Similar AFM results for CdTe@ZnS-GSH-ZnPc(COOH)<sub>4</sub>-linked were obtained.



**Figure 3.7: AFM size distribution histograms for (A) CdTe@ZnS-GSH QDs and (B) CdTe@ZnS-GSH-ZnPc(COOH)<sub>8</sub>-linked.**

### 3.1.5 XPS spectra of coreshell QD alone and in the presence of ZnPc(COOH)<sub>8</sub>

**Figure 3.8** shows the XPS spectra of (i) CdTe@ZnS-GSH QDs and (ii) CdTe@ZnS-GSH-ZnPc(COOH)<sub>8</sub>-linked. The S 2p peak at 164 eV and S 2s peak at 223 eV for CdTe@ZnS-GSH QDs become weaker after linking to the Pc since the ZnS is now partially shielded by the Pc in CdTe@ZnS-GSH-ZnPc(COOH)<sub>8</sub>-linked. The C 1s (at 284.8 eV) and O 1s (at 531 eV) peak areas increase on conjugation due to the presence of additional carbon and oxygen atoms in ZnPc(COOH)<sub>8</sub> conjugate. The Zn 2p peak (at 1020 eV), for example, is more greatly enhanced for CdTe@ZnS-GSH than for CdTe@ZnS-GSH-ZnPc(COOH)<sub>8</sub>-linked due to the presence of additional Zn atoms on the surface for the QD as a result of the presence of ZnS.



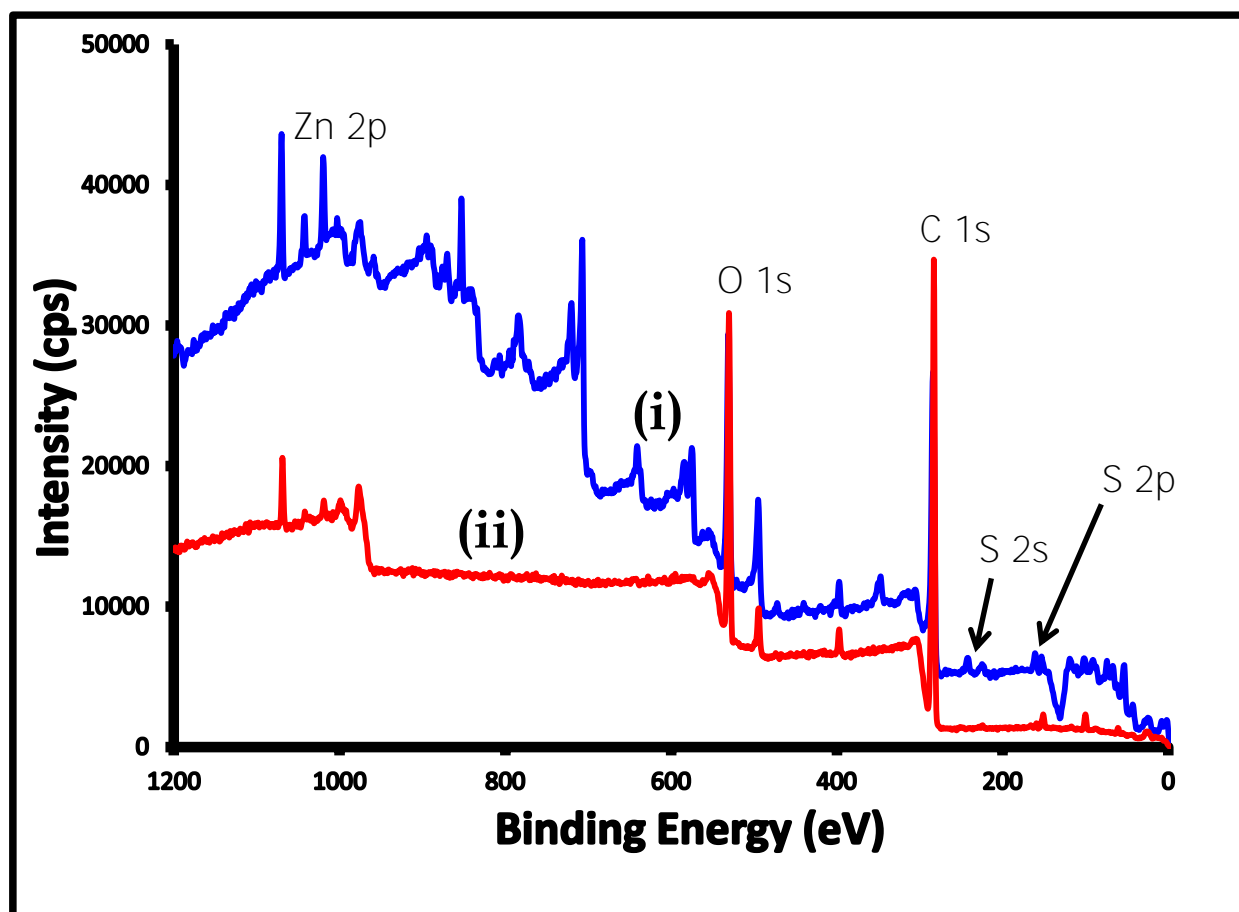


Figure 3.8: XPS spectra of (i) CdTe@ZnS-GSH QDs and (ii) CdTe@ZnS-GSH-ZnPc(COOH)<sub>8</sub>-linked.

### 3.1.6 UV-Vis spectra

Figure 3.9A shows the UV-Vis spectra of CdTe-TGA and CdTe@ZnS-GSH. Red shifting of the spectrum is observed on the UV-Vis spectrum of CdTe@ZnS-GSH as a direct result of nanoparticle growth. The absorption spectra are broad and the emission spectra are narrow as is typical of QDs. Figure 3.9B shows typical absorption spectra of (i) ZnPc(COOH)<sub>8</sub> in NaOH (0.1 M) showing no aggregation.

Aggregation is due to coplanar association of rings which may result in the splitting and broadening of spectra with a blue shifted peak at  $\sim 630$  nm being due to the so called "H" aggregates [44]. It has been reported that positively charged phthalocyanines form aggregates in the presence of negatively charged QDs, which results in complete collapse of the Q band and the formation of a broad band [125,126]. In the current work both the QDs and Pcs are negatively charged and the type of aggregation reported in literature was not observed. For the QDs mixed or linked to ZnPc derivatives, there is an increase in the absorption from 600 nm and below due to QDs absorption, **Figure 3.9B**. There was no change in the Q band maxima when comparing the mixed and linked conjugates. Also there is no shifting of the Q band of the conjugate compared to ZnPc(COOH)<sub>8</sub> alone.

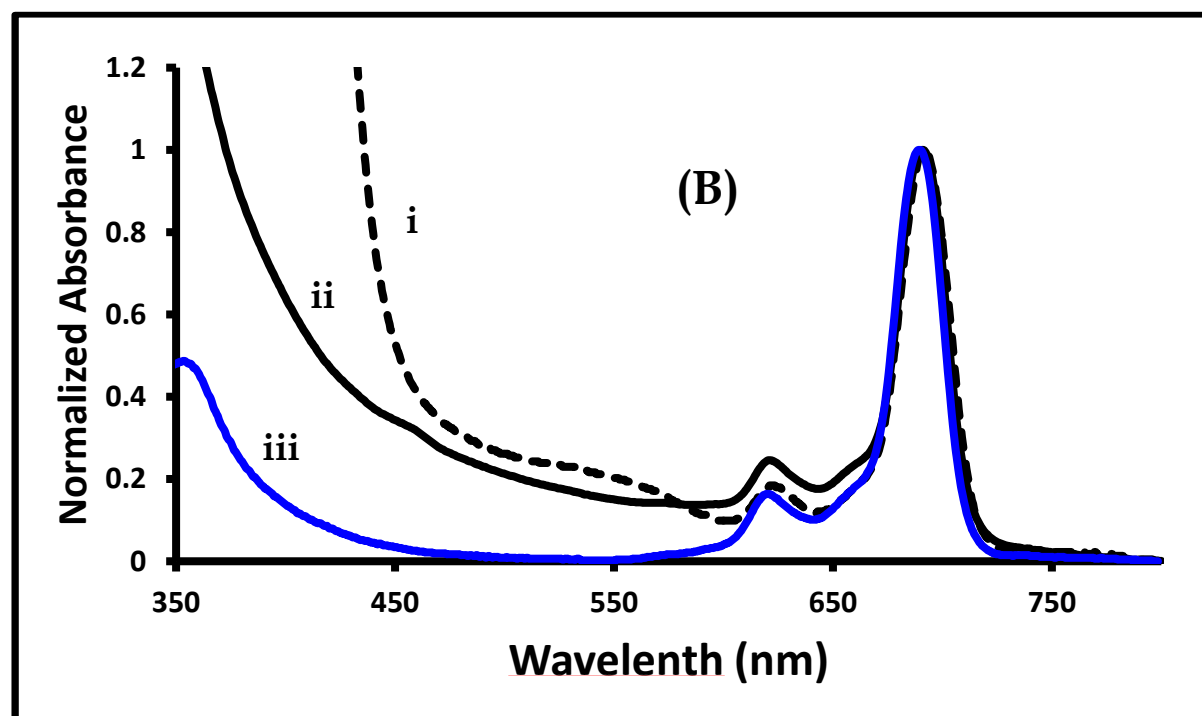
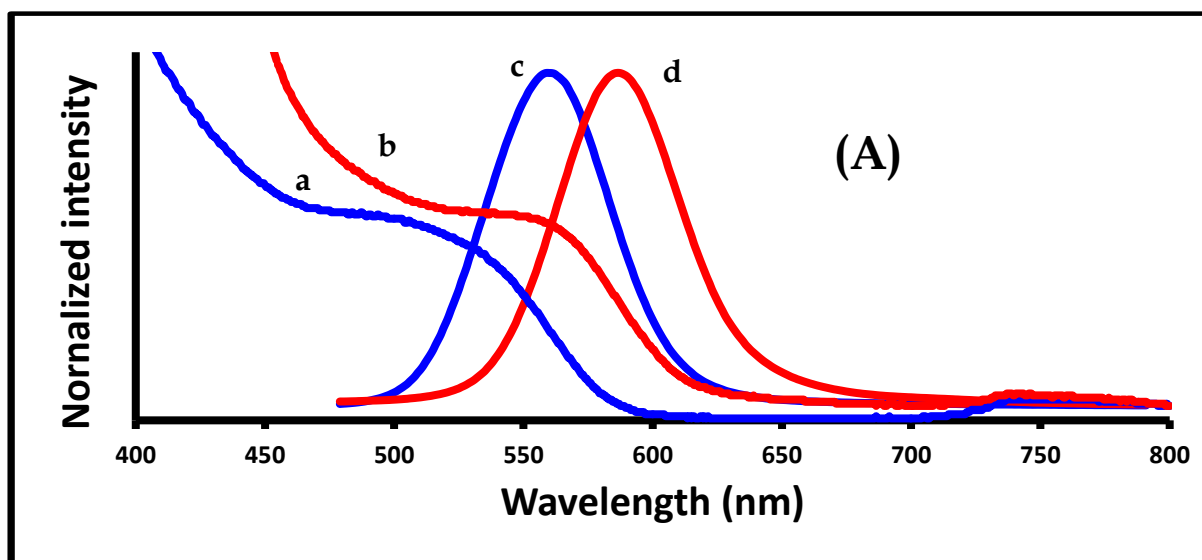


Figure 3.9: (A) Absorption (a,b) and fluorescence (c,d) spectra of CdTe-TGA (a,c) and CdTe@ZnS-GSH (b,d) and (B) absorbance spectra of (i) CdTe@ZnS-Zn(COOH)<sub>8</sub>-mixed, (ii) CdTe@ZnS-Zn(COOH)<sub>8</sub>-linked and (iii) Zn(COOH)<sub>8</sub> in NaOH (0.1 M) alone.

**Figure 3.10A** shows the typical absorption spectra for  $\text{ZnPc}(\text{COOH})_4$  in NaOH (0.1 M) and in a NaOH (0.1 M):ethanol (1:1) mixture.  $\text{ZnPc}(\text{COOH})_4$  shows severe aggregation in NaOH alone. This aggregation was reduced by dissolving the  $\text{ZnPc}(\text{COOH})_4$  in a mixture of NaOH (0.1 M) and ethanol in a 1:1 ratio. Ethanol was chosen in our study as a suitable additional solvent in aqueous media since organic solvents are able to break the aggregates to give monomers.

**Figure 3.10B** shows the absorption spectrum of  $\text{CdTe@ZnS-GSH-ZnPc}(\text{COOH})_4$ -linked,  $\text{CdTe@ZnS-GSH-ZnPc}(\text{COOH})_4$ -mixed and  $\text{ZnPc}(\text{COOH})_4$  in NaOH (0.1 M):ethanol (1:1). The presence and increase in absorption from 600 nm and below (**Figure 3.10B (ii)**) for the  $\text{CdTe@ZnS-GSH-ZnPc}(\text{COOH})_4$ -linked and  $\text{CdTe@ZnS-GSH-ZnPc}(\text{COOH})_4$ -mixed complexes are due to QD's absorption. For the mixed solutions, **Figure 3.10B**, there is a slight red shift in the Q band, while no shift is observed for the conjugate compared to  $\text{ZnPc}(\text{COOH})_4$  alone.

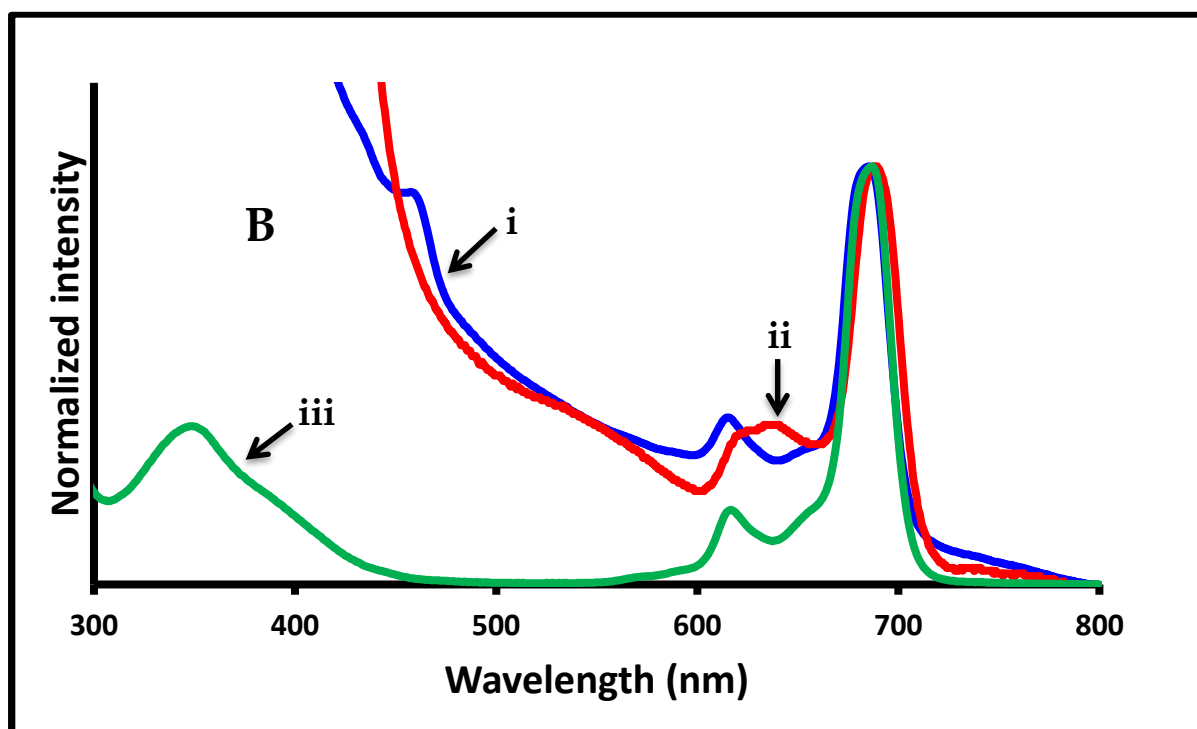
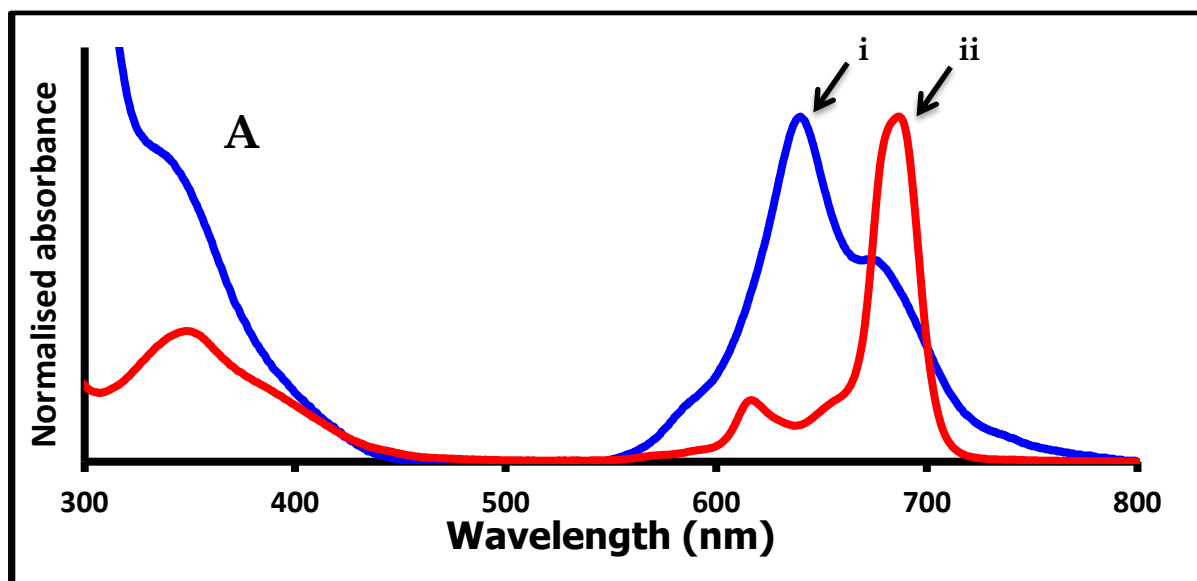


Figure 3.10: Absorbance spectra of (A) ZnPc(COOH)<sub>4</sub> in NaOH (0.1 M) (i) and in a NaOH (0.1 M):ethanol (1:1) mixture (ii); and (B) absorption spectra of CdTe@ZnS-GSH-ZnPc(COOH)<sub>4</sub>-linked (i), CdTe@ZnS-GSH-ZnPc(COOH)<sub>4</sub>-mixed (ii) and ZnPc(COOH)<sub>4</sub> (iii) in a NaOH (0.1 M):ethanol (1:1) mixture.

## 3.2 Photophysical parameters

### 3.2.1 Fluorescence quantum yields and lifetimes

The fluorescence lifetimes of CdTe-TGA, CdTe@ZnS-GSH, ZnPc(COOH)<sub>8</sub>, and conjugates were determined by TCSPC. The fluorescence decay curves of CdTe@ZnS-GSH and CdTe@ZnS-GSH-ZnPc(COOH)<sub>8</sub>-linked conjugates are similar to those shown in **Figure 3.11A** and **B** for CdTe@ZnS-GSH and CdTe@ZnS-GSH-ZnPc(COOH)<sub>4</sub>-linked conjugates. **Table 3.1** shows the amplitude weighted lifetimes (average lifetimes) for QDs and conjugates as well as a single lifetime for ZnPc(COOH)<sub>8</sub>. The fitting of the fluorescence decay curves for QDs or conjugates resulted in three lifetimes for QDs.

The longer lifetime for QDs may be due to the involvement of surface states in the carrier recombination process [127]. The second (intermediate) fluorescence lifetime component, is a result of radiative electron-hole recombination processes due to surface defects [128-130] and the shortest lifetime is caused by the band-edge recombination at the surface [131].

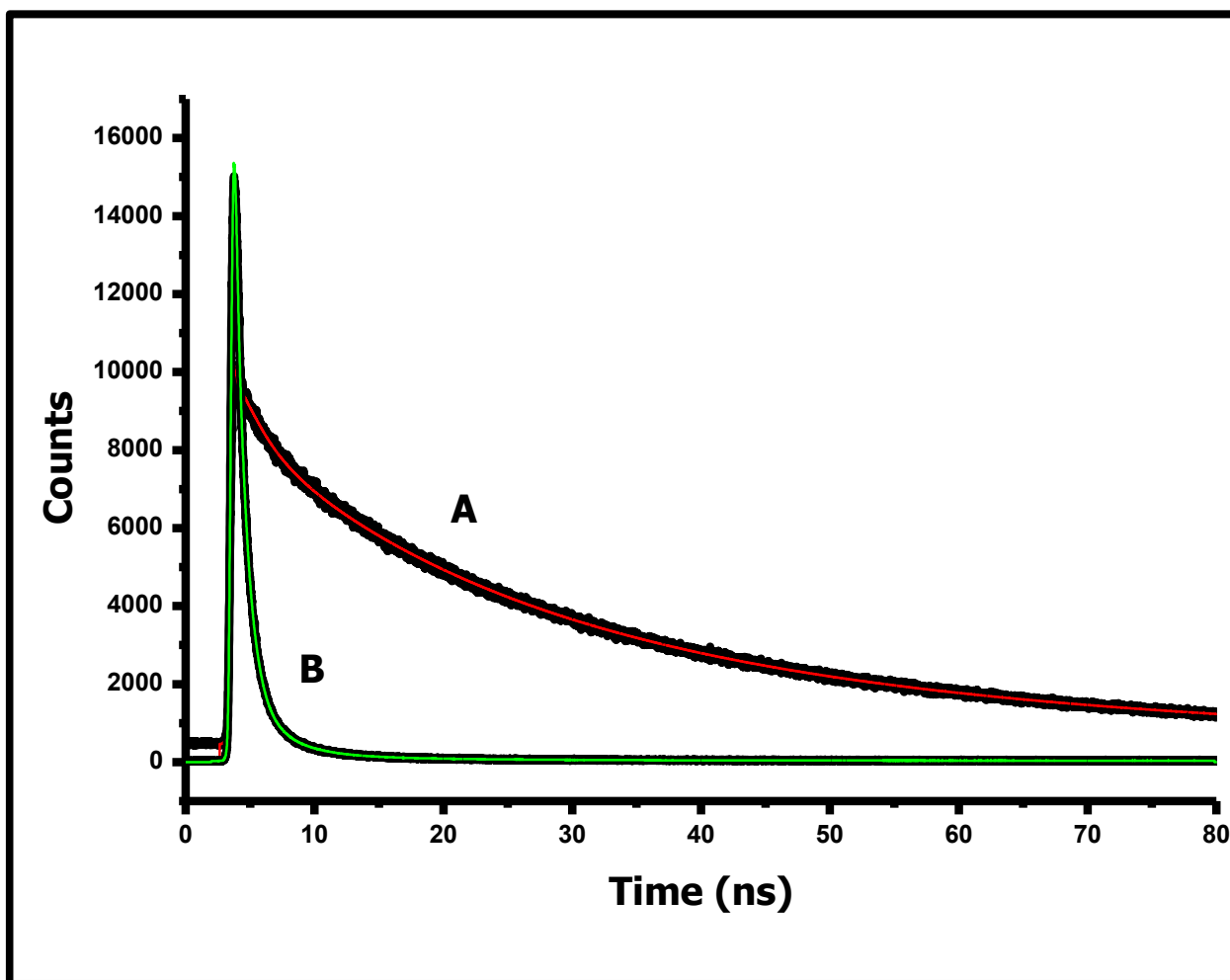


Figure 3.11: Fluorescence decay curves of (A) CdTe@ZnS-GSH and (B) CdTe@ZnS-GSH-ZnPc(COOH)<sub>4</sub>-linked in NaOH:ethanol (1:1).

When ZnPc(COOH)<sub>8</sub> alone was excited at 705 nm, one lifetime was obtained showing purity of the complexes. The fluorescence lifetimes at 2.9 ns are typical of Pc complexes [132]. The fluorescence decay curves with a tri-exponential fit for CdTe@ZnS-GSH and CdTe@ZnS-GSH-ZnPc(COOH)<sub>4</sub>-linked are shown in **Figure 3.11A** and **B**. The lifetime of QDs were shorter for the conjugates of QDs with

ZnPc(COOH)<sub>8</sub>, due to energy transfer from the former to the latter to be discussed later. Average lifetimes are listed in **Table 3.2**. Similar quenching in the fluorescence lifetimes of QDs was found for ZnPc(COOH)<sub>4</sub>-linked and -mixed conjugates, **Table 3.2**. The shortening of lifetimes was more pronounced for the tetrasubstituted complexes than for the octasubstituted derivatives. This could be related to residual aggregates for the former which may not have been broken with ethanol. Fluorescence lifetimes are shortened by aggregation.

The  $\Phi_F$  values for QDs in the mixed and linked conjugates were found to be lower than  $\Phi_F$  values for QDs alone as shown **Tables 3.1** and **3.2**. This is due to the quenching of the QD's fluorescence by ZnPc(COOH)<sub>8</sub> or ZnPc(COOH)<sub>4</sub>, which will be discussed later.

The decrease in the  $\Phi_F$  value of QDs of the same size is more pronounced for the CdTe@ZnS-GSH-ZnPc(COOH)<sub>8</sub>-linked conjugate **Table 3.1**, compared to that of CdTe@ZnS-GSH-ZnPc(COOH)<sub>4</sub>, **Table 3.2**. This contradicts the more enhanced shortening of the fluorescence lifetimes for the latter.



**Table 3.1: Fluorescence quantum yields and lifetime data of QDs, ZnPc(COOH)<sub>8</sub> and the conjugates in NaOH (0.1 M).**

| Compound   | <sup>a</sup> $\Phi_{F(QD)}^{Mix/Linked}$<br>( $\pm 0.04$ ) | <sup>b</sup> $\tau_{av}$<br>(ns)<br>( $\pm 0.91$ ) | $\chi^2$<br>for $\tau$ values | $J$<br>( $\times 10^{-13} \text{ cm}^6$ ) | $R_0$<br>( $\text{\AA}$ ) | $r$<br>( $\text{\AA}$ ) | Eff  |
|--|--|--|-------------------------------|---|---------------------------|-------------------------|------|
| CdTe@ZnS-GSH-<br>ZnPc(COOH) <sub>8</sub> -<br>linked | 0.019  | 13.3   | 1.30                          | 9.49                                      | 68.1                      | 68.6                    | 0.49 |
| CdTe@ZnS-GSH-<br>ZnPc(COOH) <sub>8</sub> -<br>mixed  | 0.20   | 17.1   | 1.19                          | 3.83                                      | 58.5                      | 64.9                    | 0.35 |
| CdTe-TGA-<br>ZnPc(COOH) <sub>8</sub> -<br>mixed      | 0.27   | 11.2   | 1.19                          | 2.4                                       | 62.3                      | 70.7                    | 0.47 |
| CdTe-TGA   | 0.39   | 21.2   | 1.05                          | -   | -                         | -                       | -    |
| CdTe@ZnS-GSH   | 0.56   | 26.2   | 1.05                          | -   | -                         | -                       | -    |
| ZnPc(COOH) <sub>8</sub>                              | $\Phi_{F(MPc)} =$<br>0.23 [117]                            | 2.9  | 1.01                          | -   | -                         | -                       | -    |

<sup>a</sup>Excitation wavelength = 510 nm for QDs (alone, linked or mixed) . References are in square brackets. For linked and mixed complexes the fluorescence quantum yields are represented as

$\Phi_{F(QD)}^{Mix}$  or linked  $\Phi_{F(QD)}^{linked}$ , respectively in the text <sup>b</sup> Excitation wavelength = 574 nm for CdTe@ZnS-

GSH (alone, linked or mixed). For ZnPc(COOH)<sub>8</sub> alone, the excitation wavelength is 705 nm and

only one lifetime was obtained, hence  $\tau_{av} = \tau$  .

**Table 3.2: Fluorescence quantum yield and lifetime data of QDs, ZnPc(COOH)<sub>4</sub> and the conjugates.**

| Compound                                      | <sup>a</sup> $\Phi_{F(QD)}^{Mix/Linked}$<br>( $\pm 0.04$ )<br>$\lambda_{exc} = 500 \text{ nm}$ | $\tau_{av}$<br>(ns) <sup>b</sup><br>$\pm 0.9$<br>( $\chi^2$ ) | $J$<br>( $\times 10^{-13} \text{ cm}^6$ ) | $R_0$<br>( $\text{\AA}$ ) | $r$<br>( $\text{\AA}$ ) | Eff  |
|---|--|---|---|---------------------------|-------------------------|------|
| CdTe@ZnS-GSH-ZnPc(COOH) <sub>4</sub> - linked | 0.044  | 9.7<br>(1.20)   | 7.13                                      | 64.4                      | 58.9                    | 0.63 |
| CdTe@ZnS-GSH-ZnPc(COOH) <sub>4</sub> - mixed  | 0.10   | 10.7<br>(1.20)  | 6.76                                      | 63.9                      | 60.1                    | 0.59 |
| ZnPc(COOH) <sub>4</sub> -CdTe-TGA-mixed       | c  | c   | c   | c                         | c                       | c    |
| ZnPc(COOH) <sub>4</sub>                       | $\Phi_{F(MPc)} < 0.01$ [76]  | 3.2<br>(1.02)   | -   | -                         | -                       | -    |
| CdTe-TGA                                      | 0.11   | c   | -   | -                         | -                       | -    |
| CdTe@ZnS-GSH                                  | 0.56   | 26.2<br>(1.05)  | -   | -                         | -                       | -    |

Footnote the same as for Table 3.1. c = not determined.

It has been reported before that the addition of quenchers to QDs caused a decrease in the fluorescence quantum yield with less effect on the fluorescence lifetime [133]. This was explained in terms of the quencher occupying hole sites on the QDs. It is possible by modifying the surface of the QDs with phthalocyanines, the fluorescence quantum yields and lifetimes are effected differently. This is because fluorescence lifetimes do not depend upon factors that influence the fluorescence intensity such as fluorophore concentration, and are largely unaffected by photobleaching of the fluorophores [134].

### 3.2.2 Triplet quantum yields, lifetimes and singlet oxygen quantum yields

A triplet decay curve for CdTe@ZnS-GSH-ZnPc(COOH)<sub>8</sub>-linked is shown in **Figure 3.12**. The increase in  $\tau_T$  values (**Table 3.3**) has been observed before [80, 84]. The increase could be related to the protection of the Pc by the QDs. However, for ZnPc(COOH)<sub>8</sub>-mixed and linked, there was a trivial difference observed in the  $\tau_T$  values.  $\Phi_T$  values increase was due to heavy atom effect of quantum dots, **Table 3.3**. **Figure 3.13** shows singlet oxygen kinetics decay curve of ZnPc(COOH)<sub>8</sub>. The  $\Phi_T$  and  $\Phi_\Delta$  values of ZnPc(COOH)<sub>8</sub> complex were lower than those of CdTe@ZnS-GSH-ZnPc(COOH)<sub>8</sub>-mixed or -linked. Such a difference is due to intersystem crossing being enhanced on CdTe@ZnS-GSH-ZnPc conjugates.  $\Phi_T$ ,  $\tau_T$  and  $\Phi_\Delta$  for ZnPc(COOH)<sub>4</sub> and its conjugates were not determined.

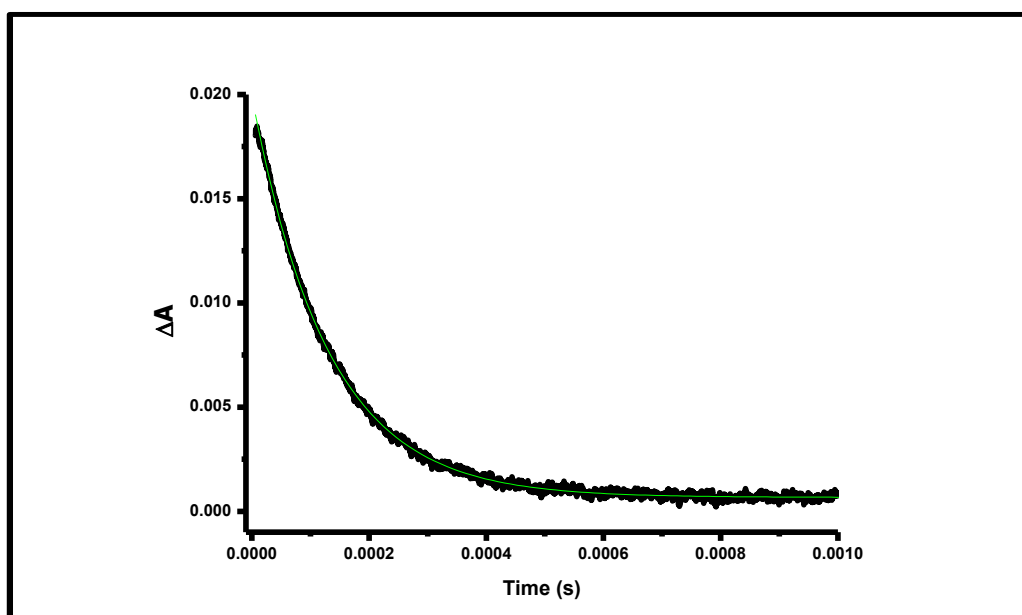


Figure 3.12: Triplet lifetime decay curve of CdTe@ZnS-GSH-ZnPc(COOH)<sub>8</sub>-linked in NaOH (pH 11).

Table 3.3: Triplet quantum yields and lifetime values of ZnPc(COOH)<sub>8</sub> and its conjugates dissolved in NaOH (pH 11).

| Complex   | $\Phi_T$<br>$\lambda_{exc} = 674 \text{ nm}$ | $\Phi_\Delta$<br>$\lambda = 674 \text{ nm}$ | $\tau_T (\mu s)$<br>$\lambda = 674 \text{ nm}$ |
|---|--|---|--|
| ZnPc(COOH) <sub>8</sub>                           | 0.38   | 0.24  | 69   |
| CdTe@ZnS-GSH-<br>ZnPc(COOH) <sub>8</sub> - linked | 0.65   | 0.29  | 130  |
| CdTe@ZnS-GSH-<br>ZnPc(COOH) <sub>8</sub> - mixed  | 0.59   | 0.27  | 128  |

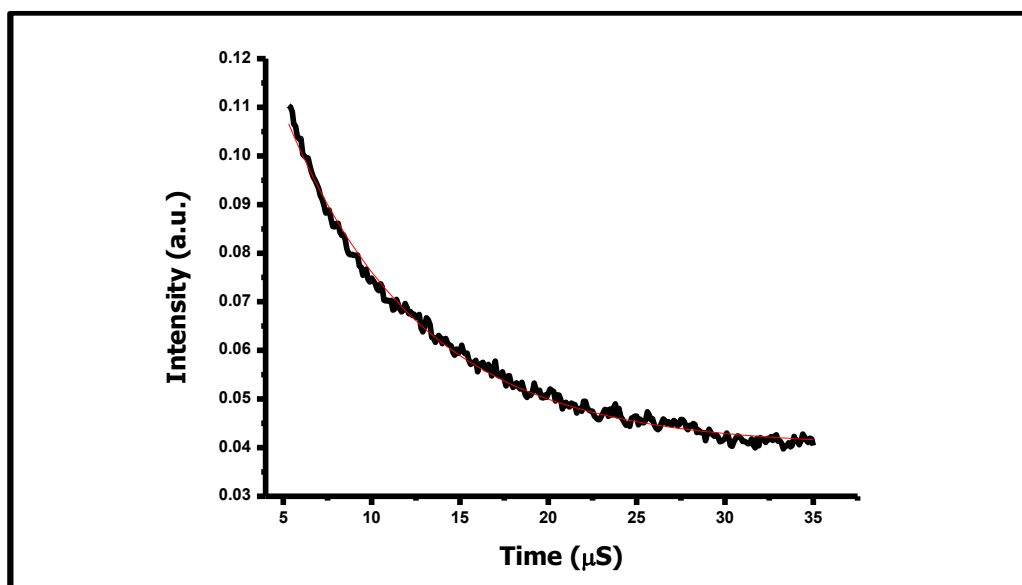


Figure 3.13: Singlet oxygen kinetics decay curve of  $\text{ZnPc}(\text{COOH})_8$  in NaOH (pH 11).

### 3.2.3 Förster Resonance Energy Transfer (FRET) Parameters

FRET was observed between CdTe@ZnS-GSH and  $\text{ZnPc}(\text{COOH})_8$  in NaOH. The non-radiative energy transfer from the donor to the acceptor is facilitated by the good spectral overlap between the donor (QD) emission and the acceptor ( $\text{ZnPc}(\text{COOH})_8$  derivatives) absorbance spectra (Figure 3.14).

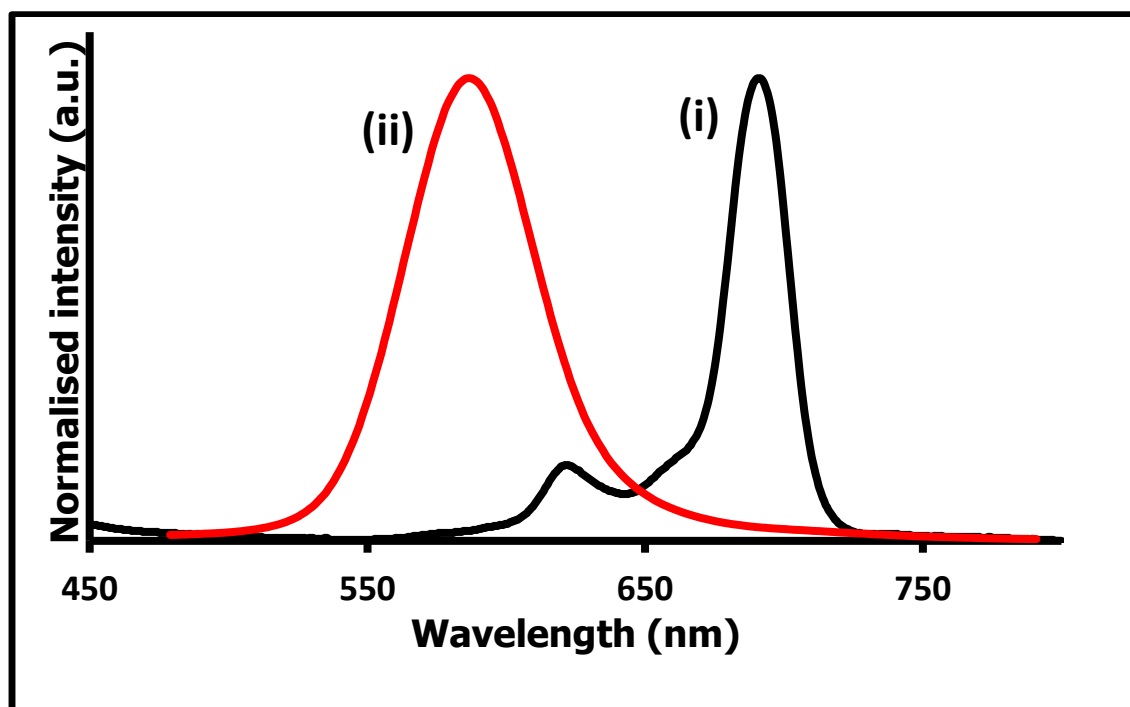


Figure 3.14: Normalized absorption spectrum of (i) ZnPc(COOH)<sub>8</sub> in NaOH (0.1 M) and emission spectrum of (ii) CdTe@ZnS-GSH in NaOH.

Figure 3.15A and B shows fluorescence emission enhancement via FRET by exciting the mixed or linked conjugate of CdTe@ZnS-GSH with ZnPc(COOH)<sub>8</sub> at the wavelength where QDs absorb and Pcs do not ( $\lambda = 510$  nm). There is greater enhancement of the Pc fluorescence for the mixed CdTe@ZnS-GSH-ZnPc(COOH)<sub>8</sub>-mixed than for the CdTe@ZnS-GSH-ZnPc(COOH)<sub>8</sub>-linked conjugate. The relative amounts of Pc and QDs will be different in the mixed and linked conjugates, making comparison difficult. The FRET parameters were determined from the photoluminescence decrease of the donor.

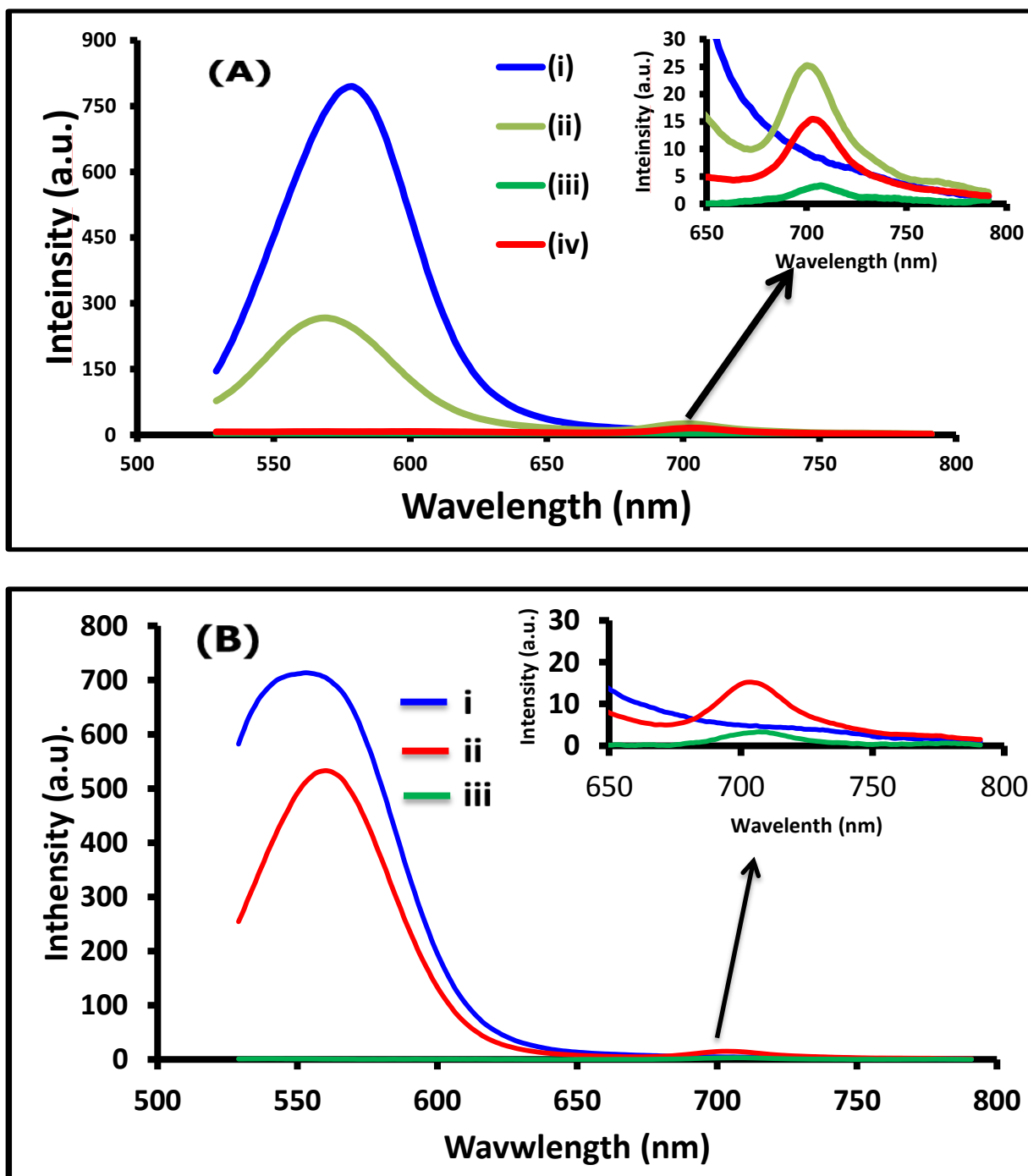


Figure 3.15: Emission spectra of (A) (i) CdTe@ZnS-GSH, (ii) CdTe@ZnS-GSH-ZnPc(COOH)<sub>8</sub>-mixed (iii) ZnPc(COOH)<sub>8</sub> and (iv) CdTe@ZnS-GSH-ZnPc(COOH)<sub>8</sub>-linked. (B) (i) CdTe-TGA, (ii) CdTe-TGA-ZnPc(COOH)<sub>8</sub>-mixed (iii) and ZnPc(COOH)<sub>8</sub>. Excitation wavelength = 510 nm.



There are many factors reported (and are still under debate) that influence photoluminescence decrease other than FRET [135-137]. It has been reported that for QD-Porphyrin nano-composites, the major part of the observed quenching of QD photoluminescence can neither be assigned to FRET nor to photoinduced charge transfer between the QD and the porphyrin [137]. This photoluminescence quenching was dependent on QD size and shell and is stronger for smaller quantum dots. It was concluded (from experimental data and quantum mechanical calculations) that QD photoluminescence quenching in QD-Porphyrin nano-composites can be explained in terms of a tunnelling of the electron (of the excited electron-hole pair) followed by a self-localization of the electron or formation of trap states. Similar explanation may be provided in the case of  $\text{ZnPc}(\text{COOH})_8$  - QDs conjugates. Thus the values of  $\text{Eff}$  presented here are estimates and will be used only for comparative purposes. The emission spectra of the conjugates show broadening in **Figure 3.15B** compared to **Figure 3.15A** (when the QDs are mixed with Pcs without a chemical bond). Broadening in the emission of QDs is associated with inhomogeneity or aggregation [85]. Compared with the TEM images in **Figure 3.6**, we suggest that the broadening of the emission peaks in **Figure. 3.15B** may be associated with aggregation.

The spectral term ( $J$ ) was estimated by overlapping QD emission with the absorbance of ZnPc derivative. The PhotochemCAD program gives  $J$  units as  $\text{cm}^6$  following the use of  $\epsilon_{\text{ZnPc}}$  in  $\text{M}^{-1}\text{cm}^{-1}$  and the wavelength  $\lambda$  in nm. The  $J$  and  $R_0$  values in this work were computed using PhotochemCAD [114] whilst the  $r$  values were calculated using Equation 1.10 and are listed in **Tables 3.1 and 3.2**. For porphyrin-

based complexes,  $J$  values are generally of the order of  $10^{-14}$   $\text{cm}^6$ . The  $J$  values obtained for QDs (CdTe@ZnS-GSH) mixed with ZnPc(COOH)<sub>8</sub> or for CdTe@ZnS-GSH-ZnPc(COOH)<sub>8</sub>-linked were of the order of  $10^{-13}$   $\text{cm}^6$ , **Tables 3.1 and 3.2**. Such  $J$  values indicate a good spectral overlap of the emission spectrum of the donor and the absorption spectrum of an acceptor. The efficiency of FRET ( $\text{Eff}$ ) values were computed using Equation 1.9. Since the value of  $r$  was greater than that of  $R_0$  for CdTe@ZnS-GSH-ZnPc(COOH)<sub>8</sub>-linked and CdTe@ZnS-GSH-ZnPc(COOH)<sub>8</sub>-mixed,  $\text{Eff}$  values less than 50% were obtained, **Table 3.1**. The values are larger for the conjugates due to the presence of the chemical bond. The advantage of time-resolved (using Equation 1.9) over steady state (using Equation 1.8) techniques for FRET efficiency determinations is that donor-acceptor separation distances can be mapped with greater quantitative accuracy in the former. As stated above, this is because fluorescence lifetimes do not depend upon factors that influence the fluorescence intensity such as fluorophore concentration, and are largely unaffected by photobleaching of the fluorophores [134], hence the  $\text{Eff}$  determined by fluorescence lifetimes may be more accurate.

FRET was observed to take place between CdTe@ZnS-GSH QDs and the ZnPc(COOH)<sub>4</sub> complexes in a NaOH (0.1 M):ethanol (1:1) mixture. A spectral overlap, **Figure 3.16**, similar to that of ZnPc(COOH)<sub>8</sub> (**Figure 3.14**), was observed for the ZnPc(COOH)<sub>4</sub> complex.

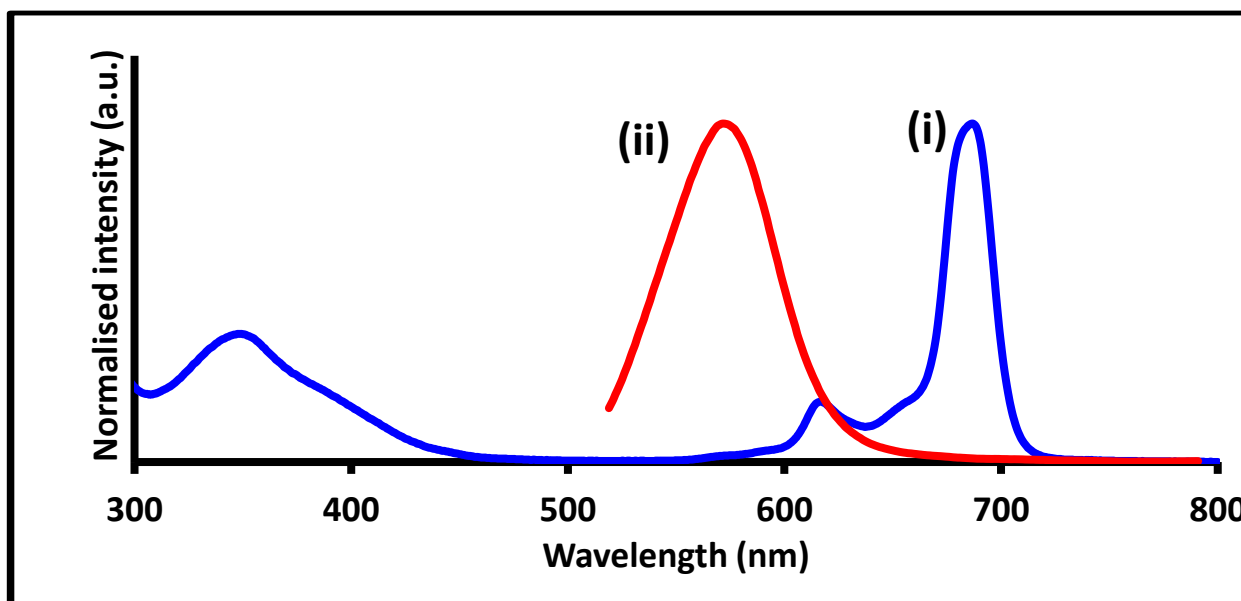


Figure 3.16: (i) Normalized absorption and (ii) emission spectra of  $\text{ZnPc}(\text{COOH})_4$  and  $\text{CdTe@ZnS-GSH}$  in  $\text{NaOH}$  (0.1 M):ethanol (1:1) mixture, respectively.

Figure 3.17 shows the emission spectra of the Pc upon excitation at 500 nm (inset), where only the QD absorbs (thus emission from the Pc is not expected). This stimulated, weak Pc emission (obtained for both the mixed and linked samples) is due to the non-radiative energy transfer from the donor QD to the  $\text{ZnPc}(\text{COOH})_4$ . A large reduction in the emission intensity of the QDs is also observed.

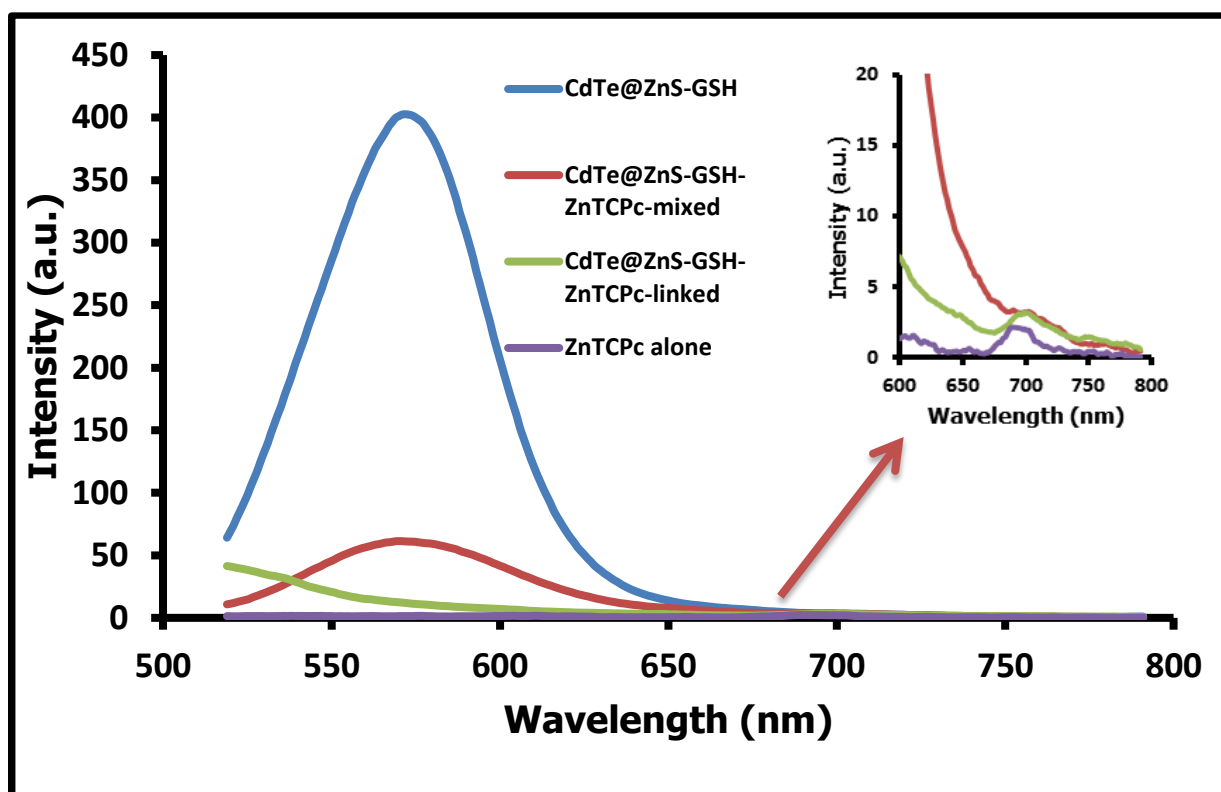


Figure 3.17: Emission spectra for the CdTe@ZnS-GSH QDs, CdTe@ZnS-GSH-Zn(COOH)<sub>4</sub>-mixed conjugate, CdTe@ZnS-GSH-ZnPc(COOH)<sub>4</sub>-linked conjugate and ZnPc(COOH)<sub>4</sub> alone in a NaOH (0.1 M):ethanol (1:1) mixture. Excitation wavelength = 500 nm.

The calculated  $r$  distances were found to be smaller than the  $R_0$  values for the CdTe@ZnS-GSH-ZnPc(COOH)<sub>4</sub>-linked (or mixed) conjugates, implying efficiencies ( $Eff$ ) greater than 50% (Table 3.2) except for core CdTe-TGA-mixed where  $Eff < 50\%$ . The opposite is true for the CdTe@ZnS-GSH-ZnPc(COOH)<sub>8</sub> - linked conjugates where  $r > R_0$ . The FRET efficiencies were found to be relatively high for the linked complexes compared to their mixed counterparts, suggesting that linking the MPcs

complexes to the QDs is beneficial to energy transfer efficiencies as the distance between the donor and acceptor are shorter compared to mixed conjugates. Also, the FRET efficiencies are lowered when the number of substituents are increased (CdTe@ZnS-GSH-ZnPc(COOH)<sub>8</sub> conjugates). The tetrasubstituted Pc is, however, a mixture of isomers and upon conjugation to QDs, the isomers may behave differently in solution.

# CHAPTER FOUR

## CONCLUSIONS

## General conclusions

The spectroscopic techniques, including UV/Vis, IR and XPS spectroscopies as well as TEM and AFM, confirmed successful coordination of ZnPc derivatives to coreshell CdTe@ZnS quantum dots capped with glutathione (GSH). Upon conjugation with ZnPc derivatives, the fluorescence quantum yields and the fluorescence lifetimes of the QDs decreased due to energy transfer from the latter to the Pc. A stimulated emission of ZnPc derivatives was also observed in the presence of QDs.

The CdTe@ZnS-GSH-ZnPc(COOH)<sub>4</sub> samples showed higher FRET efficiencies than those for the similarly sized QD conjugate, CdTe@ZnS-GSH-ZnPc(COOH)<sub>8</sub>. The triplet quantum yield, lifetime and singlet oxygen quantum yield of ZnPc(COOH)<sub>8</sub> increased upon conjugation with QDs.

---

## References

1. F. H. Moser and A. L. Thomas, Phthalocyanine compounds, Reinhold Publishing Corporation, New York, 1963.
2. W. Bauer, H. Berneth, T. Clausen, A. Engel, M. Filosa and P. Gregory, Industrial Dyes chemistry, properties and applications, ed. K. Hunger, WILEY-VCH Verlag GmbH & Co. KGaA, Weinheim, 2003.
3. N. C. Jain, The Pilgrimage of the Wonder Macromolecule: Phthalocyanine, Res. J. Chem. Sci. 1 (2011) 1-5.
4. L. R. Milgrom, The Colours of Life, an introduction to the chemistry of porphyrins and related compounds, Oxford University Press Inc., New York, 1997.
5. R. Bonnett, Chemical aspects of photodynamic therapy, Gordon and Breach Science Publishers, Germany, 2000.
6. A. C. Tedesco, J. C. G. Rotta and C. N. Lunardi, Curr. Org. Chem. 7 (2003) 187-196.
7. M. O. Liu, C.-H. Tai, M.-Z. Sain, A. T. Hu and F.-I. Chou, J. Photochem. Photobiol. A 165 (2004) 131-136.
8. S. V. Rao, P. T. Anusha, T. S. Prashant, D. Swain and S. P. Tewari, Mater Sci and Appl 2 (2011) 299-306.
9. L. Ma, Y. Zhang, and P. Yuan, Opt. Express 18 (2010) 17667 - 17670.
10. G. de la Torre, P. Vázquez, F. Agulló-López and T. Torres, J. Mater. Chem. 8 (1998) 1671-1681.



11. E. Ben-Hur and I. Rosenthal, *Int. J. Radiat. Biol.* 47 (1985) 145–147.
12. D. Frackowiak, A. Planner and K. Wiktorowicz, Near-infrared applications in medicine, in *Near-Infrared Applications in Biotechnology*, ed. R. Raghavachari, Marcel Dekker, Inc. New York, Basel, 2001, pp. 151–183.
13. A. Minnock, D. I. Vernon, J. Schofield, J. Griffiths, J. H. Parish and S. B. Brown, *J Photochem Photobiol B Biol* 32 (1996) 159-164.
14. N. Sekkat, H. van den Bergh, T. Nyokong and N. Lange, *Molecules* 17 (2012) 98-144.
15. H. S. Majumdar, A. Bandyopadhyay and A. J. Pal, *Org. Electron.* 4 (2003) 39–44.
16. K. S. Yook, B. D. Chin, J. Y. Lee, B. E. Lassiter and S. R. Forrest, *Appl. Phys. Lett.* 99 (2011) 1-3.
17. A. Varotto, C.-Y. Nam, I. Radivojevic, J. Tomé, J. A. S. Cavaleiro, C. T. Black and C. M. Drain, *J. Am. Chem. Soc.* 138 (2010) 2552–2554.
18. S. Eu, T. Katoh, T. Umeyama, Y. Matano and H. Imahori, *Dalton Trans.* 40 (2008) 5476–5483.
19. G. Rajagopal, S. S. Kim and J. M. Kwak, *Bull. Korean Chem. Soc.* 27 (2006) 1907–1909.
20. J. Brunet, A. Pauly, L. Mazet, J. P. Germain, M. Bouvet and B. Malezieux, *Thin Solid Films* 490 (2005) 28–35.
21. D. Hohnholza, S. Steinbrecherb and M. Hanacka, *J. Mol. Struct.* 521 (2000) 231–237.

22. D. Wöhrle, G. Schnurpfeil, S. G. Makarov, A. Kazarin and O. N. Suvorova, *Macroheterocycles* 5 (2012) 191–202.
23. C. G. Claessens, U. Hahn and T. Torres, *Chem. Rec.* 8 (2008) 75–76.
24. X. Song, Y. She, H. Ji and Y. Zhang, *Org. Process. Res. Dev.* 9 (2005) 297–301.
25. K. Sakamoto and E. Ohno, *Prog. Org. Coat.* 31 (1997) 139–145.
26. N. A. Wiederkehr, *J. Braz. Chem. Soc.* 7 (1996) 7–13.
27. M. Keyanpour-Rad, *Iran. Polym. J.* 10 (2001) 224–226.
28. M. A. A. El-Ghaffar, N. R. El-Halawany and H. A. Essawy, *J. Appl. Polym. Sci.* 108 (2008) 3226–3227.
29. A. R. A Shoukat, J. Keshavayya, M. N. K. Harish, A. H. Shridhar, T. Rajesha and A. G. Prashantha, *Int.J. ChemTech Res.* 3 (2011) 1145–1147.
30. C. C. Leznoff, In *Phthalocyanines: Properties and Applications*, eds. C. C. Leznoff, A. B. P. Lever, VCH publishers, New York, Vol. 1 (1989)1, Chp. 1.
31. M. J. Stillman and T. Nyokong, In *Phthalocyanines: Properties and Applications*, eds. C. C. Leznoff, A. B. P. Lever, VCH publishers, New York, Vol. 1 (1989) 133.
32. J. Mack and M. J Stillman, *J. Porphyrins Phthalocyanines.* 5 (2001) 67–76.
33. E. A. Ough, Z. Gasyna and M. J. Stillman, *Inorg. Chem.* 30 (1991) 2301–2310.
34. T. H. Huang, K. E. Reickhoff and E. M. Voight, *J. Chem. Phys.* 77 (1982) 3424–3441.
35. H. Zhan, M. Wang and W. Chen, *Mater. Lett.* 55 (2002) 97–103.

36. R. D. George, A.W. Snow, J. S. Shirk and W. R. Barger, *J. Porphyrin Phthalocyanines*. 2 (1998) 1-7.
37. K. Kameyama, A. Satake and Y. Kobuke *Tetrahedron Lett.* 45 (2004) 7617-7620.
38. A. C. H. Ng, X. Li and D. K. P. Ng, *Macromolecules* 32 (1999) 5292-5298.
39. P. Tau and T. Nyokong, *Inorg. Chimica Acta* 360 (2007) 2615-2655.
40. S. Moeno and T. Nyokong, *J. Photochem. Photobiol. A: 201* (2009) 228-236.
41. M. E. Daraio, P. F. Aramendia, E. A. San Roman and S. E. Braslavsky, *Photochem. Photobiol.* 54 (1991) 367-373.
42. T. G. Truscott, *J. Chem. Soc., Faraday Trans. 2*, 82 (1986) 2177-2181.
43. J. P. Zelina and J. F. Rusling, *Microporous Mesoporous Mater.* 5 (1995) 203-210.
44. T. Nyokong and H. Isago, *J. Porphyrins Phthalocyanines* 8 (2004) 1083-1090.
45. L. Qi and X. Gao, *Expert Opin. Drug Deliv.* 5 (2008) 263-267.
46. I. L. Medintz, H. Mattoussi and A. R. Clapp, *Int J Nanomedicine* 3 (2008) 151-167.
47. P. Yang and N. Murase, *Adv. Funct. Mater.* 20 (2010) 1258-1265.
48. A. Wolcott, D. Gerion, M. Visconte, J. Sun, A. Schwartzberg, S. Chen and J. Z. Zhang, *J. Phys. Chem. B* 110 (2006) 5779-5789.
49. A. M. Smith, G. Ruan, M. N. Rhyner and S. Nie, *Ann. Biomed. Eng.* 34 (2006) 3-14.
50. Y. Wang and L. Chen, *Nanomedicine* 7 (2011) 385-402.

51. R. D. Tilley, *Chem. N.Z.* (2008) 146-150.
52. D. Bera, L. Qian, T.-K. Tseng and P. H. Holloway, *Materials* 3 (2010) 2265 – 2321.
53. S. Zhu, J. Zhang, C. Qiao, S. Tang, Y. Li, W. Yuan, B. Li, L. Tian, F. Liu, R. Hu, H. Gao, H. Wei, H. Zhang, H. Sun and B. Yang, *Chem. Commun.* 47 (2011) 6858-6860.
54. G. P. C. Drummen, *Int. J. Mol. Sci.* 11 (2010) 154–163.
55. V. A. Fonoberov and A. A. Balandin, *J. Nanoelectron. Optoelectron.* 1 (2006) 19–37.
56. K. L. Wang, D. Cha, J. Liu and C. Chen, *Proc. IEEE* 95 (2007) 1866 – 1881.
57. Y.-Y. Zhang, J.-Y. Kim, Y. Kim and D.-J. Jang, *J Nanopart Res* 14 (2012) 1-9.
58. F. O. Silva, M. S. Carvalho, R. Mendonça, W. A. A. Macedo, K. Balzuweit, P. Reiss and M. A. Schiavon, *Nanoscale Res Lett* 7 (2012) 1-10.
59. Z. Yuan, J. Wang and P. Yang, *Luminescence* In press  
<http://dx.doi.org/%2010.1002/bio.2358>.
60. L. Zou , Z. Gu, N. Zhang, Y. Zhang, Z. Fang, W. Zhu and X. Zhong, *J. Mater. Chem.* 18 (2008) 2807–2815.
61. Z. Yuan, P. Yang and Y. Cao, *ISRN Spectroscopy* (2012) 1-8.
62. P. Reiss, M. Protière and L. Li, *Small* 5 (2009) 154–168.
63. Y.-F. Liu, J.-S. Yu, *J. Colloid Interface Sci.* 351 (2010) 1–9.
64. M. Grabolle, J. Ziegler, A. Merkulov, T. Nann and U. Resch-Genger, *Ann. N.Y. Acad. Sci.* 1130 (2008) 235-236.

- 
65. A. Verma, S. Nagpal, P. K. Pandey, P. K. Bhatnagar and P. C. Mathur, J. Nanopart. Res. 9 (2007) 1125–1130.
66. V. Biju, T. Itoh, A. Anas, A. Sujith and M. Ishikawa, Anal. Bioanal. Chem. 391 (2008) 2469-2495.
67. A. N. Al-Ahmadi, QUANTUM DOTS – A VARIETY OF NEW APPLICATIONS, InTech, Croatia, 2012.
68. T. G. Kryshchak, L.V. Borkovska, O.F. Kolomys, N.O. Korsunskaya, V. V. Strelchuk, L.P. Germash, R. Y. Pechers'ka G. Chornokur, S. S. Ostapenko, C. M. Phelan and O.L. Stroyuk, Superlattices Microstruct. 51 (2012) 353 – 362.
69. C. P. Shah, M. Rath, M. Kumar and P. N. Bajaj, Beilstein J. Nanotechnol. 1 (2010) 119-127.
70. J. M. Pérez-Donoso, J. P. Monrás, D. Bravo, A. Aguirre, A. F. Quest, I. O. Osorio-Román, Ricardo F. Aroca, T. G. Chasteen and C. C. Vásquez, PLoS ONE 7 (2012) 1-9.
71. A. C. S. Samia, X. Chen and C. Burda, J. Am. Chem. Soc. 125 (2003) 15736-15737.
72. J. C. B. Huarac, M. S. Tomar, S. P. Singh, O. Perales-Perez, L. Rivera and S. Peña, Nanotec 3 (2010) 405-408.
73. A. C. S. Samia, S. Dayal and C. Burda, Photochem. Photobiol. 82 (2006) 617-625.
74. D. A. Tekdaş, M. Durmuş, H. Yanik and V. Ahsena, Spectrochim. Acta, Part A 93 (2012) 313-320.

- 
75. M. Idowu and T. Nyokong, *J. Lumin.* 129 (2009) 356–360.
76. S. Moeno and T. Nyokong, *Polyhedron* 27 (2008) 1953-1958.
77. A. Erdogmus, S. Moeno, C. Litwinski and T. Nyokong, *J. Photochem. Photobiol. A* 210 (2010) 200-208.
78. L. Li, J.-F. Zhao, N. Won, H. Jin, S. Kim and J.-Y. Chen, *Nanoscale Res. Lett.* 7 (2012) doi:10.1186/1556-276X-7-386, 19 pages.
79. J. Ma, J. Y. Chen, M. Idowu and T. Nyokong, *J. Phys. Chem. B* 112 (2008) 4465-4469.
80. M. Idowu, J. Y. Chen and T. Nyokong, *New J. Chem.* 32 (2008) 290-296.
81. S. Dayal, R. Krolicki, Y. Lou, X. Qiu, J.C. Berlin, M.E. Kenney and C. Burda, *Appl. Phys. B*, 84 (2006) 309-315.
82. S. Dayal, Y. Lou, A.C.S. Samia, J.C. Berlin, M.E. Kenney and C. Burda, *J. Am. Chem. Soc.* 128 (2006) 13974-13975.
83. S. Dayal, J. Li, Y. S. Li, H. Wu, A. C. S. Samia, M. E. Kenney and C. Burda, *Photochem. Photobiol.* 84 (2007) 243-249.
84. J. Britton, E. Antunes and T. Nyokong, *J. Photochem. Photobiol. A* 210 (2010) 1-6.
85. S. D' Souza, E. Antunes, C. Litwinski and T. Nyokong, *J. Photochem. Photobiol. A*: 220 (2011) 11-19.
86. S. D' Souza, E. Antunes and T. Nyokong, *Inorg. Chim. Acta* 367 (2011) 173–181.
87. W. Chidawanyika, C. Litwinski, E. Antunes and T. Nyokong *J. Photochem. Photobiol., A* 212 (2010) 27-35.

- 
88. N. Masilela and T. Nyokong, *J. Photochem. Photobiol. A* 247 (2012) 82-92.
  89. J. R. Lakowicz, *Principles of Fluorescence Spectroscopy*, 3rd ed., Springer Science+Business Media, LCC, New York, 2006.
  90. L. B. Josefsen and R. W. Boyle, *Theranostics* 2 (2012) 916-966.
  91. Y.-Y. Huang, S. K. Sharma, T. Dai, H. Chung, A. Yaroslavsky, M. Garcia-Diaz, J. Chang, L. Y. Chiang and M. R. Hamblin, *Nanotechnol Rev.*, 1 (2012) 1-36.
  92. M. Durmuş and T. Nyokong, *Photochem. Photobiol. Sci.* 6 (2007) 659-668.
  93. V. Chauke, M. Durmuş and T. Nyokong, *J. Photochem. Photobiol. A*. 192 (2007) 179-187.
  94. U. Resch-Genger, M. Grabolle, S. Cavaliere-Jaricot, R. Nitschke and T. Nann, *Nat. Methods* 5 (2008) 763-775.
  95. M. D. Leistikow, J. Johansen, A. J. Kettelarij, P. Lodahl and W. L. Vos, *Phys. Rev. B* 79 (2009) 1-9.
  96. S. Fery-Forgues and D. Lavabre, *J. Chem. Educ.* 76 (1999) 1260-1264.
  97. A. Gilbert and J. Baggott, *Essentials of molecular photochemistry*, library of congress, USA, (1995).
  98. T. H. Tran-Thi, C. Desforge and C. Thiec, *J. Phys. Chem.* 93 (1989) 1226.
  99. T. Nann, *Nano Biomed. Eng.* 3 (2011) 137-143.
  100. J. F. Lovell, T. W. B. Liu, J. Chen and Gang Zheng, *Chem. Rev.*, 110 (2010) 2839-2857.
  101. I. Rosenthal, *Photochem. Photobiol.* 53 (1991) 859-870.

- 
102. J. B. Hudson, V. Imperial, R. P. Haugland and Z. Diwu, *Photochem. Photobiol.* 65 (1997) 352-354.
103. J. D. Spikes, *Photochem. Photobiol B: Biol.* 6 (1990) 259-274.
104. B.-C. Bae and K. Na, *International Journal of Photoenergy*, (2012) 1-14.
105. K. Ishii, *Coord. Chem. Re.* 256 (2012) 1556-1568.
106. W. Spiller, H. Kliesch, D. Wöhrle, S. Hackbarth, B. Röder and G. Schnurpfeil. *J. Porphyrins Phthalocyanines*, 2 (1998) 145-158.
107. K. Langa, J. Mosinger and D.M. Wagnerová, *Coordination Chemistry Reviews*, 248 (2004) 321-350.
108. I. Seotsanyana-Mokhosi and T. Nyokong, *J. Porphyrins Phthalocyanines*, 8 (2004) 1214-1221.
109. A. O. Ogunsipe and T. Nyokong, *J. Porphyrins Phthalocyanines*, 9 (2005) 121-129.
110. M. S. Patterson, S. J. Madsen and R. Wilson, *J. Photochem. Photobiol. B: Biol.* 5 (1990) 69-84.
111. L. Stryer, *Annu. Rev. Biochem.* 47 (1978) 819-846.
112. E.Z. Chong, D.R. Matthews, H.D. Summers, K.L. Njoh, R.J. Errington and P.J. Smith, *J. Biomed. Biotech.* 2007 (7) (2007) 54169-54175.
113. L. Lankiewicz, J. Malicka and W. Wizck, *Acta Biochim. Pol.* 44 (1997) 477-489.
114. H. Du, R.A. Fuh, J. Li, L.A. Cockan and J.S. Lindsey, *Photochem. Photobiol.* 68 (1998) 141-142.



- 
115. A. Ambroz, A. Beeby, A. J. MacRobert, M. S. C. Simpson, R. K. Svensen and D. Phillips, *J. Photochem. Photobiol. B: Biol.* 9 (1991) 87-95.
116. A. Shavel, N. Gaponik and A. Eychmüller, *J. Phys. Chem. B* 108 (2004) 5905-5908.
117. T. Nyokong and E. Antunes, in: *The Handbook of Porphyrin Science*. Eds. Kadish, K. M.; Smith, K. M.; Guillard, R., Academic Press: New York, Vol. 7, chapt. 34 pp 247-349, World Scientific, Singapore, 2010.
118. P. R. Barber, S.M. Ameer-Beg, J. Gibey, L.M. Carlin, M. Keppler, T.C. Ng and B. Vojnovic, *J. R. Soc. Interface* 6 (2009) S93-S105.
119. J. Fernandes, M. Bilging and L. Grossweiner, *J. Photochem. Photobiol. B:* 37 (1997) 131-140.
120. X. Cai, Y.. Zhang , X. Zhang and J. Jiang, *J. Molec. Struct. THEOCHEM* 801 (2006) 71-80
121. N. E. Triggs and J. J. Valentini, *J. Phys. Chem.*, 1992, 96, 6922-6931.
122. L. Rogach, L. Katsikas, A. Kornowski, D. Su, A. Eychmuller and H. Weller, *Ber. Bunsen-Ges. Phys. Chem.*, 100 (1996) 1772-1778.
123. C. Yan, F. Tang, L. Li, H. Li, X. Huang, D. Chen, X. Meng and J. Ren, *Nanoscale Res Lett.* 2010; 5(1): 189-194.
124. P. Chawla, G. Sharma, S. P. Lochab and N. Singh, *Bull. Mater. Sci.*, 33 (2010) 535-541.
125. S. Moeno and T. Nyokong, *J. Photochem. Photobiol. A:* 215 (2010) 196-204.
126. M. Idowu and T. Nyokong, *Spectrochim. Acta: A* 75 (2010) 411-416.

127. X. Wang, L. Qu, J. Zhang, X. Peng and M. Xiao, *Nano Lett.* 3 (2003) 1103-1106.
128. M. Lunz and A. L. Bradley, *J. Phys. Chem. C* 113 (2009) 3084-3088.
129. J. Zhang, X. Wang and M. Xiao, *Opt. Lett.* 27 (2002) 1253-1255.
130. M. G. Bawendi, P.J. Carroll, W.L. Wilson and L.E. Bruce, *J. Chem. Phys.* 96 (1992) 946-954.
131. M. Sanz, M.A. Correa-Duarte, L.M. Liz-Marzán and A. Douhal, *J. Photochem. Photobiol. A: Chem.* 196 (2008) 51-58.
132. K. Ishii and N. Kobayashi in *The Porphyrin Handbook*. K.M. Kadish, K.M. Smith, R. Guilard, Eds. Vol. 16, Chp. 1, Elsevier (2003).
133. R. E. Galian and J. C. Scaiano, *Photochem. Photobiol. Sci.*, 2009, 8, 70-74.
134. A. V. Agronskaia, L. Tertoolen and H. C. Gerritsen, *J. Biomed. Opt* 9 (2004) 1230-1237.
135. C. L. Takanishi, E. A. Bykova, W. Cheng and J. Zheng, *brain research* 1091 (2006) 132-139.
136. T. Blaudeck, E. I. Zenkevich, F. Cichos and C. von Borczyskowski, *J. Phys. Chem. C*, 112 (2008) 20251-20257.
137. E. I. Zenkevich, T. Blaudeck, A. Milekhin and C. von Borczyskowski, *Inter. J. Spectr.* 2012, ID 971791, 14 pages.